University of the Witwatersrand

Masters Dissertation

Lagrange Modelling and Control for a Linear DC Machine

Author:
Mohlalakoma Therecia Ngwako

A Dissertation submitted in fulfillment of the requirements for the degree of Master of Science in Engineering

in the

School of Electrical and Information Engineering

12 September 2019

Declaration

I, **Mohlalakoma Therecia Ngwako**, declare that this Dissertation titled, "**Lagrange Modelling and Control for a Linear DC Machine**" and the work presented in it are my own. I confirm that:

- This work was done wholly or mainly while in candidature for a research degree at this University.
- Where any part of this thesis has previously been submitted for a degree or any other qualification at this University or any other institution, has been clearly stated.
- Where I have consulted the published work of others, this is always clearly attributed.
- Where I have quoted from the work of others, the source is always given. With the exception of such quotations, this dissertation is entirely my own work.
- I have acknowledged all main sources of help.

Signed: _____

Date: _____

UNIVERSITY OF THE WITWATERSRAND

Abstract

School of Electrical and Information Engineering

Master of Science in Engineering

Lagrange Modelling and Control for a Linear DC Machine

by Mohlalakoma Therecia Ngwako

Supervisor: Dr O.T.C Nyandoro and Dr J. van Coller

Modelling of electric machines is often a very challenging task due to the underlying electromagnetic fields. The nature of the magnetic field is that they are typically time varying and have operational issues such as saturation, hysteresis, nonlinearities and coupling etc. Further, attempts to shape the fields e.g. into sinusoidal waveforms, e.g. with salient poles are never perfect. Losses such as eddy current losses among others compound to the problem of accurately modelling the underlying electromagnetic interactions of an electric machine.

The goal of this research is to utilize a dynamic energy based modelling technique to circumvent a number of the electric machine modelling challenges. Lagrange analysis is proposed to demonstrate its two key challenges namely; dynamic energy balance via Lagrangian energy equations and follow on Euler-Lagrangian state analysis. Secondly input and instantaneous rate of dissipation Euler-Lagrange model formulation and analysis incorporates a degree of freedom analysis to perform the physical model order analysis. This Lagrangian analysis is to be demonstrated on modelling a linear DC machine controlled for various performance criteria such as speed control, current control and power control. Further proposed results and analysis are for a pair of linear DC machines one of which is a gravity fed generator whose aim is to electrically drive the tandem DC machine up a slope under various control criteria.

Overall the novelty of this work is in utilizing the Lagrangian analysis to model a linear DC machine and also to utilize the same analysis to reduce the model complexity by systematically reducing the model order.

To my mother, father, the rest of the Ngwako family, and the Matekola family.

Acknowledgements

I would like to extend my deepest gratitude to my supervisors Dr J. van Coller and Dr O. Nyandoro for their academic guidance and support and also taking their time from their busy schedules to assist me with my research. I would also like to acknowledge Eskom Power Plant Engineering Institute (EPPEI) for providing me with financial assistance. The Masters program would not have been possible without funding. I would like to thank my parents for their emotional support, encouragement and also for bestowing wisdom in me. Lastly, a special thanks to my friends for their support during the tough times.

Contents

List of Figures

List of Tables

Publications

Overlapping	Peer-reviewed journal papers directly related to this Dissertation
chapter	
[7]	**M.T Ngwako** L.I.Nkomo, A. Dove and O.T. Nyandoro, "Heaviside based optimal control for ride comfort and actuation energy optimisation in half-car suspension systems", *IFAC*, vol. 50, Issue 2, pp. 259-264, 2017.
chapter	
[3,4]	**M.T Ngwako**, O.T Nyandoro and J. van Coller, "Modelling and Control of an Autonomous Linear DC Machine based Mine Locomotive", *IFAC MMM*.
chapter	
[5]	**M.T Ngwako**, O.T Nyandoro and J. van Coller, "Dynamic Friction Loss Estimation for a Linear DC Machine Powered Mining Locomotive", *IFAC MMM*.
chapter	
[7]	**M.T Ngwako**, O.T Nyandoro and J. van Coller, " A Condition for Singular Optimal Control Formulation for a Tandem Pair of Gravity Fed Linear DC Machine Powered Mine Locomotives", *IFAC MMM*.

CHAPTER 1

Introduction

1.1 Motivation for modelling technique

Modelling of machines has been described using physics concepts and classical mechanical analysis methods. Modelling machines using physics concepts involves describing the machine using Newtonian laws and Maxwell's laws, in particular, Lorentz's laws, Faraday's laws, Ampere's laws, and Gauss' laws. Classical machine modelling is based on approximating equivalent circuit models using Thevenin and Nortorn theorems and further analyzing the equivalent circuit using Kirchhoff's laws. However, one of the limitations of using equivalent circuit models is that, equivalent circuit models often assume steady state operation. Also, equivalent circuit models are valid in either the transient state, sub-transient state or the steady state depending on the type of model provided [18]. For this reason, there are several machine equivalent circuit models specifically describing a certain state of operation. Modelling machines is of paramount importance in that it assists in understanding the behaviour of a machine. The study uses the modelling results already in existence such as the work of Chiasson [13] where a comprehensive description of machines is provided. This study is particularly based on Chapter 1 - 3 of Chiasson's work where the key focus is on modelling the linear DC machine. The core focus of this study is on investigating new ways of modelling machines using an energy based approach i.e. developing existing models albeit with new energy based approaches. This presents new opportunities of formulating comprehensive machine models for control purposes. Also, using the proposed energy based analysis to formulate machine models is beneficial in that; the energy based

technique is only concerned with the dynamic energy flow and in cases where advanced machines with rotors and stators are investigated, one of the key properties of the energy based technique (which is allowing the use of transformation formulae to move from one coordinate frame to another coordinate frame) allows directly transforming from the stator reference frame to the rotor reference frame, and vice versa. This aspect though not performed is used as motivation for future work. Another characteristic of the Lagrange analysis is that, it allows for model order reduction by reducing the degrees of freedom of a system. One key advantage of energy based modelling techniques is that the technique allows modelling of machines using physics concepts and also circuit equivalent circuit modelling. In fact, energy based techniques (particularly the Lagrange), are very powerful because the Lagrange analysis can be used to formulate Maxwell's laws, Newtonian laws and also Kirchhoff's laws. The Lagrange is a very simple way of solving complex machine modelling problems in that, the technique is very systematic and structured.

1.2 Motivation for friction modelling

Some of the losses in machines are due to object to object contact, i.e. friction force. The viscous friction model is commonly used in machine models [13]. However, viscous friction only considers kinetic friction losses. Also, viscous friction assumes that the friction force is directly proportional to the velocity. Real-life machines have a friction force where the friction force has two regions, i.e. static friction and kinetic friction. It is thus important to model the two friction regions to achieve a more comprehensive model of the friction force. A comprehensive friction force is desired because it allows for friction force compensation when designing a controller for machines. A detailed friction force model together with a detailed machine model would result in a comprehensive machine model. A comprehensive machine model allows for robust control of the machine over a wide range.

1.3 Motivation for Non-linear control

Machines tend to be unstable when there are load variations and when stochastic noises are introduced in the system of an electric machine. This necessitates the use of control algorithms to improve the performance of the machines. While there are several control algorithms to choose from, it should be noted that machines and any other real-life systems are non-linear. Thus, a robust, non-linear control algorithm suitable for real-world applications is desired to improve the performance of the machine. For this study, non-linear optimal control is considered because it is suitable to control non-linear machines. Optimal control is also a robust control algorithm compared to PID control algorithm and linear quadratic regulators.

1.4 Research hypothesis

The hypothesis of this work is that; ***It is possible to model a linear DC machine and to also control the linear DC machine using the Lagrange formulation.***

The Lagrange analysis is an energy based modelling technique that has been used for centuries for machine modelling and formulating Newtonian laws [38, 102]. The Lagrange is used to model a synchronous machine in [16, 38]. The machine model is elaborate in that the saturation of the machine is also modelled. This highlights the effectiveness and power of the Lagrange. It is very important to mention that the analysis in [38] is performed on an equivalent circuit machine model. In reference [16, 93], the Lorentz force is formulated using an electromagnetic field based Lagrange analysis. The analysis presented in [16, 93] is performed on a charged particle. Chiasson also presents and discusses a linear DC machine model in [13]. The linear DC machine analysis is based on Faraday's law, Lorentz law, also Newton laws. Integrating the work done in [13, 16, 102], the linear DC machine model by [13] can be formulated using the Lagrange based on the analysis by [16]. The goal is to achieve the same results by [13] using the Lagrange analysis. Also, controlling the linear DC machine is desirable. While several control algorithms

exist, it is important to investigate control algorithms that are suitable for real-world applications such as the non-linear optimal control. A linear DC machine is non-linear when an external force (the force could be due to gravity on an inclined plane) is taken into consideration. Now with added stochastic noise in the system the linear control algorithms could result in undesirable performance, i.e. slow response time, overshoots and the system could possibly not be controlled. This necessitates robust control algorithms such as the non-linear optimal control algorithm.

1.5 Research questions

The following research questions have to be answered in order to address the hypothesis:

- *How can the linear DC machine discussed by [13] be modelled and extended using the Lagrange analysis?*
- *How can the model order of the linear DC machine be reduced using the Lagrange analysis?*
- *How can non-linear optimal control be formulated for a linear DC machine?*
- *Does friction play any significant role in the starting and running of a linear DC machine?*

1.6 Research objectives and contributions

The work done in this study is significant in that the work demonstrates that it is possible for machine models to be formulated by using energy stored in magnetic fields. Therefore, implies that magnetic fields can be analyzed using Lagrange analysis. In existing literature, [13], develops microscopic machine models using electric and magnetic field analysis in his study. The machine models in [13] are comprehensive. This therefore implies that, comprehensive machine models

which are based on the geometry of the machine can be formulated using energy based techniques. Having comprehensive models would mean that the machine analysis is accurate. The work presented in this study demonstrates that machine modelling techniques are not limited to physics and classical methods. The study presented in this document also demonstrates that control algorithms can be used on the the models formulated using magnetic field energy based analysis to improve the performance of the machine. Real-life system are non-linear and also prone to disturbances. Therefore, non-linear control algorithms are also investigated to account for the non-linearity property of machines. Also, to demonstrate how non-linear control in machines can be performed.

The objective of this research is to:

- Prove that the Lagrange analysis can be used to model a linear DC machine.
- Formulate a detailed dynamic friction model to achieve a comprehensive linear DC machine model.
- Speed control of a linear DC machine using a state-feedback control algorithm based on pole placement to demonstrate that the speed of the machine can be controlled.
- Non-linear optimal control, particularly the singularity analysis for a linear DC machine.
- Reduce model complexity via reduction of the system models' order

1.7 Methodology

The research methodology is divided into seven stages. Each stage is aimed at answering and/or addressing the research question and also contributing towards existing knowledge. Tasks have to be completed in all the stages. Completing each stage would mean reaching a milestone. The research methodology follows a simple structure which is presented in the flow chart in fig.1.1. The first stage includes

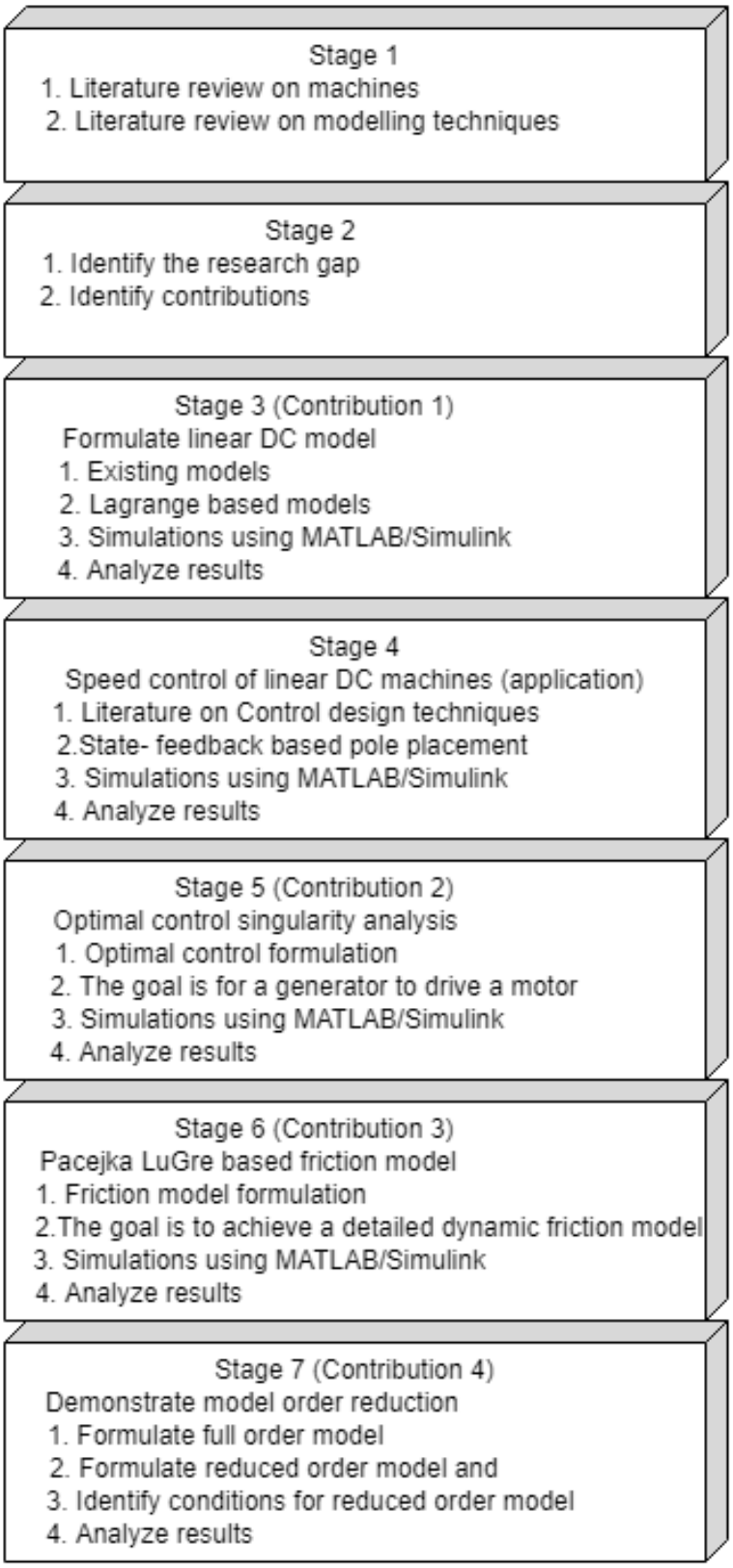

FIGURE 1.1: Research methodology

reviewing the literature on modelling techniques and also machines. The first stage is directly linked to the second stage in that a research gap and contributions are identified from the literature. Thereafter, the linear DC model is formulated, simulated and analyzed. Speed control of the linear DC machine formulated in stage three is introduced in stage four. Stage five and stage six introduce singular optimal control and LuGre based friction models where the targeted contributions are addressed. The last stage addresses another contribution. The simulations in this study are done using MATLAB/Simulink.

1.8 The Eskom Power Plant Engineering Institute

The Eskom Power Plant Engineering Institute (EPPEI) sponsored this research. Upon agreement, the research proposed to be based on a renewable energy microgrid comprising PV panels and a diesel generator. The operational conditions of the microgrid were supposed to be such that the the diesel generator supplements the PV source when there is a cloud cover and, the PV source was supposed to supply loads in a case where there is sufficient sunlight. However, the research deviated to the simplest version of a diesel generator which is a linear DC generator. The diesel generator was found to be a highly complex problem and simplifying the problem while still able to maintain using a MIMO non-linear controller brings us closer to the the real problem of modelling a diesel generator and PV panels which had to be used in a microgrid. The complex diesel generator could be modelled in the future since the fundamentals of a generator have already been addressed in this study. For speed control of the diesel generator in the future, the optimal controller or pole placement technique could be used. These control techniques have been presented in this research. The original goal of developing a comprehensive dynamic machine model via energy based methods is still covered in detail however, on a more basic machine model.

1.9 Organization of Dissertation

The rest of the dissertation is organized as follows. Chapter 2 details the literature relevant for the research, in Chapter 3, a linear DC machine model is formulated using the Lagrange analysis and the formulations are compared with a linear DC machine model formulated using classical physics methods and Kirchhoff's laws. A state feedback based on pole placement technique is found in Chapter 4. The control algorithm is used to control the speed of a linear DC machine powered mine locomotive. A friction model for the linear DC machine where the machine is used in mining applications is presented in Chapter 5. Chapter 6 details the Lagrange based model order reduction and, optimal control singularity analysis is

found in Chapter 7. Concluding remarks and future recommendations are found in Chapter 8.

CHAPTER 2

Literature Review

2.1 Modelling techniques

Analytical and numerical methods are used to describe the behaviour of machines [57, 64]. Numerical methods are used to solve Maxwell equations and often finite element methods/finite element analysis of the machine is performed using powerful computers [29, 35]. The limitation of numerical methods is that the computational time is long hence, the approach requires that powerful computers are used [108]. Analytical methods are based on electromagnetic laws and also the geometry and material of the machine are taken into consideration. Analytical methods allows for the overall behaviour of the machine under study to be explored [35]. Magnetic equivalent circuits, also known as lumped circuits, are popular in analytical methods. It should also be mentioned that most models are formulated using analytical methods and the models are fairly accurate [64]. Under the analytical approach, there are classical physics methods, classical modelling techniques and energy based modelling.

2.1.1 Classical physics methods

Electric machines can be also modelled using fundamental concepts of electricity and magnetism . In particular, the Lorentz laws, Faraday's laws, Lentz law and Amperes laws govern electromagnetic circuits. The basic idea of the Lorentz law is to describe that a current carrying conductor positioned between magnetic fields would experience a force [13]. The force is proportional to the current and also the

length of the wire between the magnetic poles. According to [13], the direction of the force would be the direction the needle of a compass would point to at that location. Further experiments also showed that the wire would only experience a force when the wire is positioned perpendicular to the magnetic poles. This force is known as the Lorentz force. Now using the same setup of a wire placed between magnetic poles to describe the Faraday's law; the Faraday's law is based on the basic principle that a changing flux induces an electromotive force. Also, the electromotive force would force current in a closed circuit to flow in the direction of the magnetic field that opposes the change in magnetic flux that produced the current [33]. It is interesting to know that the Faraday's law also describes the Lentz law. A linear DC machine modelled and analyzed using physics laws is found in [11–13].

2.1.2 Classical modelling techniques

Classical machine modelling is based on approximating equivalent circuit models using Thevenin and Nortorn theorems and further analyzing the equivalent circuit using Kirchoff's laws; Kirchoff's current law and Kirchhoff's voltage law [17]. In reference [18], an equivalent circuit of a machine comprising multiple resistor, inductor circuits and a source voltage is modelled using classical methods. The mutual inductance is also taken into consideration in the analysis [18].

2.2 Energy based modelling techniques

The Lagrange and the port-Hamiltonian are energy based techniques used to model physical systems [28, 60, 62, 65, 71, 91, 95, 102]. These techniques are similar in that they both demand identifying the kinetic energy elements, potential energy elements and dissipative energy elements [62, 70]. A key feature of both the Lagrange and Port Hamiltonian techniques is the dynamic energy balance property which physically represents the power flow of a system [9].

2.2.1 Lagrange

The Lagrange modelling technique has been used over the years for Hamiltonian formulations, optimal control formulations, Newtons formulations, Maxwell formulations and Kirchoff's formulations [8, 16, 23, 49, 50, 94, 102]. The Lagrange modelling technique has also been widely used in applications such as the simple pendulum, circuit analysis, machine analysis (particularly the synchronous generator), and also suspension systems and this technique has generated very good results in terms of modelling [49, 76, 90, 95].

One of the key characteristics of the Lagrange modelling technique is its ability to use transformation formulae by degrees of freedom analysis for model order reduction [102]. The technique also allows for the use of transformation formulae to be used to move from one coordinate frame to another coordinate frame. The aforementioned characteristic is beneficial when modelling advanced machines in that the transformation formulae are used to move from the rotor reference frame to the stator reference frame, and vice versa [13, 61, 102].

To extend on the advantages of the the Lagrange analysis, the Lagrange has an advantage of simplifying complex circuit analysis, particularly circuits with multiple meshes. To analyze a circuit with multiple meshes using mesh analysis, one cannot ignore the fact that simultaneous equations have to be solved and depending on their complexity, there are bound to be mathematical errors [17]. The Lagrange analysis addresses these limitations of traditional circuit analysis such as nodal analysis and mesh analysis by using generalized coordinate analysis which bypasses dealing with tedious equations [61, 66, 95, 102]. However, the Lagrange analysis is a longer analysis for a simple circuit since there are three main steps that have to be followed to eventually perform the analysis.

2.2.2 Lagrange on electromagnetic circuits

Just to add on the previous section, the Lagrange technique is suitable for formulation of electromagnetic circuits [86]. The RLC circuit is one electromagnetic circuit to consider. According to [16], the Lagrange technique can also be extended to the formulation of electromagnetic fields. In the work done by [16], the Maxwell's equations are derived by means of electric potentials and magnetic potentials. Thus, fundamental electric circuits based on magnetic fields and electric fields can be formulated using the Lagrange. In this study, the Lagrange technique will be used to formulate the equations of a fundamental circuit based on a magnetic field and a resistor.

2.2.2.1 Applications of the Lagrange analysis

One of the key applications of the Lagrange analysis in Electrical engineering includes applying the Lagrange technique on an RLC circuit. Given an RLC circuit with a resistor R, inductor L and capacitor C, the kinetic energy and potential energy are described by:

$$T = \frac{1}{2}L\dot{q}^2 \tag{2.1}$$

$$U = \frac{1}{2}\frac{q^2}{C} \tag{2.2}$$

The dissipation energy is in the form of heat dissipated by the resistor:

$$P = \frac{1}{2}R\dot{q}^2 \tag{2.3}$$

Where T is the kinetic energy, U is the potential energy, P is the dissipation power, L is the inductance, C is the capacitance, R is the Resistance, q is the charge and $\dot{q}$ is the current. The Lagrange equation is represented by:

$$\Gamma = T - U \tag{2.4}$$

Where Γ is the Lagrange equation.

$$\frac{d}{dt}\frac{\partial \Gamma}{\partial \dot{q}} - \frac{\partial \Gamma}{\partial q} = V - \frac{\partial P}{\partial \dot{q}} \tag{2.5}$$

Evaluating the Euler-Lagrange results in an equation of the form:

$$V = L\ddot{q} + \frac{q}{C} + \dot{q}R \tag{2.6}$$

The result is the same as the result one would obtain while using the Kirchoff's circuit analysis. Therefore, the Lagrange analysis is suitable for circuit analysis and the results of the RLC found in Eq.2.6 using the Lagrange technique confirm this.

2.2.3 Port-Hamiltonian

Similarly to the Lagrange, the port-Hamiltonian has been used to model mechatronics systems and machines[26]. The port-Hamiltonian is a modelling tool where the interaction of physical systems is described as a power exchange through power ports [9, 10, 71, 101]. The mathematical models of systems using the port-Hamiltonian modelling technique can be found using bond graphs or Dirac structures [10]. A key property of the Dirac structures is that they use power-conservation interconnection ports. Another key aspect about the port-Hamiltonian is that this technique exposes the relation between energy storage, dissipation and interconnection structure. In [26], a non-linear mathematical model of a 3-phase synchronous generator is formulated using the port-Hamiltonian approach. One disadvantage of the port-Hamiltonian is that it is notably highly complex [89].

2.3 Friction models

Object on object contact and motion typically involve friction. A linear DC machine is subject to such friction. Such friction deserves analysis as it will affect the linear DC machine performance. Several friction models exist and these models

can be classified into static and dynamic friction models [46–48, 72]. Some of these friction models are the Amonton friction model based on the work done by Amonton, the Coulomb friction model which is an extension of Amonton's work done by Coulomb, the viscous friction model by Reynolds which is often combined with the model done by Coulomb, the Stribeck friction model deduced by experimental work by Stribeck, the Dahl friction model which is a dynamic friction model based on the work done by Dahl and also the LuGre friction model which addresses the limitations of the Dahl model [2, 4, 21, 55, 58, 100, 105]. Friction has three main characteristics that were identified experimentally. These characteristics are [45];

- pre-displacement
- hysteresis
- rate dependence

Most of these characteristics are found in dynamic friction models but some more than others depending on the detail of the model. Control systems focuses on two main disciples; modelling and control design. For the purpose of system modelling, it is of paramount importance to provide a comprehensive friction model. A comprehensive system model allows for a more accurate control design where the system variations and even the system stochastic behaviour are well captured and controlled. There are two major factors that affect the correctness of a systems model; these are the details of the dynamic model without friction and the accuracy of the friction model [4]. Special focus in this work will be on the accuracy of the friction model since it is assumed that the linear DC model discussed by [13] is adequate. According to [55], studies have shown the presence of force ripples especially in linear motors and also that non-linear friction is inevitable in these motors [55]. Therefore, for control purposes in practical applications friction compensation is necessary. To proceed with friction compensation, one would need to know the nature of the non-linear friction in the motor which is only achieved through formulations of detailed dynamic models. In the literature done by [55], it is established that a dynamic friction model describes friction accurately [21].

It is in the work by [21] where the dynamic friction model is discussed. For this reason, a dynamic friction model for a linear DC machine, which is an extension of existing friction models will be formulated in this work.

2.3.1 Amonton friction model

The work done by Amonton is based on findings from an investigation performed on the motion of a sliding block on a surface [2]. Amonton found that the friction force at a sliding surface is proportional to the normal load [2, 45]. He also deduced that the friction force is independent of the contact surface area. This phenomenon is known as the Amonton paradox [45]. Another key finding by Amonton is that, the size of a block as deduced from his investigation has no influence on the friction force. However, it is the normal force that determines the quantity of the friction force. Therefore, a small and big block with the same normal force experience the same friction force [2].

2.3.2 Coulomb friction model

Coulombs friction model is an extension of the work done by Amonton [4]. Literature from [58], tells us that the Coulomb friction model is also known as the Amonton-Coulomb friction model. The Coulomb friction model is described by two regimes; static friction and kinetic friction [15]. The static friction is always greater than the kinetic friction [34, 58]. The Coulomb friction model is based on the principle that the friction force is in the opposite direction to the velocity and that the friction force is also proportional to the normal force [45, 58]. Coulombs friction model is a basis for most friction models. In contrast to the relationship of the friction model with the direction of the velocity, the friction force is independent of the magnitude of the velocity [3, 45, 58]. Also, the Coulomb friction model has limitations including the dissipation nature of the friction not being demonstrated and that, the model is based solely on the roughness theory [45]. The Coulomb friction model is denoted by:

$$F = \begin{cases} F_c sgn(\dot{x}) \ \ if \ \ \dot{x} \neq 0 \\ F_{app} \ \ if \ \ \dot{x} = 0 \ \ and \ \ F_{app} < F_c \end{cases} \tag{2.7}$$

Where F is the friction force, F_c is the coulomb friction force, F_{app} is the applied force. Also, F_c is further described by [59]:

$$F_c = \mu F_N \tag{2.8}$$

Where F_N is the normal force and μ is the coulomb friction coefficient.

2.3.3 Viscous friction model

The viscous model by Reynolds is often combined with the Coulomb friction model [58]. In the viscous friction model the friction force is a function of the viscous coefficient and sliding speed [58]. The major limitation of the viscous friction model is its poor representation of friction in the absence of a lubricant [58]. The viscous friction model is described by a linear function which is proportional to the velocity [58, 67]. Viscous friction goes to zero when motion stops. In [72], a viscous friction model is found. The viscous friction model is summarized by [59]:

$$F = k_v \dot{x} \tag{2.9}$$

Where k_v is the viscous coefficient, and $\dot{x}$ is the sliding speed in [m/s].

2.3.4 Stribeck friction model

In the work done by Stribeck, the conclusions of the friction model is based on experimental observations. Stribeck found that the friction force decreases with an increase in velocity [100]. This phenomenon is called the Stribeck effect [45]. Other friction models include the rate-and-state friction models where the friction force is a function of the velocity and the state of variables [3]. According to [58],

combining the Coulomb friction model, the viscous friction model and the Stribeck effect leads to an accurate friction model. The Stribeck friction model is of the form [96]:

$$F = F_c + (F_s - F_c)e^{-\left(\left|\frac{\dot{x}}{v_s}\right|\right)^i} sgn(\dot{x}) + k_v\dot{x} \tag{2.10}$$

Where F is the friction force, F_c is the coulomb friction force, F_s is the static friction force, $\dot{x}$ is the sliding velocity, v_s is the stribeck velocity, i is an exponent and k_v is the viscous friction coefficient.

2.3.5 Dahl friction model

Dahl introduced a dynamic friction model which is able to model the pre-displacement and hysteresis [100]. In the Dahl friction model a spring-like behaviour during stiction is deduced. It is worthwhile to mention that the Dahl model is preferred for extensive hysteresis analysis [58]. The Dahl model is an extension of Coulomb with a friction lag when the direction of motion changes [58]. Also, the Dahl model is a function of the velocity and displacement [100]. The limitation of the Dahl model is its inability to capture the Stribeck effect, static friction and stick-slip motion [45, 58, 105]. The Dahl friction model is described by [22, 79]:

$$\frac{dF}{dx} = \sigma_0 \left(1 - sgn(v)\frac{F}{F_C}\right)\left|1 - sgn(v)\frac{F}{F_C}\right|^{\delta_D} \tag{2.11}$$

The equation in Eq.2.11 can further is further simplified to Eq2.12 for the purposes of making the numerical implementation easy [79].

$$\begin{cases} F &= \sigma_0 z \\ \dot{z} &= v sgn\left(1 - sgn(v)\frac{\sigma_0 z}{F_C}\right)\left|1 - sgn(v)\frac{\sigma_0 z}{F_C}\right|^{\delta_D} \end{cases} \tag{2.12}$$

Where F is the friction force in [N], v is the sliding velocity in [m/s], z is the body displacement in [m], σ_0 is the asperity stiffness in [N/m], and δ_D is the parameter that determines the shape of the stress-strain curve [75].

2.3.6 LuGre friction model

To address the limitations of the Dahl friction model, the control groups; Lund Institute of Technology and INPG Grenoble collaborated to extend the work done by Dahl. They came up with the LuGre friction model which is a short word for the two control groups. The LuGre model is an extension of the Dahl friction model incorporating the Stribeck effect. However, the LuGre model failed to address the stick-slip motion [100]. The LuGre friction model is represented by [59, 96];

$$\begin{cases} F & = \sigma_0 z + \sigma_1 \dot{z} + \sigma_2 \dot{x} \\ \dot{z} & = \dot{x} - \sigma_0 \frac{\dot{x}}{g(\dot{x})} z \\ g(\dot{x}) & = F_c + (F_s - F_c) e^{-\left(\left|\frac{\dot{x}}{v_s}\right|\right)^i} sgn(\dot{x}) \end{cases} \tag{2.13}$$

Where σ_0 is the contact stiffness, σ_1 is the viscous friction coefficient, x is the relative displacement, $g(\dot{x})$ is the Stribeck effect, F_s is the static friction force, F_c is the coulomb friction force, and F is the friction force.

From the review on friction models, it is clear that the dynamic nature of a system necessitates a dynamic friction model to capture the truest behaviour of a system. Without a dynamic friction model, a system would be exposed to variable environmental conditions whilst the friction model is stationary. This would be contradictory to the findings by Reynolds, Dahl and LuGre. The work done by the aforementioned are the advanced friction models and they have been found to mimic friction in real systems.

2.4 Control algorithms

2.4.1 Linear control algorithms

Linear control methods such as the negative state feedback exists. The negative state feedback will be discussed in the section that follows.

2.4.1.1 Negative state feedback based on pole placement

Linear control techniques exist in abundance. Most are negative feedback based, a typical approach is the negative state feedback. The negative state feedback based on pole placement is a control technique to consider [1, 27, 53, 68, 83, 103]. The goal of the control algorithm is to determine the control input capable of driving the states of a plant to zero for a regulation problem. This control technique requires that the closed-loop poles of the system are selected to meet the desired performance criteria [7]. The poles determine the settling time, the rise time and percentage overshoot [7]. The control follows a control law which is specified by a feedback gain matrix [1, 27]. The feedback gain matrix is obtained based on the desired closed-loop poles [7].

2.4.1.2 Linear quadratic regulator

The Linear Quadratic Regulator (LQR) is another controller to be considered. This controller is based on optimal control law for a linear system where the control objective is to minimize a quadratic performance index [7]. The control law is also obtained by computing Algebraic Riccati equations [69, 81]. The goal is to determine a gain feedback matrix that drives the states to zero. The LQR is based on a quadratic cost function which aims to minimize the output error while using a reasonable control input. The cost function is used to quantify the performance of the control system. The LQR is used in many applications due to its flexibility in selecting a cost function. However, the LQR is also limited to initial test conditions and requires the measurement of the entire state during implementation. Moreover, this controller assumes linear systems. The limitation of this approach is its application to strictly linear state models. A more general approach would be on linear quadratic control. A challenge on this approach is to address input constraints as well as the singularities that often appear [54].

Other optimal controllers include the bang-bang controller and the linear quadratic Gaussian controller which has additive white Gaussian noise [52, 56, 74].

2.4.2 Non-linear control

Nonlinear control methods can be used to control nonlinear systems. It is known that linear controllers have a small range operation [5, 92]. This means that the accuracy of the control decreases as the range increases. While nonlinear controllers operate accurate over a wide range, nonlinear controllers also account for the fact that physical system are inherently nonlinear. Nonlinear control techniques ensure that the control system maintains stability when exposed to the stochastic nature of practical systems.

2.4.2.1 Hamiltonian based optimal control

Th Hamiltonian based optimal control is a nonlinear, multiple input, multiple output control algorithm. One of the applications of the control technique is found in the work done by [6, 41, 99]. The Hamiltonian based optimal control algorithm entails defining the control problem which is followed by computing the performance index. The Hamiltonian associated with the control problem of the system is then computed. The Hamiltonian is used to determine the adjoint of the system. The transversality condition follows [5, 84]. The switching function is also determined. The time derivative of the switching function is evaluated to find the singular control [99]. The advantage of the Hamiltonian based controller would be its robustness.

2.5 Summary

From the brief literature provided, the advantages of the Lagrange approach have been highlighted. As such, the approach will be adopted in this study. The novelty of this study is that, there exists no magnetic field based Lagrange model of a machine The key focus in this study is on a linear DC machine without using an equivalent circuit approach. The properties of the Lagrange modelling technique will also be investigated. Also a detailed friction model is important in that it

results in a more comprehensive model. Control has been motivated for, linear negative state feedback and non-linear optimal control.

CHAPTER 3

Linear DC Machine Modelling

3.1 Overview

Chapter 3 introduces the dynamic model of a linear DC machine formulated using energy based approach, i.e. Lagrange analysis. The results of the dynamic model are compared with results obtained using classical physics laws i.e. Newtons laws, Kirchhoff's laws and Faraday's laws. Sections discussing the Lagrange analysis, generalized coordinates, holonomic and non-holonomic constraints are presented. The aforementioned sections are necessary in that they are the building blocks for understanding the Lagrange analysis before the Lagrange analysis is applied on a linear DC machine. The results of the linear DC machine are also presented and discussed.

3.2 Linear DC machine in the mining sector

In the mining sector, underground mine locomotives are a form of transportation for coal, ore and also materials in underground mines [80]. There are several types of underground locomotives such as battery locomotives, diesel locomotives and electric locomotives [24, 31, 80]. Battery locomotives have been found to have an advantage of lack of emission of harmful gases compared to diesel locomotives [80]. Nonetheless, mine locomotives generally offer an advantage compared to rope haul and the conveyor belt [80]. According to [88], underground working conditions include hard physical work and also, the conditions underground automatically expose mine workers to various health hazards due to environmental

conditions [88]. The environmental conditions in an underground mine include humid, dusty and noisy conditions - due to the nature of the work which involves drilling through rocks. Introducing autonomous machinery in mining is of great benefit not only to the mine worker but also to the company. For the mine worker autonomous machinery would mean less physical work and it would also improve safety significantly. In fact, fatal accidents would improve by 80% while from the 80%, fatal accidents would improve by 50% [44]. For the mining company, autonomous machinery would mean transport productivity, and the study in [44], estimated an improvement of 6% - 17%. Although the study in [44] was done years ago, its still remains that the mine workers safety and the mine transport productivity would improve although the statistics would differ.

This Chapter advocates for the modelling of a linear DC machine used for powering a mine locomotive. The control of a linear DC machine used to power a mine locomotive is found in Chapter 4. The suspension system of the mine locomotive will not be modelled since the linear DC machine for locomotion is the area of interest. The objective is to use energy-based modelling to model a linear DC machine and also control it. The result found using energy-based techniques, particularly the Lagrange should be the same as the result one would obtain using physics laws as discussed by [13]. It is desirable to achieve a speed of typically 3 m/s for a loaded locomotive, this is the speed for practical systems. Also, the mine locomotive should be autonomous. A key feature that could be added on the mine locomotive would be a sensor, that is used to track the surface of the the mining track so that the necessary control is performed to ensure the speed of the train is maintained. The mine locomotive could also have a positioning system used to track the distance travelled so that the locomotive knows the location where it is supposed to stop.

3.3 Existing electromagnetic linear DC machine analysis

The following analysis summarizes the linear DC machine modelling and analysis by [13]. The electromagnetic circuit analysis by [13] is based on laws of physics

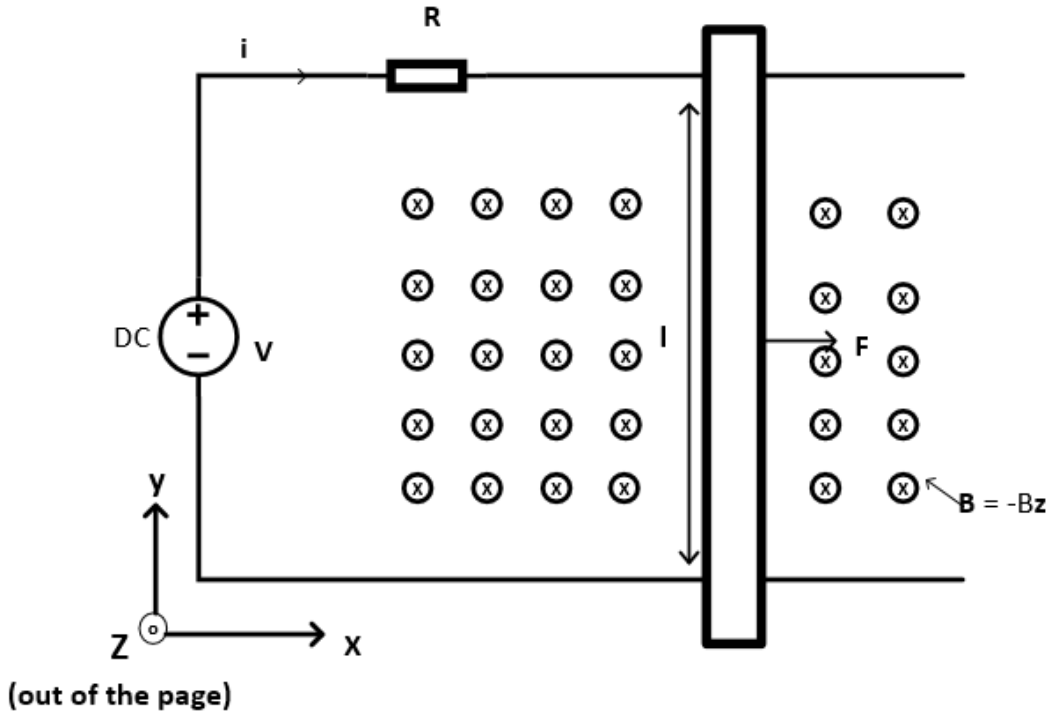

FIGURE 3.1: Linear DC machine [13]

in that, the Lorentz law, Faraday's law, Newton's law and Kirchhoff's law are applied on an elementary machine, the linear DC machine [13]. For this analysis, consider a linear DC machine as shown in figure 3.1. The machine comprises a voltage source V, a resistor R due to copper losses, and a sliding bar placed on a pair of rails. It should be noted that the bar can only move in the $\hat{\boldsymbol{x}}$ direction. Also, the electrical circuit described is placed in a constant magnetic field $\boldsymbol{B}$ in the $\hat{\boldsymbol{z}}$ direction where the magnetic field is associated with the flux density and the magnetic field takes the direction of the magnetic lines. Magnetic field notation is such that 'x' points into the page and 'o' points out of the page. The current flowing along the circuit is denoted by 'i' and the length $\boldsymbol{l}$ of the bar is in the $\hat{\boldsymbol{y}}$ direction. B is the magnitude of the magnetic field.

Notation: $\hat{\boldsymbol{x}}$ is a unit vector to the right of the page, $\hat{\boldsymbol{y}}$ is a unit vector to the top of the page and $\hat{\boldsymbol{z}}$ is a unit vector out of the page.

Notation: If a vector is represented in bold face, $\hat{\boldsymbol{z}}$ represents the unit vector in the direction of $\boldsymbol{z}$. The positive F represents the magnitude of $\boldsymbol{F}$. F is a force experienced by the bar.

When a current flows in the circuit, the bar experiences a Lorentz force which is described by:

$$\boldsymbol{F_L} = i\boldsymbol{l} \times \boldsymbol{B} \tag{3.1}$$

Where $\boldsymbol{F_L}$ is the Lorentz force. For the linear DC machine shown in figure 3.1, the resultant force is expressed by:

$$\begin{aligned} \boldsymbol{F_L} &= il(-\hat{\boldsymbol{y}}) \times B(-\hat{\boldsymbol{z}}) \\ &= ilB\hat{\boldsymbol{x}} \end{aligned} \tag{3.2}$$

Using Kirchhoff's law, the current flowing along the circuit is found and it is described by;

$$i = \frac{V - Bl\dot{x}}{R} \tag{3.3}$$

$Bl\dot{x}$ is the back emf as used by Chiasson and the back emf is a result obtained by Chiasson after applying Faraday's law [13]. Where $\dot{x}$ is the velocity of the bar. The current is dynamic in that it changes as the bar accelerates. The motion of the bar is found using Newton's law where including an applied force as used by [12] yields:

$$m_l\ddot{x} - ilB = F_{app} - b\dot{x} \tag{3.4}$$

where m_l is the mass of the bar, F_{app} is an external force applied to the bar and b is the coefficient of the rail friction of the sliding bar.

This brief summary is the modelling and analysis of a linear DC machine as modelled by [13].

3.4 Lagrange electromagnetic linear DC machine analysis

The Lagrange is applied on an electromagnetic circuit where the key contribution is the magnetic field based Lagrange analysis. The Lagrange analysis is performed on a linear DC machine under the same assumptions as Chiasson's linear DC

machine which are typically ideal electromagnetic conditions such as eddy current losses, no saturation, perfectly constant B. The objective of this study is to obtain Chiasson's model to demonstrate the correctness of the field based Lagrange analysis. The Lagrange analysis is commonly known for energy based modeling of RLC circuits, AC machines [19, 20]. It is desirable that models must satisfy reciprocity conditions to be physically acceptable hence, the Lagrange, energy based approach [19]. is one way of satisfying these conditions. Therefore, the Lagrange analysis is preferred due to its merits. The Lagrange analysis steps can be summarized as follows:

- Identify the kinetic energy
- Identify the potential energy
- Identify the dissipation power
- Perform degree of freedom and holonomic constraint analysis
- Compute the Lagrange equation
- Evaluate the Euler-Lagrange
- Formulate the state space model

For the Chiasson linear DC machine, the kinetic energy is due to the motion of the bar, the dissipation power is due to copper losses and friction losses whilst the potential energy is due to the magnetic field [16]. The potential energy is due to the magnetic field because the magnetic field is the primary field in that it actuates the electromagnetic circuit without the help of the voltage source.

3.4.1 Generalized coordinates

Generalized coordinates are independent coordinates describing the position of a particle P or the position of a system of N particles, subject to constraints; such

as the particle/s moving along a circular wire or even a rigid body moving along a slope [94, 102]. The generalized coordinates are described by [94];

$$\boldsymbol{r} = (r_1, r_2, ..., r_n) \tag{3.5}$$

Where n is the number of generalized coordinates. n is also the number of degrees of freedom. As such, a particle/s in the Euclidean space is described by polar coordinates thus the generalized coordinates in a Euclidean space are (x,y,z) [66]. For a cylinder and a sphere, the generalized coordinates are described by (ρ,ϕ,z) and (r, θ, ϕ), respectively. The time derivative of the generalized coordinates is known as the generalized velocity and the generalized velocity is described by;

$$\dot{\boldsymbol{r}} = (\dot{r_1}, \dot{r_2}, ..., \dot{r_n}) \tag{3.6}$$

3.4.2 Holonomic and non-holonomic constraints

Many practical systems have various constraints restricting the motion of a particle or system of particles. For instance, the particle could be restricted to move along a curved surface, a paraboloid or even a flat surface. If all the constraints imposed on the particle are dependent on the generalized coordinates and time, then the constraints are known as holonomic constraints [94]. The holonomic constraints take the form [94]:

$$\Omega(\boldsymbol{r_1}, \boldsymbol{r_2}, ..., \boldsymbol{r_N}, t) = 0 \tag{3.7}$$

Where $\boldsymbol{r}$ is the position vector and t is the time. If the constraints are independent of either the generalized coordinates or time, or even both the generalized coordinates and time then, the constraints are non-holonomic.

3.4.3 Degrees of freedom

The number of degrees of freedom of a system is associated with the number of generalized coordinates. For N particles with n coordinates, the number of degrees

of freedom is:

$$DOF = nN \tag{3.8}$$

Where DOF is the number of degrees of freedom, N is the number of particles and n is the number of coordinates describing the position of the particle. Suppose the particles are constrained by a total number of k holonomic constraints, then:

$$DOF = nN - k \tag{3.9}$$

For example:
A particle in a Euclidean space with the coordinates (x,y,z) has:

$$DOF = 3 \tag{3.10}$$

Imposing constraints where the particle is restricted to only move along the x-axis would mean that $y = 0$, and $z = 0$. This means that there are two holonomic constraints in the system of a particle moving along a Euclidean space, therefore:

$$DOF = 3 - 2 \tag{3.11}$$

3.4.4 Identifying energies

The Lagrange standard notation used in [94, 102] is utilized for the purpose of explaining the Lagrange formulation. Hence, the following is a summary of the theoretical description provided in [94, 102]. The kinetic energy and potential energy are denoted by T and U respectively. Where both types of energies are a function of generalized coordinates and generalized velocities. It should be noted that each generalized coordinate has a force associated to it.

The kinetic and potential energy are generally described by [61];

$$T(t, r_1, r_2, ..., r_n, \dot{r_1}, \dot{r_2}, ..., \dot{r_n}) \tag{3.12}$$

$$U(t, r_1, r_2, ..., r_n) \tag{3.13}$$

Where T is the kinetic energy and U is the potential energy. Both energies are a function of generalized coordinates. The above Lagrange formulation is the summary of the Lagrange formulation as presented in [102].

3.4.5 Computing the Lagrange equation

The Lagrange equation is the kinetic energy less the potential energy. This is shown in the equation Eq.3.14.

$$L = T(t, r_1, r_2, ..., r_n, \dot{r_1}, \dot{r_2}, ..., \dot{r_n}) - U(t, r_1, r_2, ..., r_n) \tag{3.14}$$

Where L is the Lagrange equation. It can be seen that the Lagrange equation is also a function of generalized coordinates and generalized velocities.

3.4.6 Evaluate the Euler-Lagrange

The Euler-Lagrange is further evaluated. For a loss-less system with a zero generalized force, the Euler-Lagrange is given by;

$$\frac{d}{dt}\frac{\partial L}{\partial \dot{r}} - \frac{\partial L}{\partial r} = 0 \tag{3.15}$$

However, the Euler-Lagrange is expressed as a function of n independent generalized coordinates and generalized velocities. Therefore, there are n Euler-Lagrange equations for a system with n generalized coordinates. For cases where a generalized force is applied to the system, the Euler-Lagrange has the form;

$$\frac{d}{dt}\frac{\partial L}{\partial \dot{r}} - \frac{\partial L}{\partial r} = Q \tag{3.16}$$

The generalized force Q is the input applied to the system and it can be a voltage in electric circuits or even a torque in mechanical systems. Now, consider a system

with losses, such a system is described by the equation that follows;

$$\frac{d}{dt}\frac{\partial L}{\partial \dot{r}} - \frac{\partial L}{\partial r} = Q - \frac{\partial P}{\partial \dot{r}} \tag{3.17}$$

It follows that P is the dissipation power function. The dissipation function may result in either of the three types of systems; under-damped system, critically damped system or the over-damped system. The dissipation function is the force that acts in the opposite direction to the motion of a system. The dissipation function is also non-conservative because it is dependent on the path of an object. It is common that a system oscillates when a disturbance is applied to the system. The dissipation force influences the behaviour of system in that the dissipation force attempts to stop the oscillations. In cases where there is no dissipation force, by law of conservation of energy, the system oscillates infinitely. For low losses, the system oscillates. However, the dissipation force acting on the system will result in a system that decays exponentially so that the system can be forced back to equilibrium. Now, considering a system with a high dissipation function, the system will not oscillate. However, this does not mean that the system reaches its equilibrium fast. A system of this nature is over-damped. A system with not too low or high losses does not oscillate and it reaches the equilibrium fast. This means that a critically-damped system is achieved.

3.4.7 Lagrange potential energy

The purpose of this section is to explain the Lagrange analysis on a simpler problem. Also, the gravitational and the electromagnetic field explanation will be extended. This because the fields have to be thoroughly understood before proceeding with the energy based analysis of a linear DC machine. The goal is to be able to relate the potential energy and kinetic energy of a simple pendulum with the Lagrange kinetic and Lagrange potential energy of the linear DC machine.

The Lagrange analysis demands that the Lagrange kinetic energy, Lagrange potential energy and dissipation power are identified. The potential energy of a simple pendulum is due to the gravitational force exerted on the ball of the pendulum to move the ball from one position to another position. The ball may exist in a gravitational field and therefore experiences a gravitational force.

For a linear DC machine where an electromagnetic circuit is placed in a magnetic field, there may be two fields, namely; magnetic field and gravitational field. The magnetic field is analogous to the gravitational field of the pendulum in a linear DC machine. The magnetic field is also the field of concern. Therefore, the potential energy of the magnetic circuit is due to the magnetic force acting on the bar. Table 3.1 summarizes some of the parameters equivalent to one another for a pendulum and linear DC machine.

TABLE 3.1: Analogous Lagrange potential energy parameters between a pendulum and linear DC machine

	Pendulum	Linear DC machine
Field type	Gravitational field	Magnetic field
Other fields	-	Load may be in gravitational field (bar)
Force	Gravitational force (F_g)	Lorentz force (F_L)
Potential energy	$\int_{y_1}^{y_2} F_g \hat{\boldsymbol{y}} \cdot d\boldsymbol{l}$	$\int_{x_1}^{x_2} F_L \hat{\boldsymbol{x}} \cdot d\boldsymbol{l}$

3.4.8 Lagrange kinetic energy

When a force is applied on a simple pendulum that has potential energy, the ball starts moving. The energy the ball possesses due to motion when an external force is applied is called the kinetic energy. Similarly to the pendulum, when the Lorentz force is applied to the bar, the bar starts moving. The bar is the load, therefore it may exist in a gravitational field. The Lorentz force applied to the bar is the external force that initiates the motion of the bar. The energy the bar possesses due to motion is called the kinetic energy of the bar. Table 3.2

summarizes some of the parameters analogous to one another for a pendulum and a linear DC machine.

TABLE 3.2: Analogous Lagrange kinetic energy parameters between a pendulum and linear DC machine

	Pendulum	Linear DC machine
Field type	Gravitational field	Magnetic field
Other fields	-	Load may be in gravitational field (bar)
Force	External force	External force
kinetic energy	$\frac{1}{2}m_p v^2$ (ball)	$\frac{1}{2}m_b v^2$ (bar)

3.4.9 Lagrange analysis of a simple pendulum

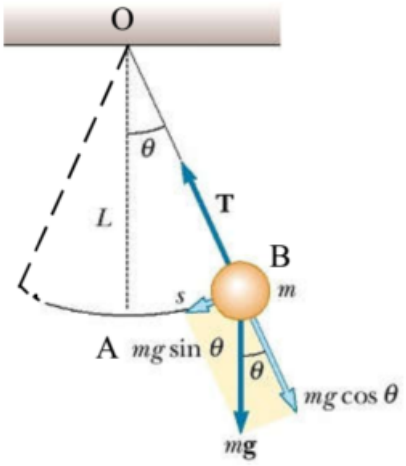

FIGURE 3.2: Simple pendulum [43]

Now performing the Lagrange analysis on a simple pendulum, the Lagrange kinetic energy of the pendulum is described by:

$$T = \frac{1}{2}mL^2\dot{\theta}^2 \tag{3.18}$$

The height of the pendulum is expressed by:

$$y = L(1 - cos(\theta)) \tag{3.19}$$

Therefore the Lagrange potential energy against gravity is described by:

$$U = \int_0^y mg\hat{\boldsymbol{y}} \cdot d\boldsymbol{l} \tag{3.20}$$

Substituting y yields:

$$U = mgL(1 - cos(\theta)) \tag{3.21}$$

To avoid confusing the Lagrangian equation with the length of the pendulum pivot described by L, the Lagrangian will be represented by Γ, where the equation describing the Lagrange is given:

$$\Gamma = T - U \tag{3.22}$$

$$= \frac{1}{2}mL^2\dot{\theta}^2 - mgL(1 - cos(\theta))$$

Where Γ is the Lagrange equation, T is the Lagrange kinetic energy and U is the Lagrange potential energy. Assuming there is no energy losses, evaluating the Euler Lagrange:

$$\frac{d}{dt}\frac{\partial\Gamma}{\partial\dot{\theta}} - \frac{\partial\Gamma}{\partial\theta} = Q - \frac{\partial P}{\partial\dot{\theta}} \tag{3.23}$$

Where Q is the generalized force $\dot{\theta}$ is the time derivative of the angle. Evaluating the Euler-Lagrange yields:

$$\boxed{\ddot{\theta} + \frac{g}{l}sin(\theta) = 0} \tag{3.24}$$

The key result in this analysis is the equation describing the behaviour of the simple pendulum.

3.4.10 Lagrange analysis of a linear DC machine

Standard notation shall be used for analysis e.g. as is done by [94]. L is the Lagrange equation, T is the kinetic energy, and U is the potential energy. This allows for the results of this work to follow the standard use by other works. The kinetic energy of the bar is:

$$T_r = \frac{1}{2} m_l \dot{x}^2 \tag{3.25}$$

The potential energy of the bar in the presence of the magnetic field is given by [37]:

$$U_M = \int_0^x -\dot{q} l B \hat{\boldsymbol{x}} \cdot d\boldsymbol{l} \tag{3.26}$$

The potential energy is the path integral of the Lorentz force where $\dot{q}$ is the current and U_M is the potential energy due to the magnetic field. The dissipation power is described by [76, 95, 102] :

$$P_1 = \frac{1}{2} R \dot{q}^2 \tag{3.27}$$

$$P_2 = \frac{1}{2} b \dot{x}^2 \tag{3.28}$$

Where R is the resistance of the electrical circuit and b is the viscous friction coefficient. The total dissipative power is given by;

$$P = \frac{1}{2} R \dot{q}^2 + \frac{1}{2} b \dot{x}^2 \tag{3.29}$$

The Lagrange equation is given by;

$$L(x, \dot{x}, q, \dot{q}) = \frac{1}{2} m \dot{x}^2 + \dot{q} l B x \tag{3.30}$$

Where x and q are the generalized coordinates and $\dot{x}$ and $\dot{q}$ are the generalized velocities. As described in Eq.3.14 - 3.17 after obtaining Eq. 3.30. The key step of the Lagrange analysis is to perform the Euler-Lagrange.

Evaluating the Euler-Lagrange with respect to x:

$$\frac{d}{dt}\frac{\partial L}{\partial \dot{x}} - \frac{\partial L}{\partial x} = F - \frac{\partial}{\partial \dot{x}}(\frac{1}{2}R\dot{q}^2 + \frac{1}{2}b\dot{x}^2) \tag{3.31}$$

Where F is the applied force, yields:

$$m_l\ddot{x} - \dot{q}lB = F - b\dot{x} \tag{3.32}$$

Whilst evaluating the Euler-Lagrange with respect to the generalized coordinate q:

$$\frac{d}{dt}\frac{\partial L}{\partial \dot{q}} - \frac{\partial L}{\partial q} = V - \frac{\partial}{\partial \dot{q}}(\frac{1}{2}R\dot{q}^2 + \frac{1}{2}b\dot{x}^2) \tag{3.33}$$

Where V is the input voltage, yields;

$$\dot{q} = \frac{1}{R}(V - lB\dot{x}) \tag{3.34}$$

Since $\dot{q}$ is the current, the dynamic model of the linear DC can be represented as:

$$\boxed{m_l\ddot{x} - ilB = F - b\dot{x}} \tag{3.35}$$

$$\boxed{i = \frac{1}{R}(V - lB\dot{x})} \tag{3.36}$$

3.4.11 Equivalent of electromagnetic modelling

At this juncture it is worthwhile highlighting the key results obtained so far. The same model i.e. Eq.3.3 - 3.4 obtained by Chiasson in modelling the linear DC machine has been obtained by Lagrange analysis i.e. Eq.3.35 - 3.36. With the same assumptions as [13], where the assumptions are;

- Constant magnetic field.
- No hysteresis losses.

- The self-inductance is assumed to be zero.
- No saturation of the magnetic field when the current increases.

The Lagrange analysis result is the same as Chiasson's results that were obtained using Newtonian and Kirchoff's laws. This highlights the correctness of the Lagrange analysis.

3.4.12 Linear DC machine state space representation

Lagrange physical equations typically allow for state space model equations to be obtained as below. Further state space trajectory can be performed to accomplish system performance analysis. When we let $x_1 = \dot{x}$, and $\dot{x_2} = \dot{q}$, $V = v$ and $F = u$, the state space model is found to be;

$$\begin{aligned} \dot{x_1} &= -\frac{1}{m_l}(\frac{B^2l^2}{R} + b)x_1 + \frac{lB}{m_lR}v + \frac{u}{m_l} \\ \dot{x_2} &= \frac{1}{R}(v - lBx_1) \end{aligned} \tag{3.37}$$

3.5 Linear DC machine results

Now that the linear DC machine model is formulate, the next logical would be to analyze the behaviour of the linear DC machine. The behaviour of the linear DC machine is shown by means of figures where Simulink is used to plot the results of the linear DC machine. Using the linear DC machine parameters found in table 3.3, the results of the linear DC machine are plotted and discussed. Arbitrary parameters values are chosen for illustration purposes. The aim is to illustrate the behaviour of the linear DC under three cases where;

- A force is applied on the bar in the direction of motion of the bar.
- A force is applied on the bar in the direction opposing the motion of the bar.
- No external force applied on the bar.

TABLE 3.3: Linear DC parameters

locomotive mass (m_l)	0.25 kg
magnetic field (B)	0.5 T
rail friction coefficient (b)	0.05
rail separation length (l)	0.6 m
resistor (R)	100 $m\Omega$
input voltage (v)	1 V, 3 V, 5 V
applied force (u)	1 N, 3 N, 5 N

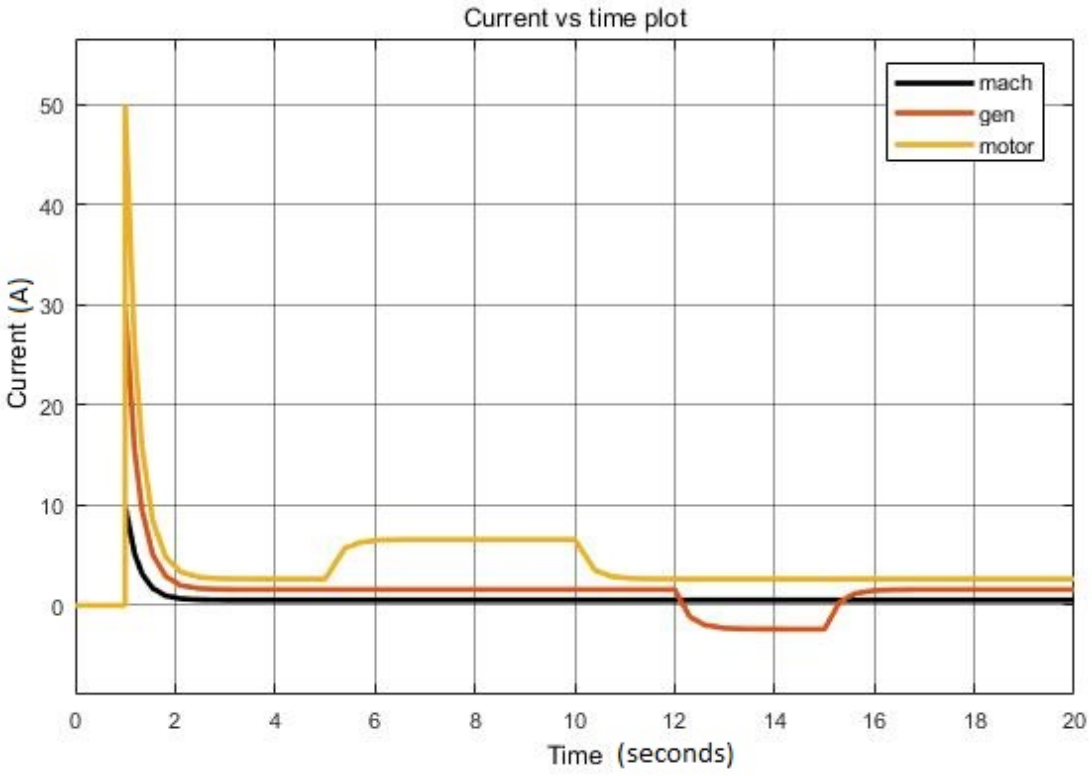

FIGURE 3.3: Linear DC machine current dynamics

From the results, it is deduced that when there is no current flowing in the electromagnetic circuit the bar is not moving. This is shown at $t = 0$ to $t = 1s$. When current starts flowing, it starts at its maximum current because electromagnetic induction does not happen instantaneously. As the current continues flowing the bar accelerates until the steady state velocity is reached where the current is also at steady state. This shown by the black lines. From fig.3.3 and fig.3.4, it is deduced that the current decreases gradually with an increase in velocity. This is due to electromagnetic induction [13].

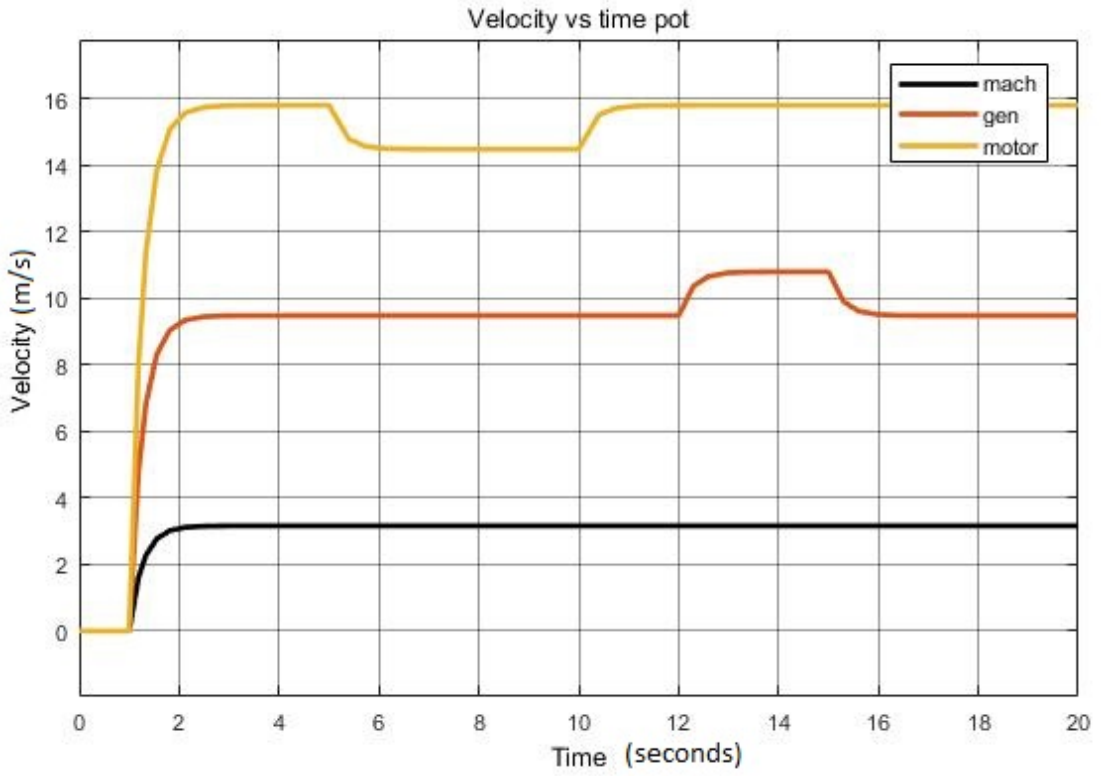

FIGURE 3.4: Linear DC machine velocity dynamics

Now consider a case where a force is applied in the direction of motion of the bar. This case happens at $t = 12s$ to $t = 15s$. The results for this case are such that when the velocity increases from steady state current ($t = 12s$ to $t = 15s$) a reverse current is obtained. The machine is operating as a ***generator***. When the force is applied in a direction opposing the direction of motion of the bar when the bar is at steady-state, the velocity decreases resulting in the current increasing. This case happens between $t = 5s$ to $t = 10s$. The machine is behaving as a ***motor***. A key result is that, the results for the linear DC machine are the same as the results obtained by [11, 12].

The power curve for an input voltage of 1 V, 3 V and 5 V, respectively, is also shown in fig.3.5. The power as shown on the aforementioned figure starts from 0 W and increases until it reaches a peak power of 2 W, 22 W, and 62 W, for the voltage of 1 V, 3 V and 5 V, respectively. Thereafter, the power decreases gradually. When an external force is applied in the direction opposing the bar of the linear DC machine at steady state, the power increases. This is shown by

the pronounced region between 5 s - 10 s. When an external force is applied in the direction of the bar of the linear DC machine at steady state, the linear DC machine supplies power. The aforementioned is shown by a pronounced region between 12 s - 15 s.

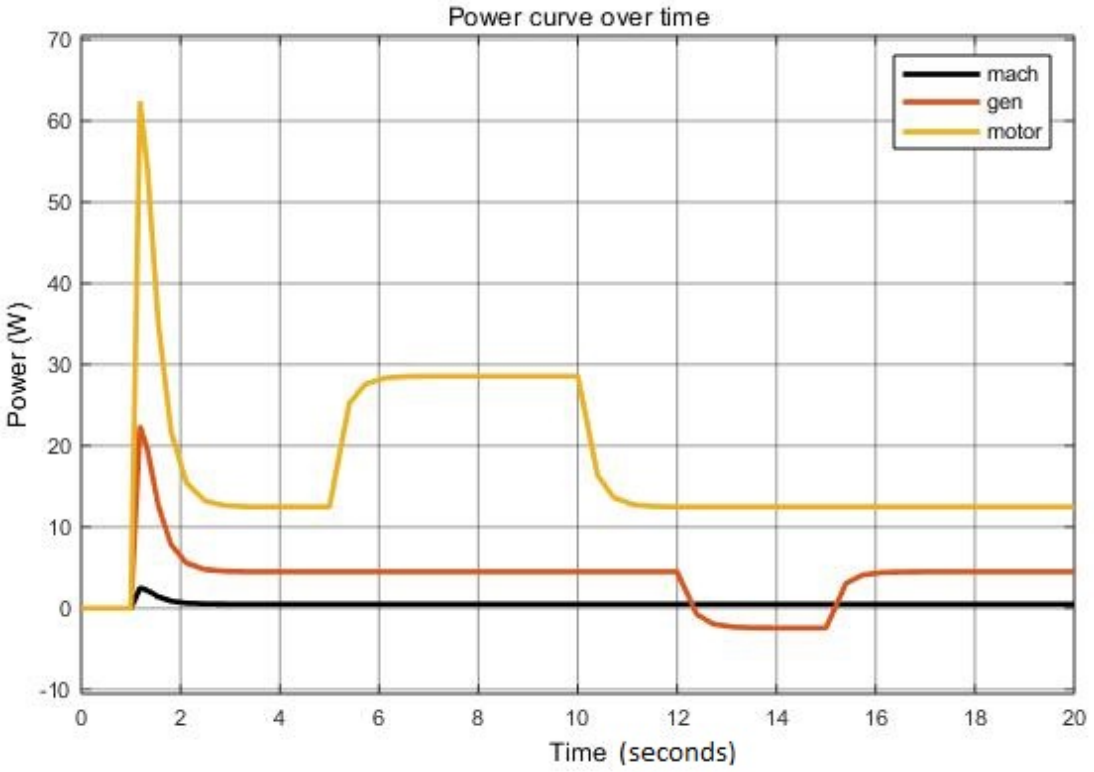

FIGURE 3.5: Power curve

3.5.1 Effects of using different inputs

From the results, it is clear that the a high input voltage results in a faster velocity. The opposite is true for a low voltage where the velocity is slow. Different input voltage and applied forces are used so that the results are well presented and such that the effects of the different inputs can be clearly seen.

3.6 Research contribution

A magnetic field based Lagrange analysis is performed on a linear DC machine. The novelty in this study lies in the fact that the model analyzed is not based on equivalent circuits comprising inductors and capacitors. Instead, the model is based on a raw magnetic field. The magnetic field based Lagrange analysis in Sec.3.4.10 is also shown to produce the same equations as existing modelling methods found in Sec.3.3.

3.7 Summary

The Lagrange analysis has been shown to generate the same physical model equations as is obtained by electromagnetic analysis of the same linear machine as modelled by [13]. Therefore Lagrange analysis is a viable and verified modelling approach for physical modelling of a linear DC machine. Consequently linear DC machine performance analysis is demonstrated by extending the Lagrange physical model to a state space model and performance analysis through state space trajectory formulation.

CHAPTER 4

Speed Control of a Linear DC Machine

4.1 Overview

Chapter 4 details the design of the negative state feedback control algorithm based on pole placement technique. The pole placement technique allows for the use of state space techniques to determine the closed loop poles of a system. The pole placement technique can be used for multiple input, multiple output systems. The negative state feedback control algorithm is used to control the speed of the locomotive formulated in Chapter 3. The controllability and observability test for the locomotive are performed and the performance specifications are selected. The closed loop poles are chosen based on the performance criteria, and the closed loop poles are used to determine the gain matrix. A summary of the control algorithm used is shown in fig.4.1.

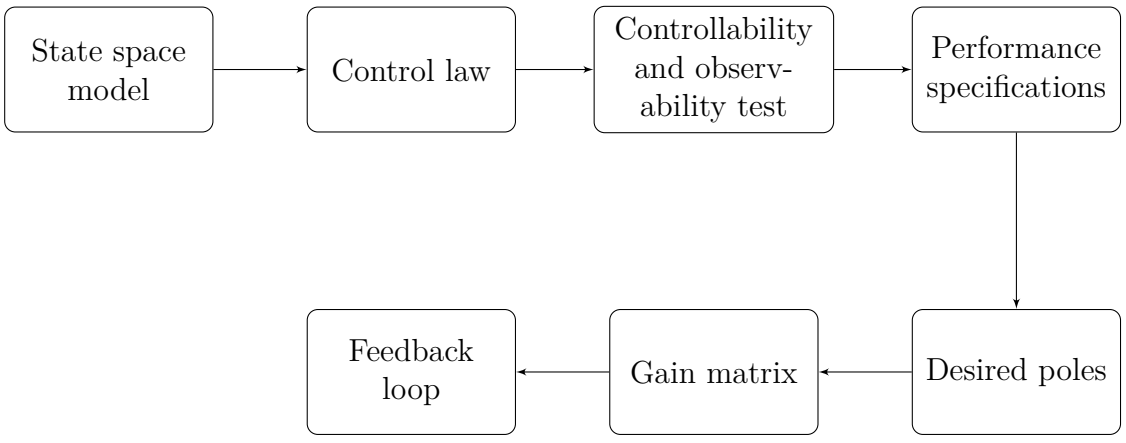

FIGURE 4.1: State feedback control based on pole placement algorithm

4.1.1 Speed control

The linear DC machine is used for various applications where the speed demand, depending on the application, vary. For instance, the magnetic-levitation train does not have the same speed as a conveyor-belt. The magnetic-levitation train is designed such that it has a very high speed whereas, the conveyor-belt moves slow. It is for this reason that speed control is necessary to address application challenges and also for the linear DC machine performance to be as desired.

4.2 State feedback based on pole placement

The control algorithm used to control the speed of the linear DC machine is based on the pole placement algorithm [53, 68, 83, 103]. Before proceeding with the control design, it should be mentioned that the plant is the linear DC machine. The mathematical model of the linear DC machine to be used in this chapter was formulated in previous chapter, chapter 3.

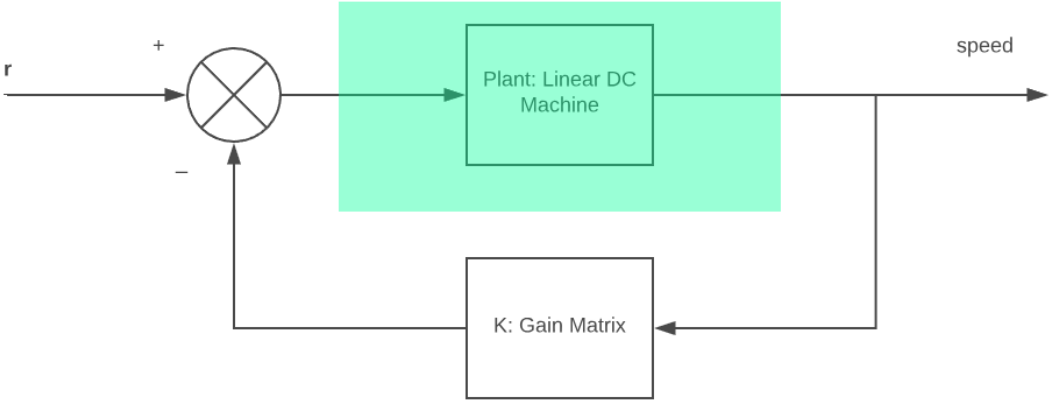

FIGURE 4.2: Controlled linear DC machine

The state-feedback using pole placement control algorithm is used to improve the performance of the linear DC machine. By performance, this refers to improving the settling time, and overshoot of the linear DC machine. The control algorithm also allows that the linear DC machine operates at the desired speed. The control design can only proceed after a controllability and observability test are performed

and the system is both controllable and observable. According to reference [7, 51] a system is controllable if a state $x(t_0)$ can be transferred to $x(t_f)$ and a system is observable if at time t_0, the state $x(t_0)$ can be determined from the output. The observability and controllability test demand the following [7]:

- a controllability and observability matrix
- the controllability and observability matrices must be of full rank

For a system with the state space equation

$$\begin{aligned} \dot{\boldsymbol{x}} &= \boldsymbol{A}\boldsymbol{x} + \boldsymbol{B}\boldsymbol{f} \\ \boldsymbol{y}(t) &= \boldsymbol{C}\boldsymbol{x} + \boldsymbol{D}\boldsymbol{f} \end{aligned} \tag{4.1}$$

and the control law is described by [7]:

$$\boldsymbol{f} = \boldsymbol{r} - \boldsymbol{K}\boldsymbol{x} \tag{4.2}$$

Where K is the state-feedback gain matrix, r is the reference input, f is the control law.

Prior to control design, it is required that a test is performed to check whether the system can be controlled and observed. An uncontrollable system does not require a controller to be design because the system cannot be controlled. When a system cannot be observed, the states cannot be measured. The controllability and observability matrix are described by [82]:

$$\boldsymbol{C} = \begin{bmatrix} \boldsymbol{B} & \boldsymbol{AB} & \dots & \boldsymbol{A^{n-1}B} \end{bmatrix} \tag{4.3}$$

$$\boldsymbol{O} = \begin{bmatrix} \boldsymbol{C} & \boldsymbol{CA} & \dots \boldsymbol{CA^{n-1}} \end{bmatrix}^T \tag{4.4}$$

Where $\boldsymbol{C}$ is the controllability matrix and $\boldsymbol{O}$ is the observability matrix. The state equation described below (formulated in chapter3) is used to determine the controllability and observability:

$$\begin{aligned} \dot{x_1} &= -\frac{1}{m_l}(\frac{B^2l^2}{R} + b)x_1 + \frac{lB}{m_lR}v + \frac{u}{m_l} \\ \dot{x_2} &= \frac{1}{R}(v - lBx_1) \end{aligned} \tag{4.5}$$

$$\boldsymbol{y} = [1 \quad 1]\boldsymbol{x} \tag{4.6}$$

Where the output is the velocity and the current.

Using the equations Eq.4.5 and Eq.4.6 into Eq.4.3 and Eq.4.4, the controllability matrix is found to have a rank of 2, i.e full rank. The observability matrix is also found to have a a rank of 2 (full rank).

4.3 Performance specifications

for the linear DC machine both matrices are found to have full rank. Therefore, the control design can proceed. For control design purposes, a second order system is assumed because the nature of a second order equation allows for the settling time, rise time and damping ratio to be determined. The aforementioned parameters are necessary to be able to realize the desired linear DC machine performance. The performance specifications of the linear DC machine is chosen such that the speed and percentage overshoot of the linear DC machine are suitable for mining applications. The specifications are presented in table 4.1.

TABLE 4.1: Linear DC performance specifications

Settling time (t_s)	0.6s
Percentage overshoot (PO)	5%
ζ	0.69
Reference velocity	3m/s
ω_n	9.4rad/s
Settling time tolerance band	$\pm$2%

4.4 Control design

Where for a chosen PO, the damping ratio is found using [7]:

$$\zeta = \sqrt{\frac{ln(\frac{PO}{100}^2}{\pi^2 + \frac{PO}{100}^2}} \tag{4.7}$$

For a settling time tolerance band of $\pm$2%, and a chosen settling time of 0.6s, the natural frequency is [7]:

$$\omega_n = \frac{-ln(\frac{2}{100})}{\zeta t_s} \tag{4.8}$$

the desired closed-loop poles are determined using a second order equation and pole placement method [7]:

$$s^2 + 2\zeta\omega_n s + \omega_n^2 \tag{4.9}$$

Now from Eq.4.9, the poles, $\boldsymbol{p}$, are found using Eq.4.10;

$$p = \frac{-b \pm \sqrt{b^2 - 4ac}}{2a} \tag{4.10}$$

Which yields

$$p = \frac{-2\zeta \pm \sqrt{(2\zeta\omega_n)^2 - 4\omega_n^2}}{2} \tag{4.11}$$

Therefore, the poles are found using the above equation to be [7];

$$\boldsymbol{p} = \begin{bmatrix} -6.5200 + 6.8375i & -6.5200 - 6.8375i \end{bmatrix}^T \tag{4.12}$$

Where K is the gain matrix, and $\boldsymbol{p}$ the poles. Substituting the control law Eq.4.2 into Eq.4.1, yields:

$$\dot{\boldsymbol{x}} = \boldsymbol{A}\boldsymbol{x} + \boldsymbol{B}(\boldsymbol{r} - \boldsymbol{K}\boldsymbol{x}) \tag{4.13}$$

The characteristic equation of the closed loop system is:

$$|s\boldsymbol{I} - \boldsymbol{A} + \boldsymbol{B}\boldsymbol{K}| = 0 \tag{4.14}$$

Where $\boldsymbol{I}$ is the identity matrix. There gain matrix if found using the Direct Comparison method [7]:

$$|s\boldsymbol{I} - \boldsymbol{A} + \boldsymbol{B}\boldsymbol{K}| = (s - \mu_1)(s - \mu_2) \tag{4.15}$$

Where μ_1 and μ_2 represent the closed loop poles. Now solve for $\boldsymbol{K}$ using Eq.4.15. The resulting gain matrix is found to be:

$$\boldsymbol{K} = \begin{bmatrix} -74.2282 & 89.2622 \end{bmatrix} \tag{4.16}$$

4.5 Simulation results and analysis

From the results it can be seen that when the speed of the linear DC machine is controlled using a negative state-feedback controller, the steady state velocity is 3m/s. Also, the controlled linear DC machine has a settling time of 0.6s while the uncontrolled linear DC machine has a settling time of 1s. The controlled linear DC machine has a steady state velocity of 3m/s whilst the uncontrolled linear DC machine has a state state velocity of 16m/s for an input voltage of 5V. This shows that the controlled linear DC machine performs better. The performance being better than the uncontrolled locomotive because the settling time of the locomotive is now faster compared to the uncontrolled locomotive. The speed is also fast enough for mining applications. For the uncontrolled locomotive, the speed is very fast and not acceptable for mining applications. In summary, the

controlled locomotive is able to meet the desired performance specifications as summarized in table 4.1. The desired performance was achieved after the found specifications were used to desire a controller.

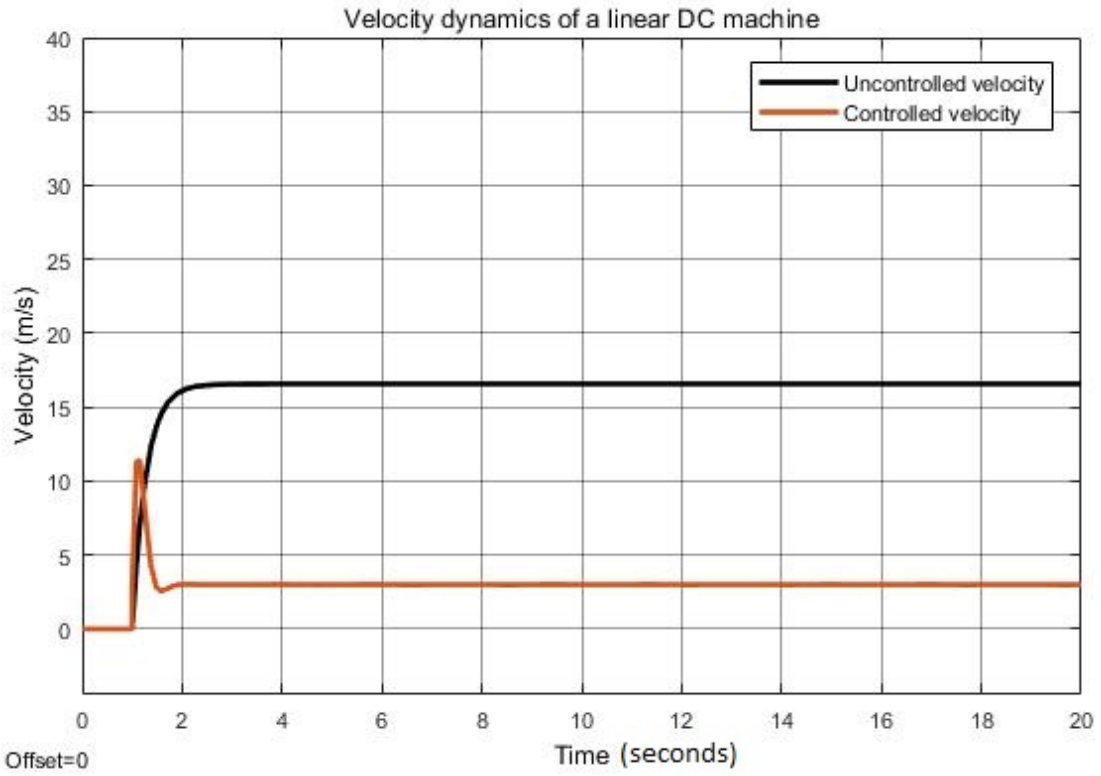

FIGURE 4.3: Linear DC machine velocity dynamics

4.6 Summary

The state feedback based on the pole placement technique is presented and used to control the speed of a locomotive to 3 m/s. The success criteria of the controller would be; achieving a settling time of 0.6 s and a speed of 3 m/s. The results presented show the desired performance (0.6 s settling time and 3 m/s speed). Therefore, the speed control of the mine locomotive is effective. In the future, non-linearity's and noise could be incorporated in the system of locomotives. This is because real life systems are not a 100% linear. Therefore, it would be an interesting exercise to analyze a highly non-linear system with stochastic noise.

CHAPTER 5

Friction Modelling

5.1 Overview

Friction modelling is of paramount importance in that it allows for a close approximation of the behaviour of a practical system to be predicted. This is especially true when the friction model is comprehensive. A detailed friction model detailing the static and kinetic region is presented. The friction model presented is for a linear DC machine powered locomotive. For this reason, the sliding friction associated with the linear DC machine and the rolling friction opposing the wheels of the locomotive are formulated. A friction model of the linear DC machine powered locomotive is presented.

5.2 Friction force

Knowing the force required to move (dispatch) an underground locomotive is important. The dispatch force should exceed the friction force where the friction force opposes the motion. This allows for the movement of the locomotive. The friction force in practical systems has a static and kinetic region [15]. The static friction force region would be the region where the dispatch force does not result in the locomotive moving. This would mean that there is no net force on the locomotive. The kinetic friction force would be the friction force from where the locomotive starts moving. Knowing the sources of the friction force is important because it allows for a thorough friction analysis for the locomotive. This would make specifying the power requirements of the locomotive possible. Subsequently,

the efficiency and performance of the mine locomotive are also determined. Suppose the underground mine locomotive is powered by a source with a power rating of 3 kW [80] and the friction losses and the overall losses of the machine sum up to an assumed power loss of 200 W. This would mean that the mine locomotive would have an efficiency of 93 %. The friction model formulated in this study tries to estimate the friction force of the mine locomotive in practice by incorporating both the static and kinetic friction regions. The linear DC machine is meant to generate a motive force that allows for the mine locomotive to be transported from one point of the mine track to the desired location.

Other design considerations which could be useful in minimizing the friction force would be deciding whether the mine locomotive should have sliding or rolling friction. In this study, sliding friction where the locomotive is positioned on the linear DC machine rail is presented. Adequate force is necessary to dispatch the mine locomotive, in essence the generated power would have to be sufficient to achieve adequate force. However, for such a set-up, the force might not be adequate. This necessitates the introduction of wheels on the mine locomotive. This would mean that the aforementioned set-up is now modified to a linear DC machine bar attached to the rolling wheels of a locomotive. This would introduce rolling friction. The force and power requirements to dispatch this mine locomotive would be lower.

It should be noted that, an extension of the model in [99] to suit the transitional motion of the linear DC machine bar which is discussed in this study, is presented. The friction model in this study does not have slip because the machine has a sliding friction. The goal is to achieve a set-up where a linear DC machine powered mine locomotive is presented and thoroughly discussed. A linear DC machine powering a locomotive is used in this study because linear machines are generally efficient which would be desired especially for commercial purpose by mining companies.

5.3 System Representation

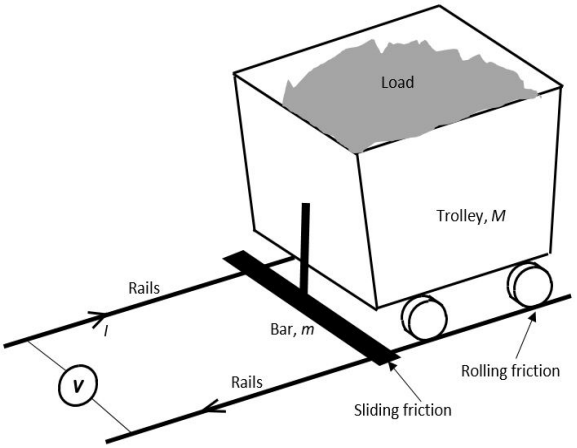

FIGURE 5.1: Linear DC machine powered mine locomotive on a rail track

Sliding friction in a system is often greater than rolling friction. A linear DC machine source requires sliding. A linear DC machine powered locomotive comprises two systems; the linear DC machine and a trolley. Reduction of overall friction while powering the locomotive with a linear DC machine which comes with sliding friction would mean using a locomotive which comes with rolling friction. Quite often, the viscous friction force is used to describe the friction force of a system. The viscous friction force is proportional to the speed [58, 67]. Therefore, the friction of the linear DC machine should be analyzed. The linear DC machine powered mine locomotive comprises a trolley used to carry coal/ore where the trolley has a mass M, the trolley is attached to a conducting bar placed on a conducting rail. The bar has a mass m and linear DC machine circuit with a voltage source V used to power the locomotive. Current i is flowing along the rail.

The electromagnetic circuit shown in fig.3.1 is described by the equations that follow. The Lorentz force experienced by the bar is expressed by:

$$\begin{aligned} \boldsymbol{F}_L &= il(-\hat{\boldsymbol{y}}) \times B(-\hat{\boldsymbol{z}}) \\ &= ilB\hat{\boldsymbol{x}} \end{aligned} \tag{5.1}$$

Where F_L is the Lorentz force. The length of the bar is a vector thus, the length has a magnitude, l, and a direction, $\hat{\boldsymbol{y}}$. The magnetic field is also a vector in

the $\hat{\boldsymbol{z}}$ direction, the positive direction of the magnetic field is represented by the magnetic field going into the page 'x' whilst, the magnetic field in the negative direction is represented by the magnetic field going out of the page 'o'. The force applied on the bar is in the $\hat{\boldsymbol{x}}$ direction where right and left represent the positive and negative direction, respectively. The induced voltage is described by:

$$e = lB\dot{x} \tag{5.2}$$

Where e is the induced voltage and $\dot{x}_1$ is the velocity of the bar. The current flowing along the electromagnetic circuit could be found using Kirchoff's laws or the Lagrange modelling technique found in section 3.4.10:

$$i = \frac{V - e}{R} \tag{5.3}$$

The nature of the induced voltage is such that the induced voltage opposes the source voltage. As such, an increase in the induced voltage results in a decrease in current. To extend on the aforementioned, a decrease in the induced voltage results in an increase in current. The current is also dynamic in that it changes with a change in the velocity of the bar. For a linear DC machine at steady-state, the induced voltage is constant. In reference to Eq.5.3, hence the current will also be constant.

The equation describing the motion of the mine locomotive follows the Newton's laws. The equation is shown by:

$$m_t\ddot{x} - ilB = F_{app} - F_{ML}(F_{app}, F_L) \tag{5.4}$$

Where the m_t is total mass of the bar and mine trolley ($m_t = M + m$), F_{app} is the external force applied on the bar, F_{ML} is the friction force which will formulate to extend the work done by Pacejka [78]. The friction force as used by [13] is the viscous friction force. However, the friction force in this work will not be assumed to be viscous friction but, the friction force will be represented as a function of the external applied force and the Lorentz force for a general case. The friction

model formulation takes into consideration the fact that some mine locomotives have external forces applied to them such as the gravitational force when the locomotive is on an inclined plane. A discussion on the friction model will be provided in the sections that follow.

5.4 Pacejka friction model

One of the key contributions in the study is to extend the Pacejka friction. The Pacejka friction model is traditionally used in tire-wheel systems i.e. for rolling friction applications [63, 77, 98]. The Pacejka friction model is extended for a bar sliding on a rail applications where the type of friction force experienced between the rail and bar is called the sliding friction. The Pacejka friction model also known as the tire magic formula is a function of slip and velocity [77, 104]. The Pacejka friction model is described by [30, 77];

$$F_y = Dsin[Carctan\{B\alpha - E(B\alpha - arctan(B\alpha))\}] \tag{5.5}$$

$$B = \frac{C_{F\alpha}}{CD} \tag{5.6}$$

The peak factor is:

$$D = \mu F_z (= F_{y,peak}) \tag{5.7}$$

The cornering stiffness is described by:

$$C_{F\alpha}(= BCD) = c_1 sin\{2arctanF_z/c_2 \tag{5.8}$$

From Eq. 5.5 - Eq.5.8, c_1 and c_2 are friction coefficients, C and E are shape parameters [77], μ is the friction coefficient and the friction coefficient is dependent on the load and speed. $C_{F\alpha}$ is the lateral slip coefficient. A slip-velocity tire friction model based on the work by Pacejka is approximated and found in [73, 97]. The approximated friction model is of the form [73]:

$$\mu(\lambda) = 2\mu_0 \frac{\lambda\lambda_0}{\lambda_0^2 + \lambda^2} \tag{5.9}$$

Where λ is the slip ratio, μ is the friction coefficient, and μ_0 is the peak friction coefficient. The slip ratio is further represented by:

$$\lambda = \frac{v - r\omega}{v} \tag{5.10}$$

A slip ratio of 1 represents free motion of the wheel while a slip ratio of 1 represents a locked wheel i.e. no motion [73, 77]. The equation Eq.5.9 is further extended for cases where there is sliding friction. It will be shown that the sliding friction presented in this study is a function of the Lorentz force and applied force where the force induce velocity in the linear DC machine.

It will be shown that Pacejka friction model can be extended for sliding friction systems where the sliding friction is due to the bar moving along the rail. The novelty in the extended model is that the Pacejka rolling model is formulated such that the Pacejka model accommodates sliding model. Another key feature on the sliding friction model would be that the extended friction model is a function of the Lorentz force and any other external force applied to the linear DC machine.

5.5 Locomotive rolling friction

The sliding friction model used in this study is based on a friction model originally formulated by Pacejka Eq.5.5. An approximation Pacejka friction model is described by Eq.5.9 [73, 97]. The approximated friction model is further extended in this study to accommodate sliding motion. Typically, the Pacejka model is formulated for rolling friction, and the model is also a function of slip and velocity. The extended model in this study is a function of the Lorentz force and other external forces experienced by the locomotive.

The rolling friction of a linear DC machine powered mine locomotive is due to the wheel-rail contact and wheel-bearing [73]. The rolling friction increases with an

increase in load and decreases with a decrease in load. Another factor affecting the rolling friction is the uneven-ness of the rail track. Modelling the rolling dynamics of the linear DC machine powered mine locomotive would result in an accurate prediction of the system behaviour [107]. The rolling friction model is formulated by Pacejka whose work is applied by [99] and [73]. An extension of Pacejka's friction model is formulated in this study [78]. First, the total force applied on the locomotive is defined as:

$$F_A = F_{app} + F_L \tag{5.11}$$

Where F_A, represents the total force applied on the locomotive, F_{app} is the applied force and F_L is the Lorentz force. The rolling friction in this study is an extension of the work done by Pacejka and the rolling friction is described by [78]:

$$\mu(F_A) = 2F_{A_0}\frac{F_{A_0}F_A}{F_{A_0}^2 + F_A^2} \tag{5.12}$$

Where μ is friction coefficient, F_{A0} is the peak applied force (total).

$$F_r = \mu(F_A)F_N \tag{5.13}$$

Where F_r is rolling friction and F_N is the normal force.

5.6 Bar sliding friction

The Dry friction force [42] is the force opposing the motion of the bar. The effects of the friction force are present when the Lorentz force or an external applied force (such as gravity) acts on the bar. Hence, the model formulated for the friction force is such that it is a function of the Lorentz and an external applied force. The friction force formulation is obtained using curve fitting where the static and kinetic friction are represented using a piece-wise function. Reference [34] tells us that the friction coefficient of a body is high when a body at rest starts sliding, this is known as the static friction. As the body continues moving, the friction

coefficient starts decreasing until a stationery value is reached, at this stage, the kinetic friction is reached [34]. The idea of the friction force dynamic model is an extension of the approach taken from [73, 99]. The dynamic friction model formulated in this study is an extension of Pacejka's friction model and the LuGre model [3, 45, 99]. The Pacejka's friction model used to represent rolling friction is such that the friction is a function of the slip coefficient and the model is formulated assuming steady state conditions [99]. However, it should be noted that the model in this study does not have slip. The LuGre model is a dynamic model, and it represents the Stribeck, Coulomb and static friction [3, 45]. The resulting friction model representing the sliding friction is described by [78]:

$$F_{fr}(F_A) = \begin{cases} F_o & 0 \leq F \leq F_N \\ \frac{k_1 \frac{F_A}{F_N}}{(\frac{F_A}{F_N})^2 + k_3} F_N & F_N \leq F \leq \infty \end{cases} \tag{5.14}$$

Where $F_{fr}(F_A)$ is the sliding friction force, F_N is the threshold static friction force (also the normal force) and k_n are constants.

It should be noted that the sliding friction is an extension of the Pacejka friction model where the Pacejka friction model in this study is based on an external applied force and the Lorentz force. Normally, the Pacejka friction force is a function of the slip and velocity. It is seen from the sliding friction model formulated that not only is the Pacejka for the translational motion of the linear DC machine powered locomotive a function of the an applied force and the Lorentz force but that, the friction model is further represented by piece-wise equations. The extended Pacejka friction model is based on:

- Piece-wise equations.
- The Pacejka friction model is a function of the Lorentz force and an external applied force (to suit the translational motion of the bar).

5.7 Friction simulation results

In fig.5.2 a dynamic friction curve for friction force based on the Pacejka and LuGre is shown. The solid lines on the curve represent sliding friction while the dotted lines on the curve represent rolling friction. Tsiotras states that the friction force in real life systems is a function of the speed and normal force [99]. The aforementioned is in accordance to Amonton [2], whose work shows that the friction force is proportional to the normal force and also Reynolds, Dahl and LuGre's work where friction force is a function of velocity [2, 21, 58, 100]. The friction model formulated in this study incorporates the speed of the bar (the current is a function of the speed) and the normal force, thereby mimicking practical systems. From the curve provided, it is deduced that the friction force opposing the motion of the bar starts by increasing with an increase in total applied force (F_A) until the threshold friction force is reached. The threshold friction force is the peak friction force observed on the dynamic curves. The friction regime from when there is no applied up until the peak friction is reached represents the static friction. As the applied force continues increasing, the friction force starts decreasing. As the friction force leaves the static friction regime, the friction force enters the kinetic friction regime where in this case, the kinetic friction is represented by a decrease in friction force starting from the peak friction. The results obtained from the friction formulation are in agreement with [34, 73, 99]. It is worthwhile to mention that the results of the dynamic friction curve comply with the findings by Amonton, Stribeck, Coulomb, Dahl and most importantly the LuGre control group.

Remark: To re-emphasize the correctness of the friction model, the results in fig.5.2 show that the friction force decreases with an increase in velocity. This complies with the results from work done in other friction studies [34, 73, 99].

Another important observation in fig.5.2 is that the sliding friction force (denoted by solid lines) is greater than the rolling friction force (denoted by dotted lines) for the same load. The linear DC machine has a bar that slides in principle, which

means a high friction force. To minimize the friction force, the mine locomotive should have wheels. This would mean that the linear DC machine would be used to pull the wheel of the mine locomotive. This is shown in the dynamic friction force curve where the maximum friction force for a full load of a mine locomotive based solely on sliding is 1.1 per unit (pu). For a mine locomotive with wheels, the sliding friction of the linear DC machine should not be ignored hence, the full load friction force would be the sum of rolling friction full load and no load sliding friction. It is worthwhile to mention that the no load friction force is represented as 0.05 of load for illustration purposes, this is because the mine locomotive still experiences a friction force opposing its motion even when it is not loaded. Therefore the maximum friction force would be 0.79 pu. Therefore, a mine locomotive with wheels is preferred.

The next step would be to approximate the desired friction model based on the results shown in fig.5.2. The desired friction model is a combination of sliding friction and rolling friction.

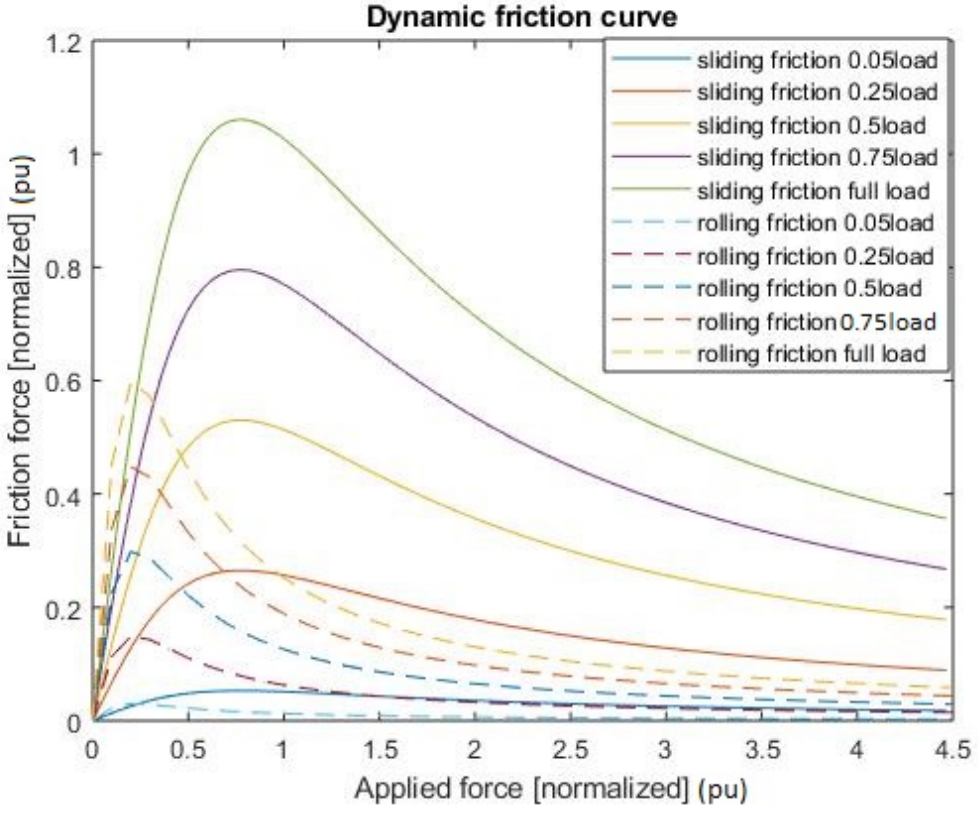

FIGURE 5.2: Dynamic friction curve

The friction force of a bar sliding on a rail has thus been formulated using extension methods of the analysis provided by Pacejka and LuGre friction models. An analysis and curve of the friction model formulated is in agreement of the findings by LuGre.

5.8 Desired locomotive friction model

The resulting friction model of the mine locomotive is the sum of the no load linear DC sliding friction force of the bar and the rolling friction force.

$$F_{ML} = F_{fr_{NL}}(F_A) + F_r \tag{5.15}$$

Where F_{ML} is the resulting friction force of the mine locomotive and $F_{fr_{NL}}(F_A)$ is the no load sliding friction force. Now that the dynamic friction model of the mine locomotive has been formulated, substituting the dynamic friction model into Eq.5.4 yields:

$$m\ddot{x} - ilB = F_{app} - F_{ML} \tag{5.16}$$

5.9 Locomotive simulation results

The simulation results are found in this section. It should be noted that a small-scale mine locomotive is simulated for purposes of proof of concept. The following parameters are used for simulation purposes:

TABLE 5.1: Mine locomotives parameters

Locomotive mass (kg)	1 kg
Bar mass (kg)	0.25 kg
Load (N)	12.25 N
Magnetic field (B)	0.5 T
Rail separation length (l)	0.6 m
Resistor (R)	$100m\Omega$
Input voltage (V)	1 V
Applied force (N)	0 N

The simulation results are a comparison of the linear DC behaviour for a case where there is friction force and when there is no friction force. The friction force formulated in sec.5.8 is in accordance with the work done by Amonton where the friction force is proportional to the normal force. From the results shown in fig.5.6 it is deduced that the linear DC machine has a lower steady state velocity when the friction force is incorporated in the system model. By Coulomb, the friction force is in the direction opposing the motion of the bar. Hence, the velocity where friction force is present is slightly lower than for a case where there is no friction force. As a result of the lower velocity in a system with friction force, the steady state current in fig.5.5 is slightly higher compared to a case where there is no friction force. This is because the current is a function of the induced emf where the induced emf is also a function of velocity as shown by Eq.5.3. The equation shows that the current decreases with an increase in velocity whilst the current also increases with a decrease in velocity. Also, the displacement of the linear DC machine shown in fig.5.4, in the presence of friction force is lower due to the bar moving at a lower velocity. Another interesting thing deduced from fig.5.6 is that the load has an effect on the friction force. In fig.5.6, the velocity dynamics of the mine locomotive are shown for load ranges of $(no-load, 0.25 \times (fullload), 0.5 \times (fullload), 0.75 \times (fullload), (fullload)$. It is deduced from these velocity dynamics that a loaded mine locomotive moves slower compared to a a no-load mine locomotive which has the highest velocity compared to all the other mine locomotives. The load is also found to affect the velocity of the locomotive

and the conclusion is that the higher the load, the slower the motion of the mine locomotive.

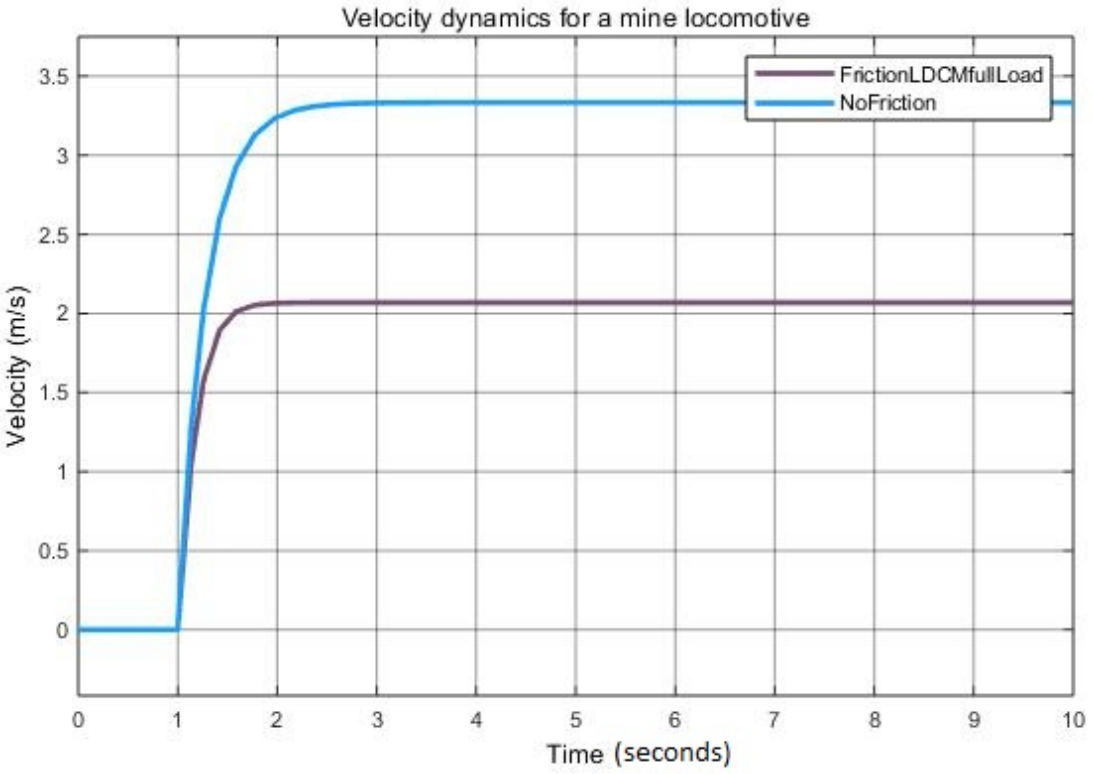

FIGURE 5.3: Velocity dynamics of the mine locomotive

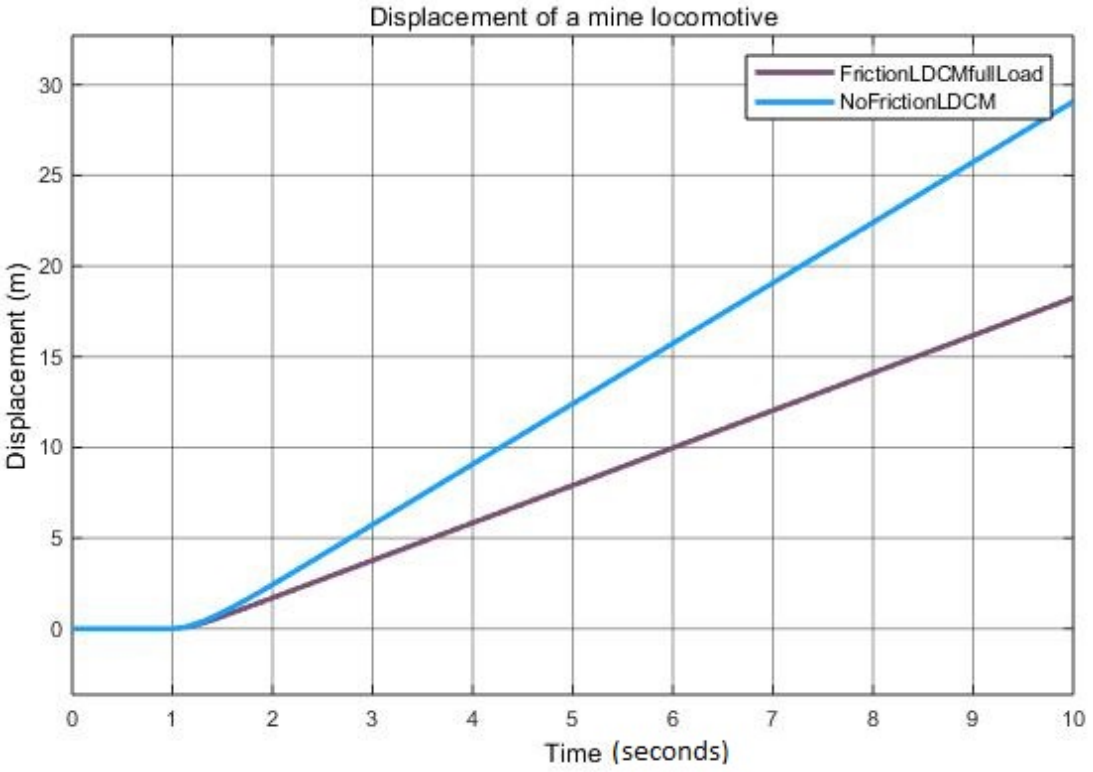

FIGURE 5.4: Displacement of the mine locomotive

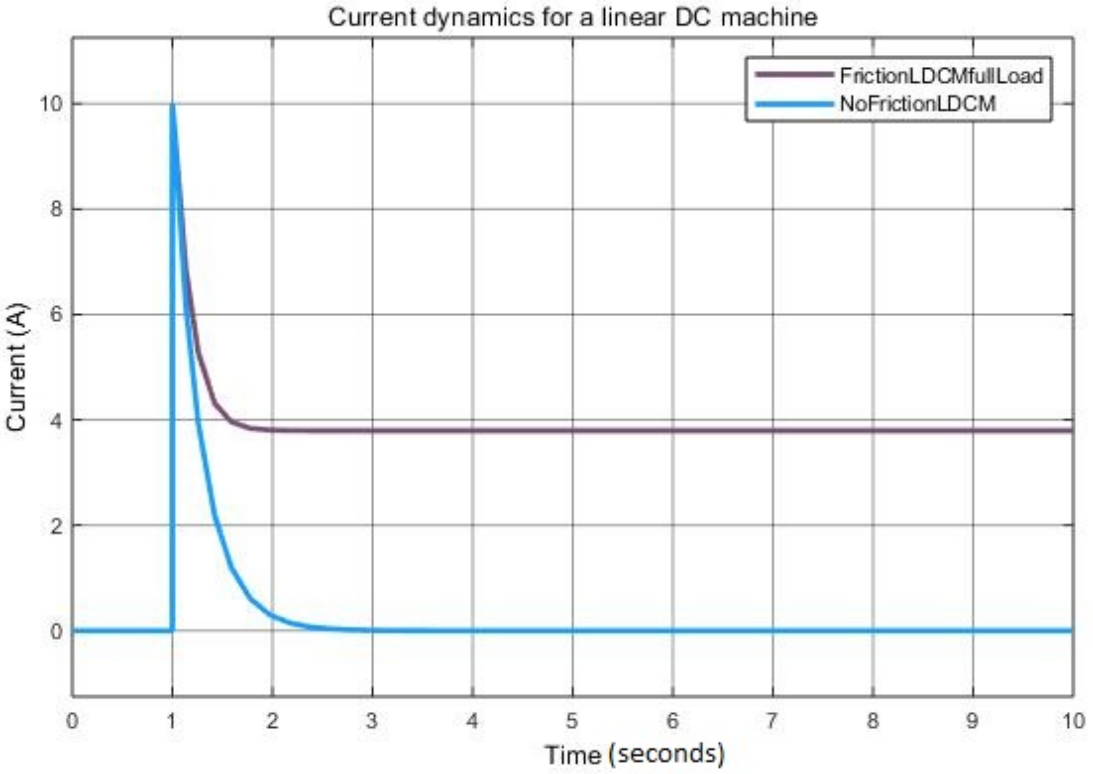

FIGURE 5.5: Current dynamics of the linear DC machine

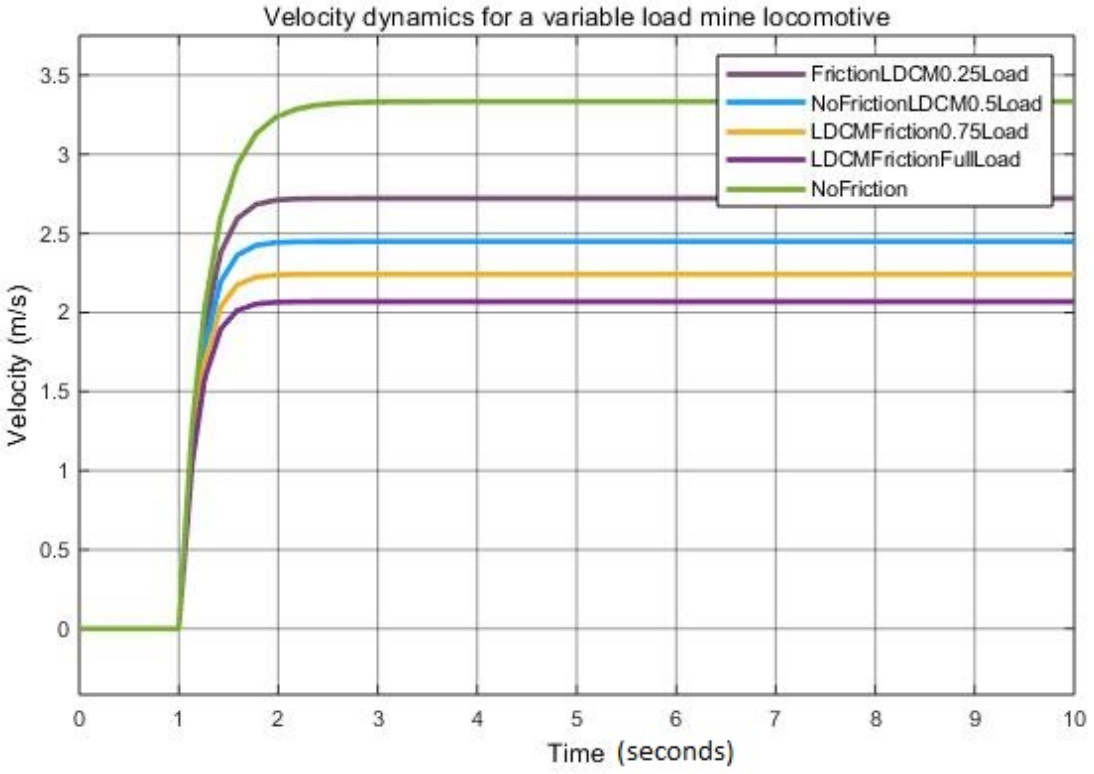

FIGURE 5.6: Velocity dynamics of the mine locomotive for variable loads

Variable voltage results of the mine locomotive are also presented. The voltage is varied from 1 V - 3 V. The results show that the lower the input voltage, the more friction losses of the mine locomotive locomotive. The results also highlight that practical systems move slightly slower than perfect systems. The results show that the system with a voltage of 1 V, 2V, 3 V respectively, moves at 37.5%, 15.6% and 12%, respectively slower than the no-load mine locomotives. This justifies the need for a comprehensive friction model.

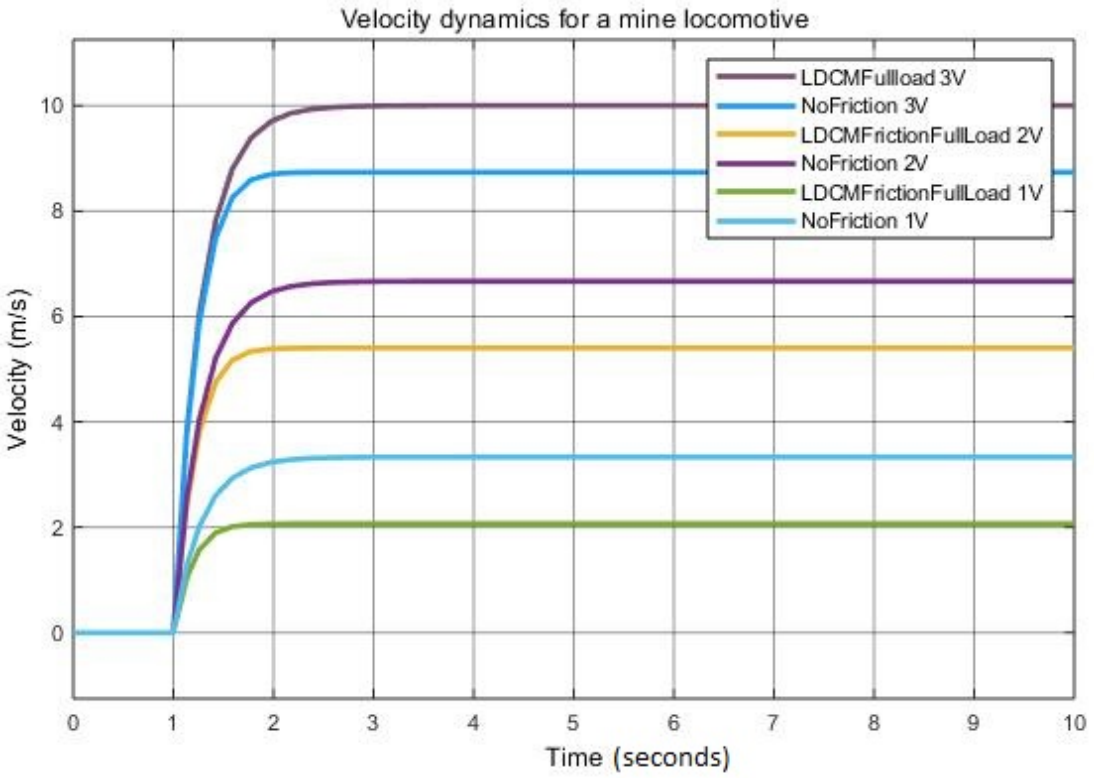

FIGURE 5.7: Velocity dynamics of the mine locomotive for variable voltage input

For future work, the stick-slip effects will be incorporated in the friction model. According to [105], the LuGre friction model does not address this limitation. Therefore, although the friction model provided is a better approximation of a real linear DC machine powered locomotive system, more work can still be done to improve the model.

5.10 Research contribution

The friction model formulated in this research is an extension of the work done by Pacejka in that the formulated friction model of the linear DC machine is a translational version of Pacejka's rolling friction model [73, 99]. Formulating a comprehensive friction model is one of the key contributions in the study. In this chapter, a friction model of a linear DC machine which incorporates the sliding friction of the linear DC machine and rolling friction of locomotive is successfully formulated. The model formulated has two regimes; the static friction regime and

the kinetic friction regime. This would mean that the friction model mimics the friction force in a practical system by having all regimes taken into consideration. One of the key results in this chapter would be, being able to demonstrate that the rolling friction is less than the sliding friction. The aforementioned is also true in real life systems. Therefore, a friction model is successfully formulated in this chapter.

5.11 Summary

A friction model for a linear DC machine powered mine locomotive is formulated and presented. The friction model accounts for the sliding friction of the linear DC machine and the rolling friction of the wheels of the locomotive. The linear DC machine model by [13] is extended with a detailed friction model. Simulation results for the friction model and detailed model of a linear DC machine are presented and analyzed. The results show that the bar tends to move slower when the friction force effects are taken into consideration. The results also show that a friction model is needed especially when modelling small-scale systems. A Pacejka model for slip based rotating motion is extended to sliding translational motion.

CHAPTER 6

Lagrange Based Model Order Reduction

6.1 Overview

Physical systems are often described by large-scale differential equations [40]. Large-scale systems are high- order systems. These high-order systems are often accurate descriptions of physical systems obtained by finite element methods, linearized models of non-linear systems and, integer order approximations of fractional order systems [87]. It is a known fact that high-order systems are a computational burden [40, 87] and they result in a complex system analysis [14]. Moreover, simulations and control design for high-order systems are challenging [87]. The complications of control design and simulations of high-order systems are due to the presence of many states and high computational power demands [87]. It is known that the optimal control algorithm is suitable for complex systems. However, in a case where a high-order system is analyzed, the complication is that each state would require a co-state hence, doubling the order of the system [99]. This would result in difficulty when analyzing the system due to the order of the system doubling. Another issue with high-order systems would be that the measurement of the states becomes increasingly difficult. Even when the state observation and estimation is considered, the observer design is difficult to analyse, calculate, and simulate. It is for these reasons highlighted that model order reduction is desirable. However, the reduction process should be able to preserve the system's dominant dynamic properties [40]. The aim of this chapter

is to provide a Lagrange based model order reduction for a tandem pair of linear DC machines using degrees of order analysis. The conditions for model order reduction are highlighted and discussed and the lowest order model is formulated.

6.2 Physical representation

A system of mine locomotives placed on a slope are used to demonstrate model order by Lagrange in this study. The physical model is shown in fig.6.1 where the area of interest is the source driving the mine locomotive. It is for this reason that the study is based on model order reduction of the source driving the mine locomotives, in this case, the linear DC machine. The zoomed version of the linear DC machine at each end of the slope marked by a maroon colour in fig.6.1 is shown on fig.6.2. Each of the linear DC machines shown has a bar which is free to travel up and down the slope depending on whether the linear DC machine is behaving as a generator or a motor. For a generator, the bar of the linear DC machine would travel down the slope due to the gravitational force pushing the bar down the slope. The linear DC machine at the bottom of the slope would behave as a motor and the bar of the linear DC machine would travel up the slope. The slope is inclined at an angle θ and this angle is fixed. Also, the linear DC machine comprises a DC battery represented by V, a series resistance R, and a conducting bar (completing the circuit) placed on a rail where the length of the bar is described as the distance from one end of the rail to another end of the rail [13]. The current, i, flows along the circuit and, the circuit is placed in a constant magnetic field B. According to the fig.6.2, 'x' represents a magnetic field into the page while 'o' represents a magnetic field out of the page. Newton's law of motion is used to describe the movement of the bar, the law of induction is used to describe the induced voltage across the bar, and Kirchoff's voltage law is used to describe the current flowing along the circuit. However, the Lagrange will be used to analyse the system of locomotives. The Lagrange should have the same structure as the analysis performed using the Newtons laws and laws governing electromagnetic circuits. The 3D Pythagoras and axis of the rail are shown in

fig.6.3. In the fig.6.2, l represents the length of the rail. The linear DC powered mine locomotive should slide down an inclined plane with a length l_2 and an angle θ.

The Lagrange is an energy based approach used for dynamic energy balance [95, 102]. The Lagrange follows steps that can be summarized as [95]:

- Identify and classify (potential/kinetic) energy
- Compute Lagrange
- Compute dissipation power
- Evaluate Euler-Lagrange

Before performing the Lagrange analysis, the following conditions should be met:

- The generalized coordinates should be independent
- The generalized coordinates should be complete
- The system has to be holonomic

Remark: In practice, the angle of inclination of the slope should adhere to mining standards. However, for the purpose of this study, the angle will be assumed for proof of concept.

Remark: The direction of either the bar, magnetic field or current is represented by a unit vector $\hat{\boldsymbol{x}}$, $\hat{\boldsymbol{z}}$ and $\hat{\boldsymbol{y}}$, respectively.

6.3 Classical physics modelling

For an independent system mine of a pair of mine locomotives on a slope where the key focus is on the linear DC machines used to power the mine locomotives, the mathematical model of the linear DC machines is found using Newtons law, law of induction and Kirchhoff's voltage law. The gravitational force acting on

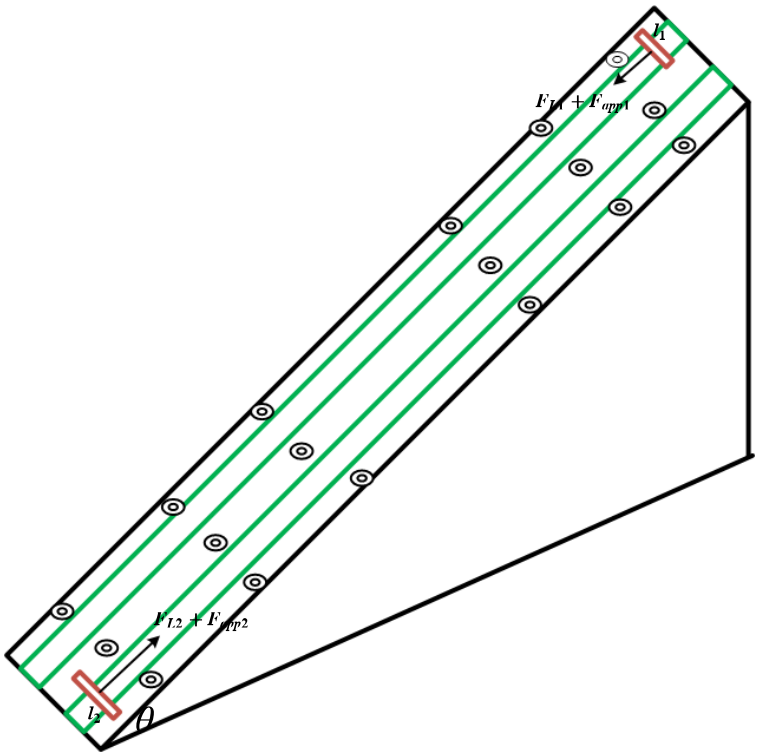

FIGURE 6.1: Linear DC machines on a slope

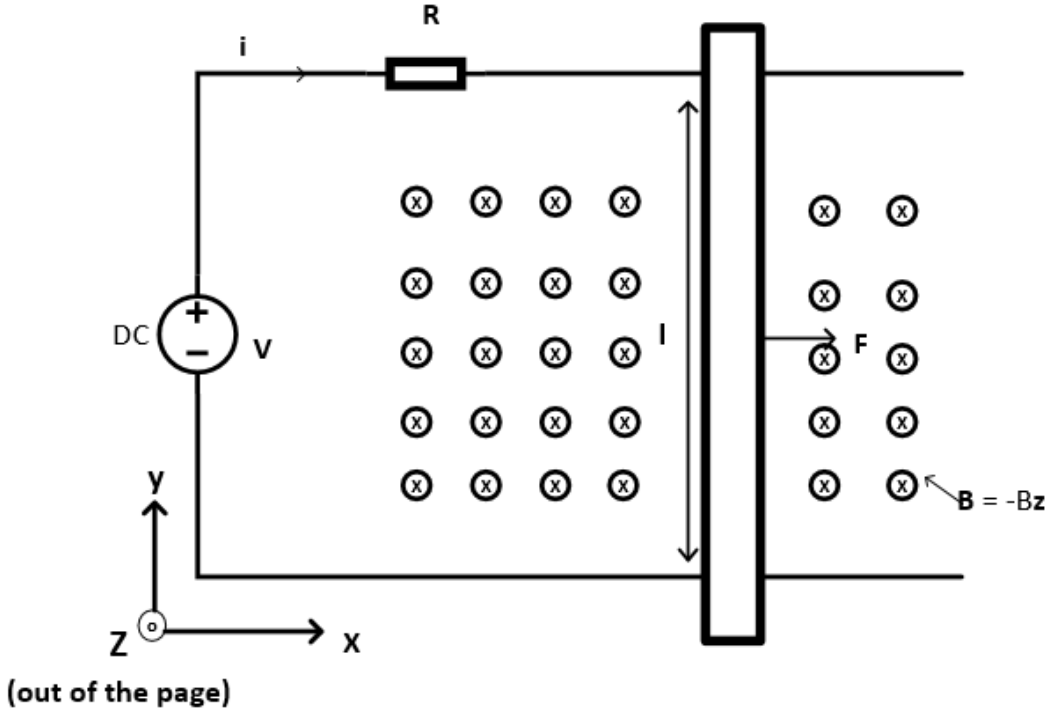

FIGURE 6.2: Linear DC machine

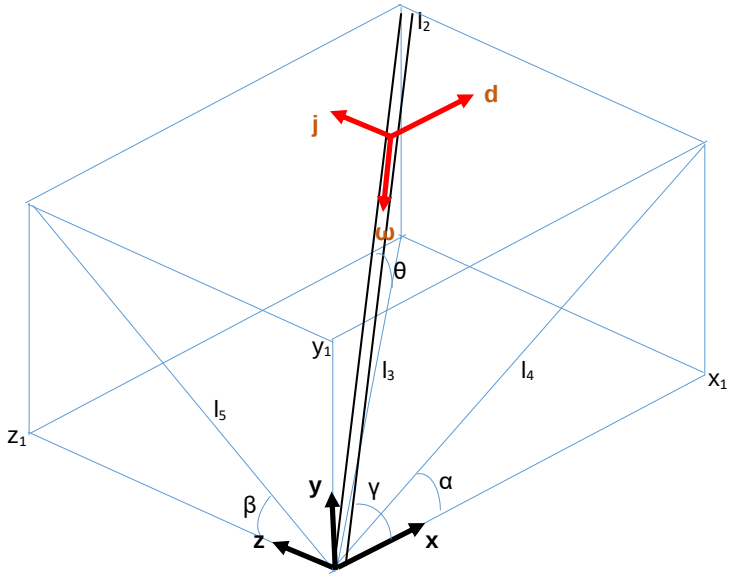

FIGURE 6.3: Coordinate frames of the rail

the locomotive has a downward direction. According the Newtons third law, there is a reaction for every action. The normal force of the locomotive would be perpendicular to the rail (contact surface). The rail is positioned on a inclined plane which would mean that the perpendicular force to the plane is the ***cos*** of the gravitational force acting on the locomotive. Newtons second law governs the motion of the locomotive. The magnetic field is perpendicular to the bar of the linear DC machine powered locomotive along all its axis. By the right hand rule, the Lorentz force would be generated along the rail, resulting in a force pulling the locomotive along the rail. A friction force opposing the motion of the locomotive is also present. Now in reference to fig.6.3, the following equations describe the position of the rail on a 3D plane:

$$sin\alpha = \frac{y_1}{l_4} \tag{6.1}$$

$$sin\beta = \frac{y_1}{l_5} \tag{6.2}$$

$$sin\gamma = \frac{z_1}{l_3} \tag{6.3}$$

Eq.6.4 is found from fig.6.3:

$$l_2^2 = x_1^2 + y_1^2 + z_1^2 \tag{6.4}$$

Where l_2 describes the length of the slope from the origin. Formulating equations related to the locomotives on the rail in the x-y-z axis using the Newtons laws would be a challenge in that the angles α, γ, β would have to be taken into consideration. Also, the force in the $\hat{\boldsymbol{y}}$ would be a function of (α, γ) and the magnetic field would also be a function of (α, β, γ). Also, visualising forces in 3D is generally challenging which complicates the analysis. To simplify the 3D analysis, the $j-w-d$ axis are defined. By inspection and the Newton's second law, the locomotive equations of motion are described. The equations describing the locomotive A are now delayed:

The normal force in the $\hat{\boldsymbol{j}}$ direction is $\perp$ to the rail. The locomotive does not move in this direction. This means that the net force is zero. The equation describing the forces in the $\hat{\boldsymbol{j}}$ direction is:

$$\hat{\boldsymbol{j}}: \quad m_{la}\ddot{j} = N_a - m_{la}gcos\theta = 0 \tag{6.5}$$

Where m_a is the mass of the locomotive, N_a is the normal force acting on the locomotive in the $\hat{\boldsymbol{j}}$ direction and $m_{la}gcos\theta$ is the reaction force. For the $\hat{\boldsymbol{w}}$ direction:

$$\hat{\boldsymbol{w}}: \quad m_{la}\ddot{w}_a - i_a l_a B_a sin\theta = m_{la}gsin\theta - b_a\dot{w}_a \tag{6.6}$$

Where l_a is the length of the bar, w is the path along which the locomotive is travelling, $\dot{w}$ is the velocity of the mine locomotive, $m_a gsin\theta$ is the applied gravitational force pushing the locomotive down the rail, B is the magnetic field and b is the viscous friction coefficient. The magnetic field is perpendicular to the locomotive from one end of the rail to another. The Fig.6.4 shows that there is

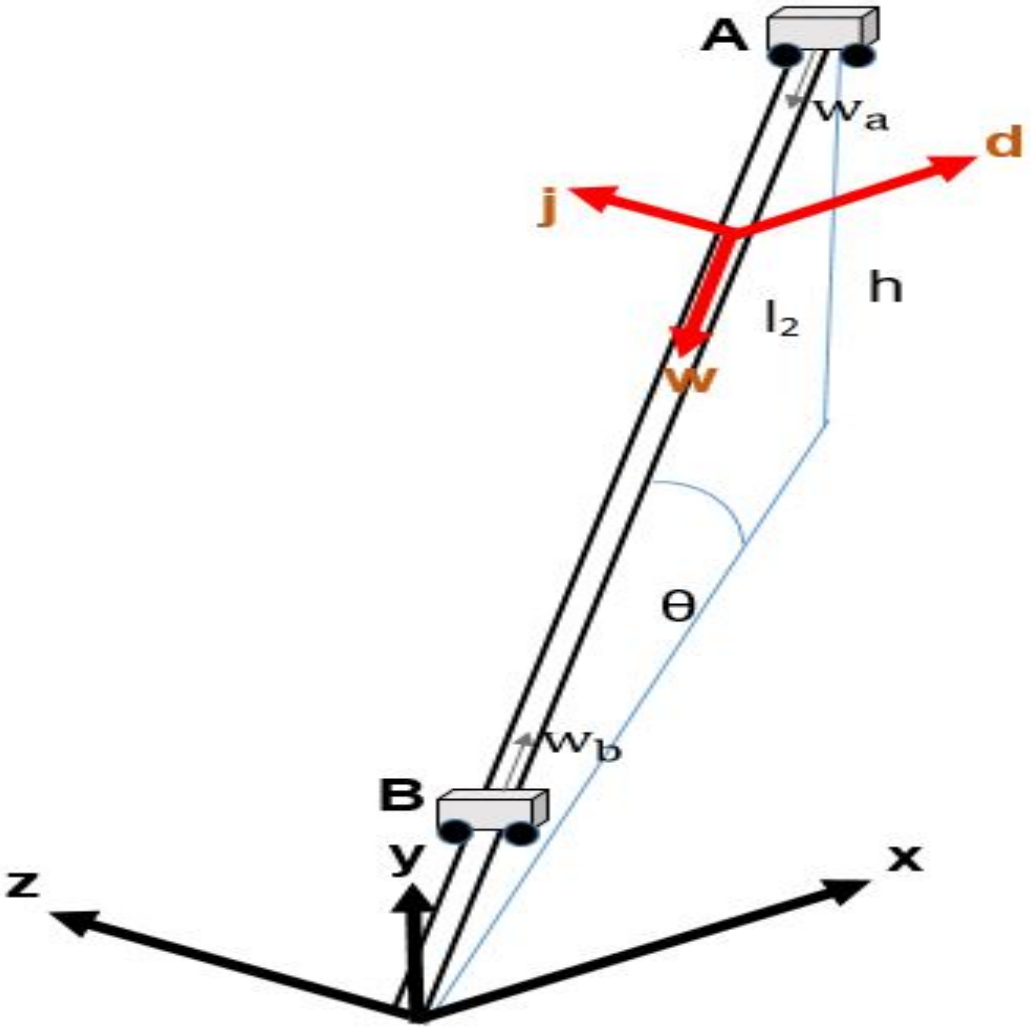

FIGURE 6.4: Mine locomotive in the **j-w-d** axis

no force in the $\hat{\boldsymbol{d}}$ direction. The locomotive is constrained from having motion in the $\hat{\boldsymbol{d}}$ direction. Therefore, the net force in the $\hat{\boldsymbol{d}}$ direction is:

$$\hat{\boldsymbol{d}}: \quad m_{la}\ddot{d}_a = 0 \tag{6.7}$$

The current is found using Kirchhoff's law:

$$i_a = \frac{1}{R_a}(V_a - l_a B_a(\dot{w}_a)) \tag{6.8}$$

Note: For the purpose of this study, the direction up and right are associated

with a positive direction and, down and left are associated with a negative direction. The equation representing the second linear DC machine are also described. The motion of bar B is also found using Newton's law of motion:

$$\hat{\boldsymbol{j}}: \quad m_{lb}\ddot{j} = N_b - m_{lb}gcos\theta = 0 \tag{6.9}$$

$$\hat{\boldsymbol{w}}: \quad m_{lb}\ddot{w}_b = m_{lb}gsin\theta + i_b l_b B_b sin\theta - b_b\dot{w}_b \tag{6.10}$$

$$\hat{\boldsymbol{d}}: \quad m_{lb}\ddot{d}_b = 0 \tag{6.11}$$

Where m_{lb} is the mass of locomotive b, N_b is the force acting on locomotive b in the direction of $\hat{\boldsymbol{j}}$ The current of bar B is also found using Kirchhoff's voltage law:

$$i_b = \frac{1}{R_b}(V_b - l_b B_b(\dot{w}_b)) \tag{6.12}$$

Remark: The power supply of locomotive A does not necessarily have to be identical to the power supply of locomotive B. The model provided caters for a general case.

Remark: The friction force is assumed to be the viscous friction force. However, the viscous friction does not entirely describe the friction force in practical systems. The viscous friction does not have a static regime. Since the key focus of this Chapter is on Lagrange based model order reduction as opposed to a detailed friction model, the viscous friction is assumed. For a comprehensive friction model of a mine locomotive, refer to Chapter 5.

Remark: The system of locomotives is non-holonomic.

6.4 Lagrange modelling based on a double rotation matrix

Formulating equations representing the dynamics of the pair of mine locomotives in a 3D plane using the Lagrange analysis/Newton analysis on the Cartesian axis

with fixed angles is challenging. The main reason is so to move away from x-y-z coordinate frame is so that the analysis can be done in a lower dimension. It should also be noted that the coordinate system must also be holonomic to proceed with the Lagrange analysis.

The focus of this study is on Lagrange based model order reduction using transformation formulae and degree of freedom analysis. A systematic model order reduction Lagrange procedure of a pair of locomotives in a 3D plane is treated and analyzed. Two mine locomotives, one at the top of an inclined plane and one at the bottom of an inclined plane are presented. The goal would be to formulate a reduced order model state space equation. When a gravitational force is applied to the system of mine locomotives, the locomotive at the top of the slope possesses motion. When the locomotive moves, the locomotive's x-y-z coordinates change because the position of the locomotive is changing. The locomotive positioned at the top of the slope assists in driving the locomotive positioned at the bottom of the slope. The locomotives are arranged such that they can only move along the slope, and the slope is at an angle $\boldsymbol{\theta}$ to the ground. A new set of axes, j-w-d is introduced in the system of the locomotives. Introducing a new set of axis is necessary in that attempting to analyze the locomotives in the x-y-z axis is a laborious task. A double rotation matrix is then used to move from the x-y-z axis to the j-w-d. The transformation from x-y-z to j-w-d is necessary in that the transformation relates the generalized coordinates (x,y,z) with the position [94]. Thereby allowing the system of locomotives to be holonomic. The transformation is followed by a Lagrange analysis.

To analyze the locomotives in terms in the x-y-z/j-w-d axis, a rotation transformation matrix is used to transform from the x-y-z axis to the j-w-d axis. The transformation matrix is based on Euler angles [25, 106]. Now transform the axis about the z-axis and the y-axis. This transformation matrix is defined by:

$$\boldsymbol{R}(\alpha, \beta) = \boldsymbol{R}_z(\alpha)\boldsymbol{R}_y(\beta) \tag{6.13}$$

The transformation equations found in [25, 106] are used to transform from x-y-z to j-w-d, and vice versa. The resulting transformation/rotation matrix is:

$$\boldsymbol{R}(\alpha,\beta) = \begin{bmatrix} cos\alpha cos\beta & sin\alpha & -cos\alpha sin\beta \\ -sin\alpha cos\beta & cos\alpha & sin\alpha sin\beta \\ sin\beta & 0 & cos\beta \end{bmatrix} \tag{6.14}$$

Where $\boldsymbol{R}(\alpha,\beta)$ is the transformation/rotation matrix, α is the angle in the x-y plane between the hypotenuse of the x-y plane and x, β is the angle in the y-z plane between the hypotenuse of y-z and z. The inverse of the transformation matrix is defined by:

$$\boldsymbol{R}^{-1}(\alpha,\beta) = \frac{1}{det(\boldsymbol{R}(\alpha,\beta))} adj(\boldsymbol{R}(\alpha,\beta)) \tag{6.15}$$

Where *det()* is the determinant of the transformation matrix $\boldsymbol{R}(\alpha,\beta)$, *adj* is the adjoint of the transformation matrix. By solving Eq.6.15, the inverse transformation matrix is found to be:

$$\boldsymbol{R}^{-1}(\alpha,\beta) = \begin{bmatrix} cos\alpha cos\beta & -sin\alpha cos\beta & sin\beta \\ sin\alpha & cos\alpha & 0 \\ -cos\alpha sin\beta & sin\alpha sin\beta & cos\beta \end{bmatrix} \tag{6.16}$$

The transformed axis is defined by:

$$\begin{bmatrix} j \\ w \\ d \end{bmatrix} = \boldsymbol{R}(\alpha, \beta) \begin{bmatrix} x \\ y \\ z \end{bmatrix} \tag{6.17}$$

Solving Eq.6.17 yields:

$$\begin{bmatrix} j \\ w \\ d \end{bmatrix} = \begin{bmatrix} xcos\alpha cos\beta + ysin\alpha - zcos\alpha sin\beta \\ -xsin\alpha cos\beta + ycos\alpha + zsin\alpha sin\beta \\ xsin\beta + zcos\beta \end{bmatrix} \tag{6.18}$$

Substituting Eq.6.18 yields equations describing the dynamics of the locomotive:

$$m_{la}(\ddot{x}cos\alpha cos\beta + \ddot{y}sin\alpha - \ddot{z}sin\alpha sin\beta) = N_a - m_{la}g\frac{\rho}{r_1} \tag{6.19}$$

$$\begin{aligned} -m_{la}\ddot{x}_a sin\alpha = &- m_{la}(cos\beta + \ddot{y}_a cos\alpha + \ddot{z}_a sin\alpha sin\beta) \\ &+ i_a l_a B_a \frac{h}{\rho} + m_{la}g\frac{h}{l\rho} + b_a(\ddot{x}sin\alpha cos\beta \\ &- \ddot{y}cos\alpha - \ddot{z}sin\alpha sin\beta) \end{aligned} \tag{6.20}$$

$$m_{la}(\ddot{x}sin\beta + \ddot{z}sin\beta) = 0 \tag{6.21}$$

6.4.1 Lagrange using transformation matrix

The Lagrange based model order reduction is shown and discussed in this work. The Lagrange based model order reduction is based on using transformation formulae and imposing physical limitations to the system of mine locomotives to restrict the type of motion (and reduce the degrees of freedom) of the locomotives. These limitations could be used in any system to restrict an object to be at a particular position or velocity. For instance, the locomotives are constrained to have an upward/downward motion along an inclined plane. The constraints depend on

the generalized coordinates and time; these constraints are known as holonomic constraints. The independent coordinates i.e. generalized coordinates describing the motion of the pair of locomotives on an inclined plane and the current flowing along the linear DC machine circuits are denoted by:

$$(x_a, y_a, z_a, \dot{q_a}, x_b, y_b, z_b, \dot{q_b}) \tag{6.22}$$

where the (x_a, y_a, z_a) are the Cartesian coordinates for locomotive A and, (x_b, y_b, z_b) are the Cartesian coordinates for locomotive B. The electromagnetic circuit of the mine locomotive A and B is denoted by the generalized coordinates (q_a, q_b), respectively. The number of degrees of freedom is related to the number of generalized coordinates. The number of coordinates for the pair of linear DC machine powered mine locomotives is eight [94]. Imposing holonomic constraints reduces the number of degrees of freedom. The number of degrees of freedom can further be described by:

$$DOF = \lambda - \eta \tag{6.23}$$

Where DOF is the number of degrees of freedom, λ is the number of coordinates for an unconstrained system, and η is the number of holonomic constraints.

Now from Eq.6.18, let:

$$\begin{aligned}
\varrho &= cos\alpha cos\beta \\
\sigma &= sin\alpha \\
\psi &= cos\alpha sin\beta \\
\iota &= sin\alpha cos\beta \\
\vartheta &= cos\alpha \\
\kappa &= sin\alpha sin\beta \\
\delta &= sin\beta \\
\zeta &= cos\beta
\end{aligned} \tag{6.24}$$

Remark: It is important to mention that the Lagrange technique can only be applied when the generalized coordinates are holonomic.

Formulating the equations describing the dynamics of the linear DC machine powered mine locomotives using the Lagrange demands following the steps in sec.6.2. The kinetic energy is identified to be due to the motion of the locomotives and the kinetic energy takes the form:

$$T_a = \frac{1}{2} m_{la}(\varrho \dot{x}_a + \sigma \dot{y}_a + \psi \dot{z}_a)^2 + \frac{1}{2} m_{la}(-\iota \dot{x}_a + \vartheta \dot{y}_a + \kappa \dot{z}_a)^2 + \frac{1}{2} m_{la}(\delta \dot{x}_a + \zeta \dot{z}_a)^2 \tag{6.25}$$

$$T_b = \frac{1}{2} m_{lb}(\varrho \dot{x}_b + \sigma \dot{y}_b + \psi \dot{z}_b)^2 + \frac{1}{2} m_{lb}(-\iota \dot{x}_b + \vartheta \dot{y}_b + \kappa \dot{z}_b)^2 + \frac{1}{2} m_{lb}(\delta \dot{x}_b + \zeta \dot{z}_b)^2 \tag{6.26}$$

$$T = T_a + T_b \tag{6.27}$$

The potential energy due to the magnetic field and the gravitational force acting on the locomotives is:

$$U_a = m_{la} g(h + (\iota x_a - \vartheta y_a - \kappa z_a)\frac{h}{l_1}) - \dot{q_a} l_a B_a \frac{h}{l_1}(-\iota x_a + \vartheta y_a + \kappa z_a) \tag{6.28}$$

$$U_b = m_{lb} g(h + (\iota x_b - \vartheta y_b - \kappa z_b)\frac{h}{l_2}) - \dot{q_b} l_b B_b \frac{h}{l_2}(-\iota x_b + \vartheta y_b + \kappa z_b) \tag{6.29}$$

The total potential energy is the sum of the potential energy of mine locomotive A and mine locomotive B.

$$U = U_a + U_b \tag{6.30}$$

The Lagrange equation of the mine locomotives is a function of the generalized coordinates $(x_a, y_a, z_a, q_a, x_b, y_b, z_b, q_b)$, and the equation is described by:

$$L(x_a, y_a, z_a, q_a, x_b, y_b, z_b, q_b) = T - U \tag{6.31}$$

Where L is the Lagrange equation, T is the kinetic energy, and U is the potential energy. The dissipation power is:

$$\begin{aligned} P =& \frac{1}{2} b_a(-\iota\dot{x}_a + \vartheta\dot{y}_a + \kappa\dot{z}_a)^2 + \frac{1}{2} b_b(-\iota\dot{x}_a + \vartheta\dot{y}_b + \kappa\dot{z}_b)^2 \\ &+ \frac{1}{2} R_a\dot{q}_a^2 + \frac{1}{2} R_b\dot{q}_b^2 \end{aligned} \tag{6.32}$$

Where P is the dissipation power.

One cannot apply Lagrange when the generalized coordinates are not holonomic. This is true for the evaluated case.

6.5 Transitioning from xyz to jwd

The transformation from the x-y-z axis to the j-w-d axis is necessary. The key thing about the transformation is that the transformation clearly shows that the transformed axis (j-w-d) is an explicit function of the x-y-z. The axis of interest (the surface along which the locomotive moves), j, is a function of x-y-z. Reducing the order when the generalized coordinates are (x,y,z) would mean analyzing the system of locomotives in a 2-D plane. However, a full analysis of the locomotives requires that all xyz coordinates are present. For this reason, the analysis of the locomotive is performed on the surface parallel to 'w' i.e. the locomotive moves along the 'w' axis. This would mean that (j,w,d) would be identified as the generalized coordinates because we are operating in the transformed axis.

6.6 Full order model in jwd axis

The full order locomotive model in the j-w-d axis where the generalized coordinates are described by:

$$(j_a, w_a, d_a, q_a, j_b, w_b, d_b, q_b) \tag{6.33}$$

is described using the Lagrange where there are no holonomic constraints on the system of locomotives. The number of degrees of freedom for these locomotives

without holonomic constraints is eight. This would also mean that the highest order for the gravity fed pair of linear DC machine powered mine locomotives is expected to be 14 (this will be shown as we proceed with the Lagrange analysis). The Lagrange steps from sec.6.2 follow, and the kinetic energy is described by:

$$T = \frac{1}{2}m_{la}(\dot{j_a}^2 + \dot{w_a}^2 + \dot{d_a}^2) + \frac{1}{2}m_{lb}(\dot{j_a}^2 + \dot{w_b}^2 + \dot{d_b}^2) \tag{6.34}$$

The potential energy follows:

$$\begin{aligned} U =& m_{la}g(h - w_a sin\theta) - \dot{q_a}l_a B_a w_a + m_{lb}g(-w_b sin\theta) - m_a g d_a cos\theta - m_a g d_b cos\theta \\ & - \dot{q_b}l_b B_b w_b \end{aligned} \tag{6.35}$$

The Lagrange equation is computed and this equation is described as the difference between the kinetic energy and potential energy:

$$L = T - U \tag{6.36}$$

According to the general steps mentioned in sec.6.2, computing dissipation power as a function of the generalized coordinates gives:

$$P = \frac{1}{2}b_a\dot{w_a}^2 + \frac{1}{2}R_a\dot{q_a}^2 + \frac{1}{2}b_b\dot{w_b}^2 + \frac{1}{2}R_b\dot{q_b}^2 \tag{6.37}$$

Evaluating the Euler-Lagrange using the following equation:

$$\frac{d}{dt}\frac{\partial L}{\partial \dot{s}} - \frac{\partial L}{\partial s} = Q - \frac{\partial P}{\partial \dot{s}} \tag{6.38}$$

Where s is the generalized coordinate. The Euler Lagrange with respect to the generalized coordinates $(j_a, w_a, d_a, q_a, j_b, w_b, d_b, q_b)$, respectively, results in equations describing the dynamics of the locomotive:

$$m_{la}\ddot{j} = N_a - m_{la}gcos\theta = 0 \tag{6.39}$$

$$m_{la}\ddot{w}_a - \dot{q}_a l_a B_a sin\theta = m_{la} g sin\theta - b_a \dot{w}_a \tag{6.40}$$

$$m_{la}\ddot{d}_a = 0 \tag{6.41}$$

$$\dot{q}_a = \frac{1}{R_a}(V_a - l_a B_a(\dot{w}_a)) \tag{6.42}$$

$$m_{lb}\ddot{j} = N_b - m_{lb} g cos\theta \tag{6.43}$$

$$m_{lb}\ddot{w}_b = m_{lb} g sin\theta + \dot{q}_b l_b B_b sin\theta - b_b \dot{w}_b \tag{6.44}$$

$$m_{la}\ddot{d}_a = 0 \tag{6.45}$$

$$\dot{q}_b = \frac{1}{R_b}(V_b - l_b B_b(\dot{w}_b)) \tag{6.46}$$

The state equations describing the dynamics of the mine locomotive are formulated and described.The state equations take the form:

$$\dot{\boldsymbol{x}} = \boldsymbol{A}\boldsymbol{x} + \boldsymbol{B}\boldsymbol{u} \tag{6.47}$$

Where $\boldsymbol{A}$ is a matrix, $\boldsymbol{x}$ is a column vector, $\boldsymbol{B}$ is a row vector and $\boldsymbol{u}$ is an input vector. Now, let $x_1 = j_a$, $\dot{x_1} = \dot{j}_a$, $x_3 = w_a$, $\dot{x_3} = \dot{w}_a$, $x_5 = d_a$, $\dot{x_5} = \dot{d}_a$, $x_7 = j_b$, $\dot{x_7} = \dot{j}_b$, $x_9 = w_b$, $\dot{x_9} = \dot{w}_b$, $x_{11} = d_b$, $\dot{x_{11}} = \dot{d}_b$, $\dot{x_{13}} = \dot{q}_a$ and $\dot{x_{14}} = \dot{q}_b$. The state equation is found to be:

$$\begin{aligned}
\dot{x_1} =& x_2 \\
\dot{x_2} =& \frac{N_a}{m_{la}} + g cos\theta \\
\dot{x_3} =& x_4 \\
\dot{x_4} =& g sin\theta + \frac{1}{m_{la}}\dot{x_{13}} l_a B_a sin\theta - \frac{b_a}{m_{la}} x_4 \\
\dot{x_5} =& x_6
\end{aligned}$$

$$
\begin{aligned}
\dot{x}_6 =& 0 \\
\dot{x_7} =& x_8 \\
\dot{x}_8 =& \frac{N_b}{m_{lb}} + gcos\theta \\
\dot{x_9} =& x_{10} \\
\dot{x}_{10} =& gsin\theta + \frac{1}{m_{lb}}\dot{x}_{14} l_b B_b sin\theta - \frac{b_b}{m_{lb}} x_{10}
\end{aligned}
\tag{6.48}
$$

$$
\begin{aligned}
\dot{x_{11}} =& x_{12} \\
\dot{x}_{12} =& 0 \\
\dot{x_{13}} =& \frac{1}{R_a} V_a - \frac{1}{R_a} l_a B_a x_4 \\
\dot{x_{14}} =& \frac{1}{R_b} V_b - \frac{1}{R_b} l_b B_b x_{10}
\end{aligned}
$$

As it has been stated, the state model of the system of locomotives has 14 states. The interesting thing to note is that the Newtons dynamic equations are generated which shows that the Lagrange analysis is a viable technique to analyze the mine locomotives even when placed on an inclined plane. The area of focus in this study is on model order reduction based on degrees of freedom analysis and using transformation formulae which are a function of the generalized coordinates.

6.7 Reduced order model

From the fig.6.3, it can be seen that the locomotive is constrained to slide down the slope. This means there is no motion in the $\hat{\boldsymbol{j}}$ and $\hat{\boldsymbol{d}}$ directions. Therefore the holonomic constraints governing the motion of the mine locomotives in the j-w-d axis are described by:

$$
\begin{aligned}
f_1 : \mathrm{J}_a =& 0 \\
f_2 : \mathrm{J}_b =& 0 \\
f_3 : d_a =& 0 \\
f_4 : d_b =& 0
\end{aligned}
\tag{6.49}
$$

The degrees of freedom are found to be:

$$DOF = 8 - 4 = 4 \tag{6.50}$$

The full order model of the mine locomotives in the transformed axis (j-w-d) has eight degrees of freedom i.e. $(j_a, w_a, d_a, \dot{q}_a, j_b, w_b, d_b, \dot{q}_b)$. Imposing four holonomic constraints on system of mine locomotives would mean that the system of locomotives has four degrees of freedom $(w_a, \dot{q}_a, w_b, \dot{q}_b)$.

The Lagrange kinetic energy is represented by:

$$T = \frac{1}{2} m_{la} \dot{w_a}^2 + \frac{1}{2} m_{lb} \dot{w_b}^2 \tag{6.51}$$

The potential energy is described by:

$$U = m_{la} g(h - w_a sin\theta) - \dot{q_a} l_a B_a w_a + m_{lb} g(h - w_b sin\theta) - \dot{q_b} l_b B_b w_b \tag{6.52}$$

The Lagrange equation is:

$$L = T - U \tag{6.53}$$

and the dissipation power is described by:

$$P = \frac{1}{2} b_a \dot{w_a}^2 + \frac{1}{2} R_a \dot{q_a}^2 + \frac{1}{2} b_b \dot{w_b}^2 + \frac{1}{2} R_b \dot{q_b}^2 \tag{6.54}$$

Evaluating the Euler-Lagrange using the following equation:

$$\frac{d}{dt} \frac{\partial L}{\partial \dot{s}} - \frac{\partial L}{\partial s} = Q - \frac{\partial P}{\partial \dot{s}} \tag{6.55}$$

Yields the equations describing the dynamics of the locomotive and its power source:

$$m_{la} \ddot{w}_a - \dot{q_a} l_a B_a sin\theta = m_{la} g sin\theta - b_a \dot{w}_a \tag{6.56}$$

$$\dot{q_a} = \frac{1}{R_a} (V_a - l_a B_a (\dot{w_a})) \tag{6.57}$$

$$m_{lb}\ddot{w}_b = m_{lb}gsin\theta + \dot{q}_b l_b B_b sin\theta - b_b\dot{w}_b \tag{6.58}$$

$$\dot{q}_b = \frac{1}{R_b}(V_b - l_b B_b(\dot{w}_b)) \tag{6.59}$$

The equations are the same as the equations found using the Newtons by the inspection method. This confirms that the Lagrange is reliable and can generate equations for 3D setups such as a mine locomotive on an inclined plane. Formulating equations using the Lagrange is found to be easy compared to the Newtons law by inspection. This is primarily because the Lagrange is only concerned with the energy while the equations describing the locomotive sort themselves out. From the equations formulated, we are only interested at Eq.6.56, Eq.6.57, Eq.6.58 and Eq.6.59 because these equations describe the motion of the locomotive and current dynamics of the locomotive whilst the other equations have a net force of 0 N. Therefore, the reduced model is described by four equations where the number of states is 6 as shown by the state equation Eq.6.60.

The state equations describing the dynamics of the mine locomotive are formulated and described. Now, let $x_1 = w_a$, $\dot{x_1} = \dot{w}_a$, $x_3 = w_b$, $\dot{x_3} = \dot{w}_a$, $\dot{x_5} = \dot{q}_a$ and $\dot{x_6} = \dot{q}_b$. This results in a state equation of the form:

$$\begin{aligned}
\dot{x_1} =& x_2 \\
\ddot{x_2} =& gsin\theta + \frac{1}{m_{la}}\dot{x}_5 l_a B_a sin\theta - \frac{b_a}{m_{la}}x_2 \\
\dot{x_3} =& x_4 \\
\ddot{x_4} =& gsin\theta + \frac{1}{m_{lb}}\dot{x}_6 l_b B_b sin\theta - \frac{b_b}{m_{lb}}x_4 \\
\dot{x_5} =& \frac{1}{R_a}V_a - \frac{1}{R_a}l_a B_a x_2 \\
\dot{x_6} =& \frac{1}{R_b}V_b - \frac{1}{R_b}l_b B_b x_4
\end{aligned} \tag{6.60}$$

Suppose for the same system of mine locomotives with the same holonomic constraints as described in Eq.6.49 and a steady state current, we are only interested in the motion of the locomotives. This would mean that it would not be necessary to represent the current dynamics. Therefore, the generalized coordinates would

be (w_a, w_b). This would mean that the Euler-Lagrange would only be evaluated with respect to the generalized coordinates (w_a, w_b). The equations describing the mine locomotives after the Euler-Lagrange is evaluated would be:

$$m_{la}\ddot{w_a} - \wp_a l_a B_a sin\theta = m_{la} g sin\theta - b_a \dot{w_a} \tag{6.61}$$

$$m_{lb}\ddot{w_b} = m_{lb} g sin\theta + \wp_b l_b B_b sin\theta - b_b \dot{w_b} \tag{6.62}$$

Where $\wp$ is the steady state current. Two equations, Eq.6.61 and Eq.6.62, are found to describe the dynamics of the mine locomotive. That means that the order of the system of locomotives is reduced to 4 as shown by Eq.6.63.

$$\begin{aligned}
\dot{x_1} =& x_2 \\
\ddot{x_2} =& g sin\theta + \frac{1}{m_{la}} \wp_a l_a B_a sin\theta - \frac{m_{la}}{b_a} x_2 \\
\dot{x_3} =& x_4 \\
\ddot{x_4} =& g sin\theta + \frac{1}{m_{lb}} \wp_b l_b B_b sin\theta - \frac{m_{lb}}{b_b} x_4
\end{aligned} \tag{6.63}$$

6.8 Reduced order model with current constraint

The next step would be to have a setup whereby the current of the linear DC machine powering locomotive A is equal to the current of the linear DC machine powering locomotive B. This would mean that the configuration of the DC machines is such that the machines are connected in series. The holonomic constraints of the locomotives would be described by:

$$\begin{aligned}
f_1 : d_a =& 0 \\
f_2 : d_b =& 0 \\
f_3 : j_a =& 0 \\
f_4 : j_b =& 0 \\
f_5 : \dot{q_a} =& \dot{q_b}
\end{aligned} \tag{6.64}$$

$$DOF = 8 - 5 = 3 \tag{6.65}$$

Increasing the number of holonomic constraints reduces the degrees of freedom. For instance, the degrees of freedom for the mine locomotives decreases from eight degrees of freedom $(j_a, w_a, d_a, j_b, \dot{q}_a, w_b, d_b, \dot{q}_b)$ to three degrees of freedom $(w_a, \dot{q}_a, w_b)$. The holonomic constraints would mean that Lagrange potential energy and dissipation power equations become Eq.6.66 and Eq.6.67, respectively:

$$U = m_{la}g(h - w_a sin\theta) - \dot{q_a} l_a B_a w_a + m_{lb}g(h - w_b sin\theta) - \dot{q_a} l_b B_b w_b \tag{6.66}$$

and

$$P = \frac{1}{2} b_a \dot{w_a}^2 + \frac{1}{2} R_a \dot{q_a}^2 + \frac{1}{2} b_b \dot{w_b}^2 + \frac{1}{2} R_b \dot{q_a}^2 \tag{6.67}$$

The kinetic energy remains the same as Eq.6.51 because the kinetic energy equation is not a function of the current. Since there is no motion in the $\hat{\boldsymbol{j}}$ and $\hat{\boldsymbol{d}}$ direction, j and d are also not considered as the generalized coordinates of the locomotives. The Euler-Lagrange described by Eq.6.55 would yield the equations:

$$m_{la}\ddot{w}_a - \dot{q_a} l_a B_a sin\theta = m_{la} g sin\theta - b_a \dot{w}_a \tag{6.68}$$

$$m_{lb}\ddot{w}_b = m_{lb} g sin\theta + \dot{q_a} l_b B_b sin\theta - b_b \dot{w}_b \tag{6.69}$$

$$\dot{q_a} = \frac{1}{R}(V - l_a B_a(\dot{w}_a + \dot{w}_b)) \tag{6.70}$$

Where $R = R_a + R_b$ and $V = V_a + V_b$. The number of equations describing dynamics of the locomotives A and B is three. The order of the system of mine locomotives is five as shown by Eq.6.71. Similarly to the setup in the previous section 6.7, if we are only interested in the motion of the mine locomotive then the equations describing the motion would be two. The order would also be four. Suppose, we are only interested in the current dynamics. The equation describing

the current would be one and the order of the system would be one. However, the aforementioned assumes that the velocity is constant i.e. the velocity is at a steady state.

$$\begin{aligned}
\dot{x_1} =& x_2 \\
\ddot{x_2} =& gsin\theta + \frac{1}{m_{la}}\dot{x}_5 l_a B_a sin\theta - \frac{b_a}{m_{la}}x_2 \\
\dot{x_3} =& x_4 \\
\ddot{x_4} =& gsin\theta + \frac{1}{m_{lb}}\dot{x}_5 l_b B_b sin\theta - \frac{b_b}{m_{lb}}x_4 \\
\dot{x_5} =& \frac{1}{R}V - \frac{1}{R}(l_a B_a x_2 + l_b B_b x_4)
\end{aligned} \tag{6.71}$$

After introducing a new holonomic constraint ($\dot{q}_a = \dot{q}_b$), the degrees of freedom of the linear DC machine powered mine locomotive decreases. The model order is also reduced from six to five compared to Eq.6.60. This highlights the fact that the model order can be reduced by adding constraints to the system of locomotives.

6.9 Minimal order formulation using relative motion

The minimal order is obtained by constraining the locomotives to a relative velocity. This would mean that we are only interested in the relative velocities of the locomotives as opposed to individual velocities. Equal currents for the locomotive A and locomotive B are maintained. Now suppose that the relative displacements are described by:

$$\begin{aligned}
w &= w_a - w_b \\
-w &= w_b - w_a
\end{aligned} \tag{6.72}$$

Now consider x as one of the generalised coordinates. This means that the generalized coordinates describing the system of locomotives is (w, q_a). Now computing the kinetic energy of the system of locomotive's based on relative motion results in:

$$T = \frac{1}{2}m_a\dot{w}^2 + \frac{1}{2}m_b\dot{w}^2 \tag{6.73}$$

Now using the relative speed, the potential energy is described by:

$$U = m_a g w cos\theta - m_b g w cos\theta + \dot{q_a} l_a B_a w sin\theta - \dot{q_a} l_b B_b w sin\theta \tag{6.74}$$

The Lagrange is computed following Eq.6.53. The losses are also described by:

$$P = \frac{1}{2} R \dot{q}_a + \frac{1}{2} b_a \dot{w}^2 + \frac{1}{2} b_b \dot{w}^2 \tag{6.75}$$

By Euler-Lagrange

$$(m_a + m_b)\ddot{w} - (m_a + m_b) g cos\theta = 0 - b_a \dot{w} - b_b \dot{w} \tag{6.76}$$

$$- (l_a B_a sin\theta - l_b B_b sin\theta)\dot{w} = V - R\dot{q}_a \tag{6.77}$$

The state equation describing the system of locomotives is:

$$\begin{aligned} \dot{x_1} =& g cos\theta - \frac{b_a}{m_a + m_b} x_1 - \frac{b_b}{m_a + m_b} x_1 \\ \dot{x_2} =& \frac{V}{R} + \frac{1}{R} l_a B_a sin\theta x_1 - \frac{1}{R} l_b B_b sin\theta x_1 \end{aligned} \tag{6.78}$$

The minimal order of the system of linear DC machines achievable using Lagrange based model order reduction is two. This minimal order is achieved when relative motion of the locomotives is taken into consideration as opposed to focusing on individual velocity's and displacements of the locomotives.

Remark: It is important to note that the reduction process occurs due to the physical constraints . The Lagrange allows for a systematic way to process model order reduction through through degree of freedom reduction by introducing holonomic constraints. While model order reduction by increasing holonomic constraints applies to all modelling approaches, the Lagrange modelling approach is more systematic compared to all the other modelling approaches.

6.10 Research contribution

The research contribution is; demonstration of a Lagrange based model order reduction. The Lagrange based model order reduction is based on using transformation formulae, imposing holonomic constraints on the system of locomotives, degree on freedom analysis and evaluating Euler-Lagrange. In this chapter, the order of a pair of locomotives positioned on a slope with an order of 14 is reduced to a minimal order of two by imposing holonomic constraints, using transformation formulae and by performing the degree of freedom analysis.

6.11 Summary

In this Chapter 6, the Lagrange analysis has been used to formulate models for a pair of locomotives on an inclined plane. The locomotives are on a 3D x-y-z plane. A new plane, j-w-d, is defined to simplify the analysis and a double rotation matrix is used to move from the x-y-z plane to the j-w-d. Thereafter, the Lagrange analysis is simplified by working in the j-w-d plane. The locomotives are constrained to move along the w-axis. The constraints of the locomotives are increased as the analysis proceeds. From the Lagrange analysis, the order of the locomotives starts off as 14 and the order reduces with an increase in constraints. The lowest order achieved is two. Therefore, a Lagrange based model order reduction is demonstrated in this Chapter. The order of the locomotive model decreases when transformation formulae are used and holonomic constraints are increased - which allows for degree of freedom analysis.

CHAPTER 7

Non-linear Control: Optimal Control Singularity Analysis

7.1 Overview

In Chapter 7, A non-linear, multiple input, multiple output control algorithm is formulated and applied on a pair of mine locomotives positioned on an inclined plane. Optimal control, particularly, singularity analysis for a pair of linear DC machine powered mine locomotives is presented. The optimal control algorithm is based on the Hamiltonian. The Pontryagin Maximum Principle is used to to determine the optimal control for the system of mine locomotives. The time derivative of the switching function yields the singular control for the pair of locomotives. Figure 7.1 summarizes the optimal control algorithm.

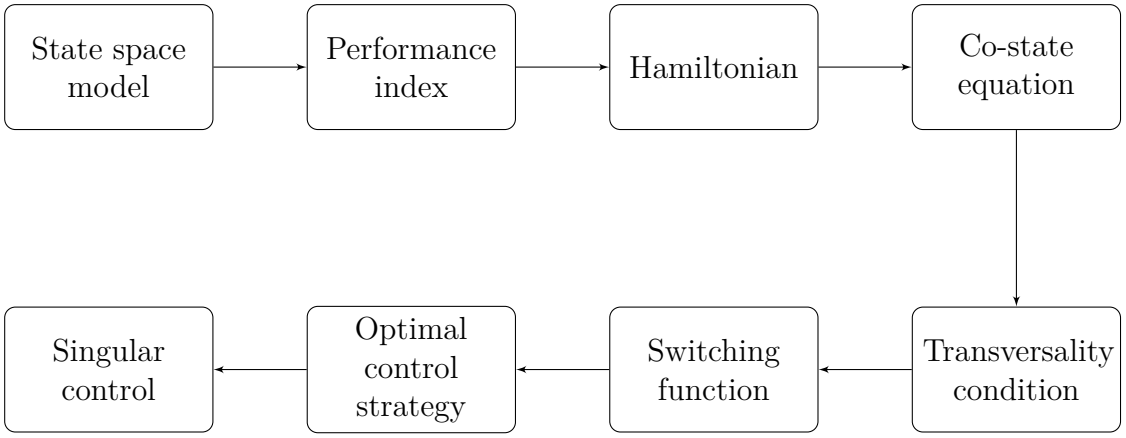

FIGURE 7.1: Optimal control, singularity analysis

7.2 Powering a pair of mine locomotives on an inclined plane

Some of the approaches used to access mine deposits from underground include; adit, decline/ramp, incline shaft and vertical shafts [85]. Adits in the South African mining sector are often found in mountainous areas where the deposits dip under the mountain [85]. Incline shafts offer quick access to the ore body which reduces cost significantly however, they are labour intensive and they have low operational efficiencies compared to vertical shafts [36, 85]. In the 1960s, incline shaft power consumption costs and maintenance costs were estimated to amount to 3.5 cents per tonne compared to vertical shafts [36]. Vertical shafts are efficient in transporting mining equipment, however, they experience difficulty in transporting large equipment. Vertical shafts are often used where the ore body is 250 - 500 m deep [85]. Decline shafts are often used in Australia and the ore is transported by truck haulage or conveyor belts [85]. The form of transportation used in mining include mine locomotives, conveyor belts and rope hauling [80]. Now introducing autonomous mine equipment, in particular, autonomous mine locomotives, would improve transport efficiency, productivity and mine safety [39, 44]. The aforementioned would also reduce the intensity of physical labour in the mining sector. A key operational concept in the mining sector where the track has a slope would be to use two mine locomotives simultaneously to fully utilize all the energies in the system. The idea is to have a set-up where one locomotive is at the top of the slope whilst the other locomotive is at the bottom of the slope. The locomotive at the top of the slope would take advantage of the gravitational force applied to it to drive the locomotive at the bottom of the slope. Therefore, the locomotive at the top of the slope would behave as a generator whilst the locomotive at the bottom of the slope would behave as motor. This approach is similar to a lift with counter-weight control problem. Optimal control algorithms based on the work by [99] could be applied for optimal speed and displacement.

7.2.1 Linear DC machine powered locomotive physical model

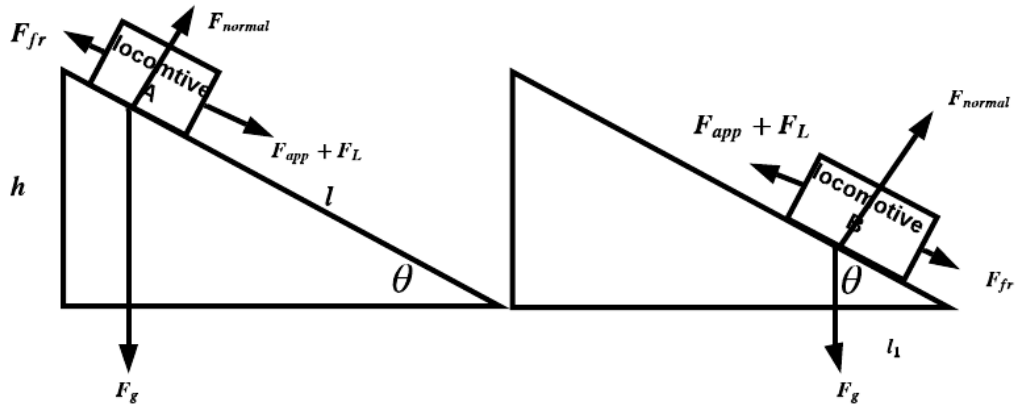

FIGURE 7.2: Free body diagram for a tandem pair of linear DC machine powered locomotives

The free body diagram of a tandem pair of gravity fed linear DC machine powered locomotives is shown in fig.7.2. The linear DC machines powered locomotives are subjected to a gravitational force F_g, an applied force which is the x-component of the gravitational force, a normal force F_{normal}, a Lorentz force F_L and a friction force F_{fr}. These tandem pair of linear DC machines powered locomotives are arranged such that a gravitational force is applied on either one of the DC machines powered locomotives when it is positioned at the top of the slope, assuming a steady state. As the gravitationally fed linear DC machine powered locomotives starts moving, from the linear DC machine, the reverse current is generated hence, the DC machine is operating as a generator. The aim is for the linear DC operating as a generator to be able to drive the second linear DC machine positioned at the bottom of the slope which behaves as a motor. The key operation feature of this exercise is getting the generator to drive the motor.

7.2.2 State equations

The model describing the dynamics of the locomotives on a slope is formulated using the Lagrange in Chapter 6. The model used is for a case where the linear DC machines have the same current. However, the friction force is assumed to be zero to simplify the analysis. The equations describing the dynamics of the locomotives are Eq.6.68 - Eq.6.70, without the friction force:

$$m_{la}\ddot{\omega_a} - \dot{q_a} l_a B_a sin\theta = m_{la} g sin\theta - b_a \dot{\omega_a} \tag{7.1}$$

$$m_{lb}\ddot{\omega_b} = m_{lb} g sin\theta + \dot{q_a} l_b B_b sin\theta - b_b \dot{\omega_b} \tag{7.2}$$

$$\dot{q_a} = \frac{1}{R}(V - l_a B_a(\dot{\omega_a} + \dot{\omega_b})) \tag{7.3}$$

From the equations describing the dynamics of the locomotives, the state space equation is formulated. To describe the state space equation, let: $x_1 = \omega_a$, $\dot{x_1} = \ddot{w}_a$, $x_2 = \dot{\omega}_b$, $\dot{x_2} = \ddot{\omega}_b$, and $\dot{x_3} = \dot{q}_a$. The following state equation is obtained:

$$\begin{aligned} \dot{x_1} =& \frac{F_{app1}}{m_{la}} + \frac{1}{Rm_{la}}(V - l_a B_a x_1 - l_b B_b x_2) l_a B_b sin^2\theta \\ \dot{x_2} =& \frac{F_{app2}}{m_{lb}} + \frac{1}{Rm_b}(V - l_b B_b x_1 - l_b B_b x_2) l_b B_b sin^2\theta \\ \dot{x_3} =& \frac{V - l_a B_a sin\theta x_1 - l_b B_b sin\theta x_2}{R} \end{aligned} \quad : \tag{7.4}$$

Remark: In practice, there is friction force due to the bar sliding along the rail of the linear DC machine and the wheel-rail contact and bearing of the locomotive. However, in this study the friction force is assumed to be negligible. This assumption is made primarily to simplify optimal control formulation, in particular, singularity analysis, which will be demonstrated in the sections that follow.

let $\alpha = \frac{F_{app}}{m}$, $f(x) = -l_a B_a sin\theta x_1 - l_b B_b sin\theta$, $u = \frac{V}{R}$, $\rho = \frac{lBsin\theta}{Rm}$, $\gamma = \frac{1}{R}$. This step is necessary in that it allows for a neater treatment of the switching function

which will be formally introduced in optimal control analysis. The state equation is now described by:

$$\begin{aligned} \dot{x_1} =& \alpha_1 + \rho_1 f(x) + \frac{u}{m_1} \\ \dot{x_2} =& \alpha_2 + \rho_2 f(x) + \frac{u}{m_2} \\ \dot{x_3} =& \gamma f(x) + u \end{aligned} \tag{7.5}$$

i.e.

$$\dot{\boldsymbol{x}} = \boldsymbol{g}(\boldsymbol{x}, \boldsymbol{u}, t) \tag{7.6}$$

Another thing to note is that, throughout this document, $\boldsymbol{g}(\boldsymbol{x}, \boldsymbol{u}, t)$ will be used to represent the state equation.

In this section, a series connected tandem pair of linear DC machine powered locomotives is presented. The model describing the dynamics of the locomotives is formulated in sec.6.8. An applied force, due to gravity, is also incorporated when modelling the DC machines whilst, the friction force is omitted. Future work in this model will incorporate a detailed friction model of the pair of DC machines. This friction model will be an extension of Pacejka's friction model and the LuGre dynamic model [99].

7.3 Hamiltonian based optimal control formulation

The Hamiltonian based optimal control from [99] is used to formulate the optimal control in this study. Formulating the optimal control demands that the control problem is well defined. A key step that follows is the Pontryagin Maximum Principle (PMP), where a first order condition necessary for optimality is used in determining an explicit solution to the optimal control problem [32]. The optimal control problem is to minimize the differential displacement of the bars of a pair of gravitational fed linear DC machines over a finite time and a space of admissible

controls [32]. The performance index:

$$J = \int_0^{t_f} L dt \tag{7.7}$$

is subjected to the state space equation:

$$\dot{\boldsymbol{x}} = \boldsymbol{g}(\boldsymbol{x}, \boldsymbol{u}, t) \tag{7.8}$$

Where J is the cost function (performance index), and L is the running cost (Lagrangian) [6]. Now consider:
$L = x_1 + x_2$,
where x_1 and x_2 are the velocities of the locomotives. Computing the Hamiltonian associated with the optimal control problem follows; the Hamiltonian for a general case is described using the Legendre transformation and this is shown by [6, 99]:

$$H = L + \boldsymbol{\lambda}^T(\boldsymbol{g}(\boldsymbol{x}, \boldsymbol{u}, t)) \tag{7.9}$$

Where H is the Hamiltonian, $\boldsymbol{\lambda}$ is a vector of co-state variables (also known as a vector of Lagrange multipliers), this vector has the same dimensions as the state vector $\boldsymbol{x}$. Evaluating the Hamiltonian yields:

$$\begin{aligned} H = x_1 + x_2 + \lambda_1(\alpha_1 + \rho_1 f(x) + \frac{u}{m_1}) + \lambda_2(\alpha_2 + \rho_2 f(x) \\ + \frac{u}{m_2}) + \lambda_3(\gamma f(x) + u) \end{aligned} \tag{7.10}$$

It follows that the time derivative of the co-state variables is equal to the Jacobian of the Hamiltonian. The relationship between the Hamiltonian and co-states variables (co-state equation) deduced by a first order optimality condition is necessary for determining the optimal control input which will be shown later in the dissertation:

$$\dot{\boldsymbol{\lambda}} = -\frac{\partial H}{\partial \boldsymbol{x}} \tag{7.11}$$

Evaluating Eq.7.11 yields the following equations:

$$\dot{\lambda_1} = \frac{\partial H}{\partial x_1} = -1 + (\lambda_1\rho_1 + \lambda_2\rho_2 + \lambda_3\gamma)\frac{\partial f(x)}{\partial x_1} \tag{7.12}$$

$$\dot{\lambda_2} = \frac{\partial H}{\partial x_2} = -1 + (\lambda_1\rho_1 + \lambda_2\rho_2 + \lambda_3\gamma)\frac{\partial f(x)}{\partial x_2} \tag{7.13}$$

$$\dot{\lambda_3} = 0 \tag{7.14}$$

Now imposing the transversality condition for finite time:

$$-\boldsymbol{\lambda}^T|_{t_f} d\boldsymbol{x}(t_f) + H|_{t_f} dt_f = 0 \tag{7.15}$$

so;

$$H(t_f) = 0 \tag{7.16}$$

therefore:

$$H(t) = 0 \quad \forall t \in [\,0, t_f\,] \tag{7.17}$$

and it is desired that:

$$\lambda(t_f) = 0 \tag{7.18}$$

The optimal control input is also given by:

$$u^* = argmin H(x, \lambda, t) \tag{7.19}$$

The admissible control input is described by:

$$u_{min} \leq u \leq u_{max} \tag{7.20}$$

Where u is the input voltage normalized with the resistance and it ranges between $u \in [\,0, 20/R\,]$

Stationary condition:

$$\frac{\partial H}{\partial \boldsymbol{u}} = 0 \tag{7.21}$$

7.3.1 Pontryagin Singular control

$$H^* \leq H \tag{7.22}$$

$$L^* + \boldsymbol{\lambda}^T(\boldsymbol{g}((\boldsymbol{x}), \boldsymbol{u}, t))^* \leq L + \boldsymbol{\lambda}^T(\boldsymbol{g}((\boldsymbol{x}), \boldsymbol{u}, t)) \tag{7.23}$$

Which yields

$$\boldsymbol{\lambda}^{T*} u^* \leq \boldsymbol{\lambda}^T u \tag{7.24}$$

The switching function is known as the coefficient of the control input deduced from the Hamiltonian represented by Eq.7.25. Thus:

$$H_1 = \rho_1\lambda_1 + \rho_2\lambda_2 + \lambda_3 \tag{7.25}$$

The control strategy is found using Eq.7.20:

$$u* = \begin{cases} u_{min} & H_1 \geq 0 \\ u_{max} & H_1 \leq 0 \\ u_{sing} & H_1 \equiv 0 \end{cases}$$

At the singular arc, $H_1 \equiv 0$, which implies that:

$$\rho_1\lambda_1 + \rho_2\lambda_2 + \lambda_3 = 0 \tag{7.27}$$

Now, taking the time derivative of the switching function:

$$\dot{H_1} = \rho_1\dot{\lambda_1} + \rho_2\dot{\lambda_2} + \dot{\lambda_3} \tag{7.28}$$

substituting Eq.7.12 - Eq.7.14 into Eq.7.28 yields:

$$(\lambda_1\rho_1 + \lambda_2\rho_2 + \lambda_3\gamma)(\rho_1\frac{\partial f(x)}{\partial x_1} + \rho_2\frac{\partial f(x)}{\partial x_2}) = \rho_1 + \rho_2$$

Since $\dot{H}_1$ does not result in an explicit solution for the optimal control problem, now evaluate:

$$\begin{aligned}\ddot{H}_1 = (\dot{\lambda_1}\rho_1 + \dot{\lambda_2}\rho_2 + \dot{\lambda_3}\gamma)(\rho_1\frac{\partial f(x)}{\partial x_1} + \rho_2\frac{\partial f(x)}{\partial x_2}) \\ + (\lambda_1\rho_1 + \lambda_2\rho_2 + \lambda_3\gamma)(\rho_1\frac{d}{dt}\frac{\partial f(x)}{\partial x_1} + \rho_2\frac{d}{dt}\frac{\partial f(x)}{\partial x_2})\end{aligned} \tag{7.29}$$

Now evaluating:

$$\frac{d}{dt}\frac{\partial f(x)}{\partial x_1} = \frac{\partial^2 f(x)}{\partial x_1^2}\dot{\boldsymbol{x_1}} + \frac{\partial^2 f(x)}{\partial x_1 \partial x_2}\dot{\boldsymbol{x_2}} \tag{7.30}$$

and

$$\frac{d}{dt}\frac{\partial f(x)}{\partial x_1} = \frac{\partial^2 f(x)}{\partial x_2^2}\dot{\boldsymbol{x_2}} + \frac{\partial^2 f(x)}{\partial x_1 \partial x_2}\dot{\boldsymbol{x_1}} \tag{7.31}$$

Recall from Eq. 7.5 that;

$$\begin{aligned}\dot{x_1} =& \alpha_1 + \rho_1 f(x) + \rho_1 u \\ \dot{x_2} =& \alpha_2 + \rho_2 f(x) + \rho_2 u\end{aligned}$$

Now Eq.7.29 can be represented as:

$$u_{sing}\zeta(x) + \beta(x) = 0 \tag{7.32}$$

Where u_{sing} is the control input at the singular arc. Therefore, rearranging Eq.7.32 results in:

$$u_{sing} = -\frac{\zeta(x)}{\beta(x)} \tag{7.33}$$

Solving Eq.7.33 yields:

$$u_{sing} = -f(x) \tag{7.34}$$

Remark: An interesting observation is made when performing an analysis on singular arc. It is found that the control input for a singularity case is independent of the mass of the locomotives. The control input is a function of $f(x)$ where only the length of the bar and the magnetic field act on the $f(x)$.

Now applying the Legendre-Clebesch second optimality condition to verify the correctness of the optimal control input on the singular arc, the following equation is used:

$$\frac{\partial}{\partial u}\frac{d^{2k}H_1}{dt} \geq 0 \tag{7.35}$$

k is the order of the optimal control input at the singular arc. The order for this system is 1. Therefore the Legendre-Clebesch condition is satisfied, making the control input on the singular arc valid.

A Hamiltonian based optimal control formulation is presented and discussed. For an optimal control formulation where a tandem pair of gravity fed LDCM locomotives is evaluated, the optimal control input at the singularity arc is found using Pontryagin's maximum principle. The Legendre-Clebesch second optimality condition is further applied to verify the existence of the control input on the singular arc.

Remark: While this approach is similar to [99] yet a maximizing friction is not needed as is done for [99] approach. In this case, the state function solves the singularity problem.

7.4 Research contribution

The key contribution in Chapter 7 is; optimal control formulation, particularly, singularity analysis for a pair of locomotives on an inclined plane. In this chapter, a non-linear Hamiltonian based optimal control is formulated where the key focus is on the singularity analysis of a pair of locomotives. From the formulations, u_{sing}, the singular control is found. The singular control is found after applying time derivatives to a switching function.

7.5 Simulation results

The current and velocity relations are observed on fig. 7.3 and fig. 7.4, respectively. As it can be seen, the pair of linear DC machines have the same current as expected. This same current is owing to the fact that the linear DC machines are connected in series. The maximum current observed is 10A whilst the steady state current appears to be 0A. As it had been mentioned prior, the friction effects are not taken into consideration hence, a steady state current of 0A. An illustration of the velocity of the pair of gravitationally fed linear DC machines is found on fig. 7.4. Again, the velocities are found to be same for both the linear DC machines. This means that both bars have the same velocities hence, the same displacement. These illustrations are for a case where there is no external force applied to the

linear DC machines. Results that will follow will show the effects of changing the slope on which the bar moves along, effects of applying a force (gravity force) on the linear DC machines, optimal control results where the performance index, displacements and velocities of the linear DC machines will be shown.

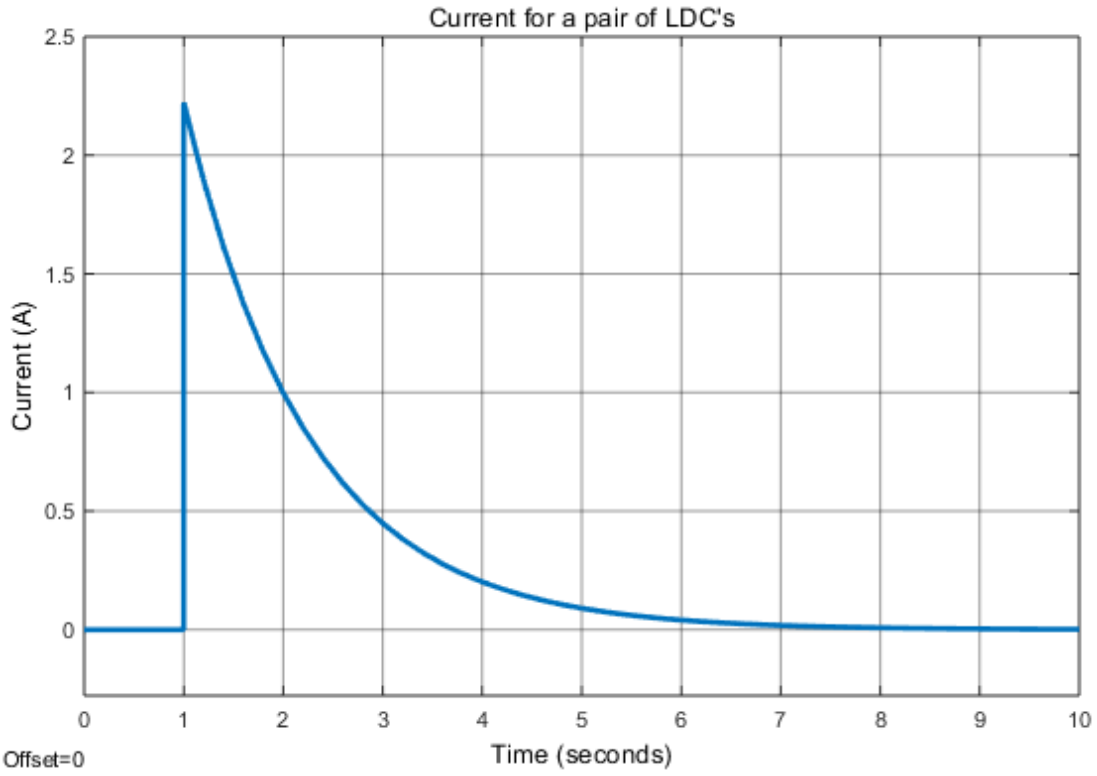

FIGURE 7.3: Current dynamics for a system of linear DC machines

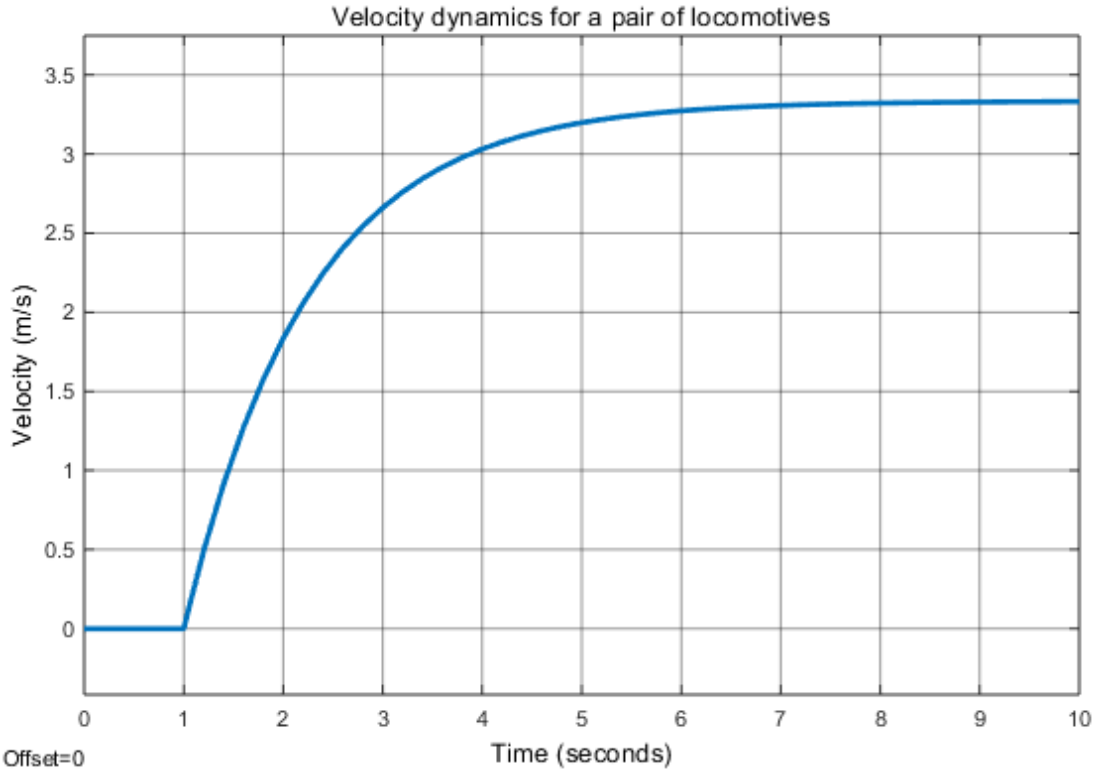

FIGURE 7.4: Velocity dynamics for a system of mine locomotives

Now, consider a case whereby the one linear DC machine is at the top of the slope whilst the other is at the bottom of the slope. Both the linear DC machines in this setup are in steady state. When the linear DC machine at the top of the slope experiences an external force due to gravity, the DC machine starts operating as a ***generator***. The generator at the top of the slope results in a reverse current in the system of linear DC machines. The reverse current is shown in fig. 7.6. The velocities of the bars of the linear DC machines are shown on fig. 7.7. When this gravity force is applied to the one linear DC machine, the DC machine start behaving as a generator hence, there is negative current in the system of linear DC machines. While a gravity force is applied to the linear DC machine at the top of the slope, the opposite force is applied to the linear DC machine at the bottom of the slope. This means that at the bottom of the slope, the linear DC machine behaves as a ***motor***. This conclusion is made based on the fact that a motor would result in a positive but equal current to the generator since a force with the same magnitude is applied to the linear DC machine at the bottom of the slope. On a general case; when a force is applied to the system of generators, they either behave as ***motors*** or ***generators*** depending on whether the force is in the direction towards or opposite the motion of the linear DC machines. It

is of paramount importance to mention that the force is applied at two seconds. But since there is a ***generator*** and ***motor*** in this system of linear DC machines, the negative and positive current due to these different modes of operation cancel each other completely. Hence, the current will remain at steady-state as can be seen on fig. 7.5 (exponential graph). Also, to illustrate that a generator behaviour is obtained when a force is applied to the system of linear DC machines, refer to fig. 7.6. The explanation provided is for an uncontrolled pair of linear DC machines. When an optimal control algorithm is applied on the system of linear DC machines with the same conditions as the linear DC machines explained; i.e. gravity force applied to the the pair of linear DC machines, the applied force is equal in magnitude but opposite in direction and the linear DC at the top of the slope is behaving as a generator whilst the linear DC machine at the bottom of the slope is behaving as a motor. After applying the co-state initial conditions that result in optimality by trial and error (transversality condition), the results are represented by the black line on fig. 7.5. The steady-state current is maintained for a controlled system.

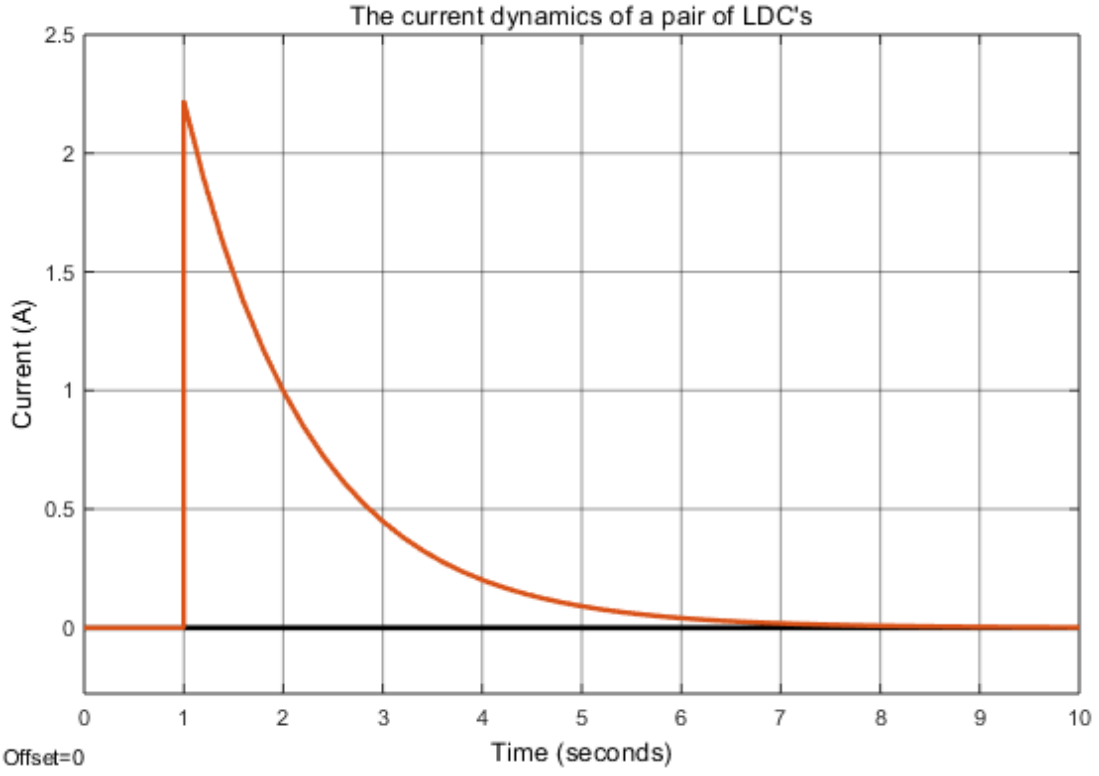

FIGURE 7.5: Optimal and uncontrolled current for a pair of linear DC machines

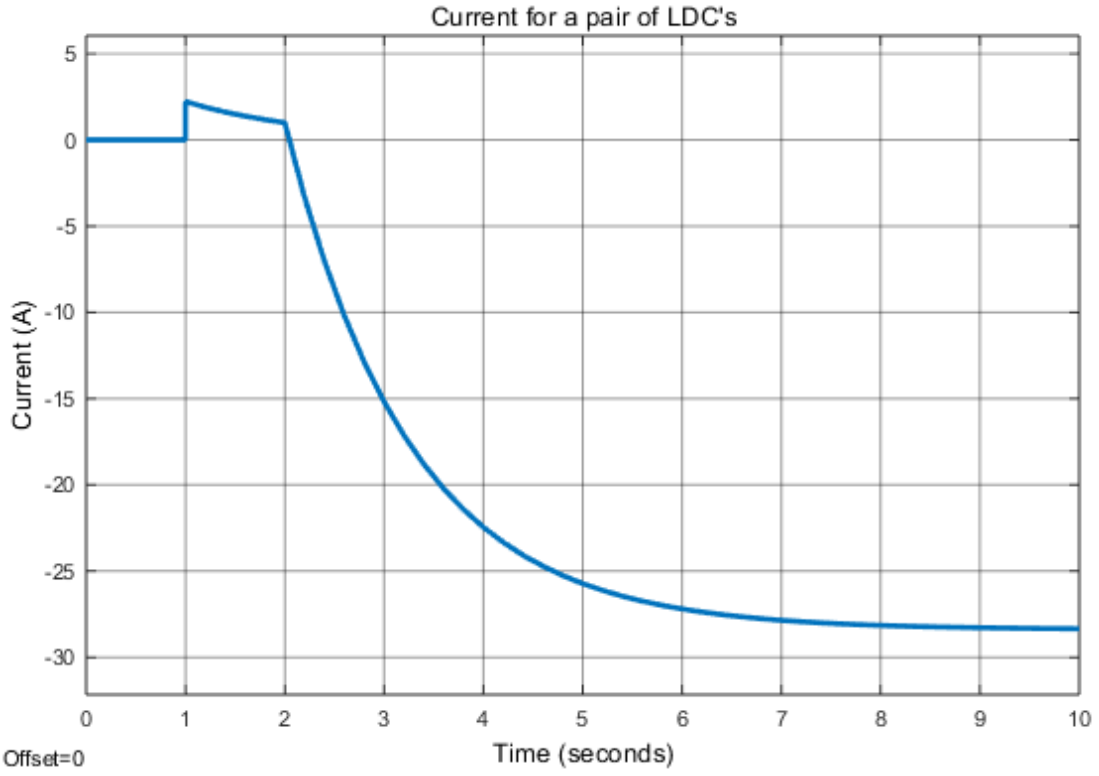

FIGURE 7.6: Current dynamics for a system of linear DC machines

The velocity is also observed and it can be seen that for an uncontrolled system of linear DC machines, the velocity starts at 0 until reaching a steady state at two seconds. At exactly two seconds, a force is applied to the system of linear DC machines and the linear DC machines accelerate in opposite direction. The aforementioned is supported by fig. 7.7 where the linear DC machines have velocities going in opposite directions. For a controlled system of linear DC machines, the velocities are shown in fig. 7.8. The velocities are equal but opposite in direction for a controlled system whilst for an uncontrolled system, there is an offset equal to the steady state velocity. Thus, if the steady state was zero, the velocities would be exactly the same in magnitude. This is because it is deduced that the velocities of the linear DC machines is the same gradient in magnitude but opposite in direction.

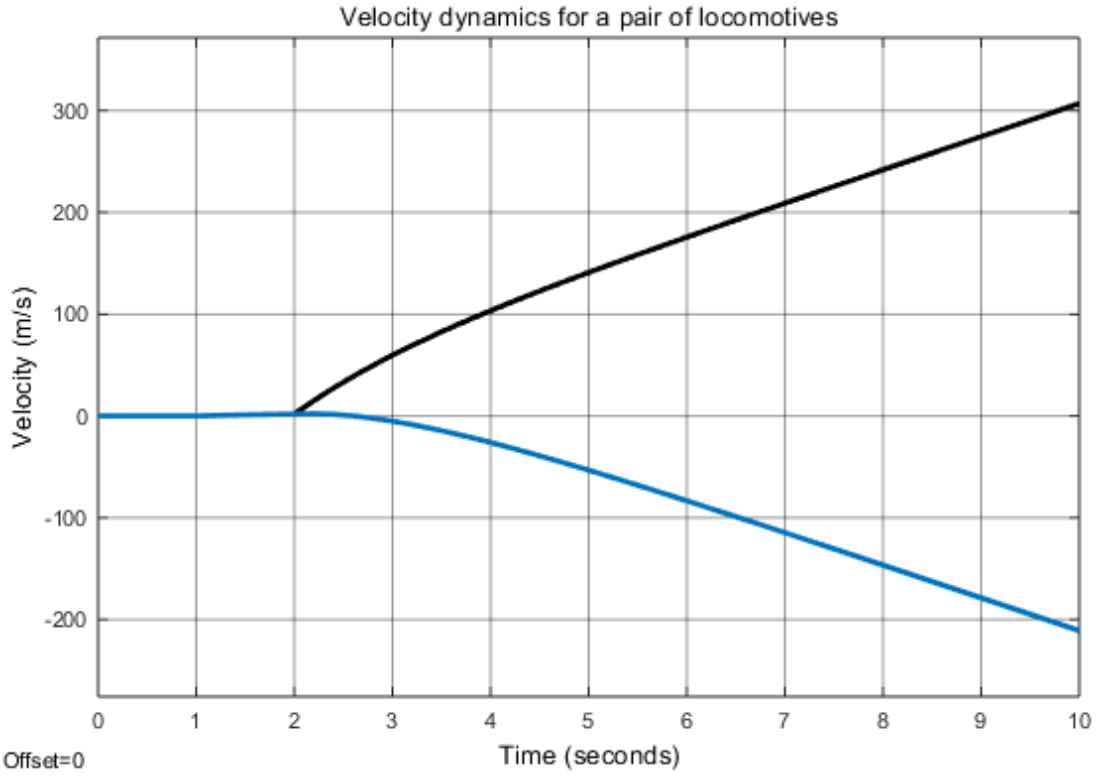

FIGURE 7.7: Velocity dynamics for a system of mine locomotives

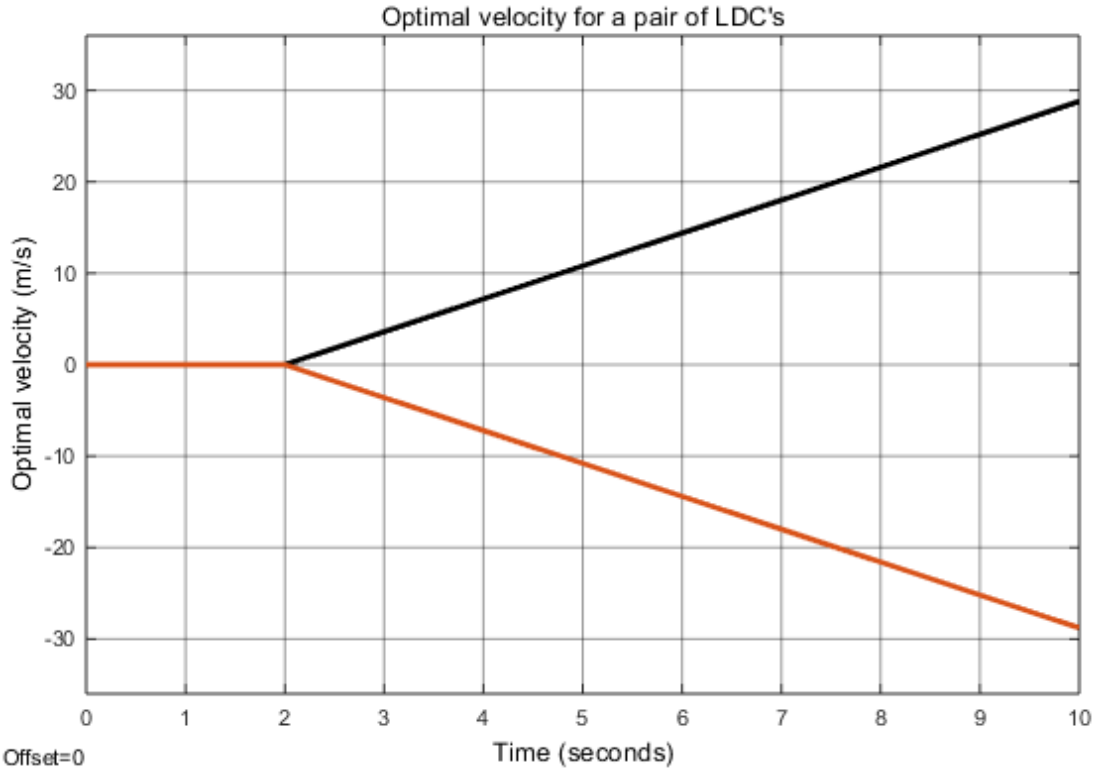

FIGURE 7.8: Optimal velocity

The displacements of the linear DC machines are also shown. It is clear from the simulations that the linear DC machines are moving in the opposite direction hence, the displacement is in the opposite direction. For a case where the optimal controller is applied, the displacements are equal but opposite in direction. More details on the displacement will be shown in the performance index plot where it will be verified that the optimal displacement is achieved. Therefore, this will mean that an optimal control solution for the optimal control problem is found and illustrated.

The performance index is shown on fig. 7.11. The performance index is also described by Eq.7.7. It can be seen from this figure that displacements of the linear DC machines have been minimized and both the linear DC machines have the same displacement in magnitude. The performance index before applying the optimal control algorithm is also illustrated on the same axis, fig. 7.11. The illustration mentioned shows that before an optimal control is applied, the performance index increases in a linear fashion until the bar has travelled the whole length along the rail. If an infinite path is considered, the performance index will also approach infinity.

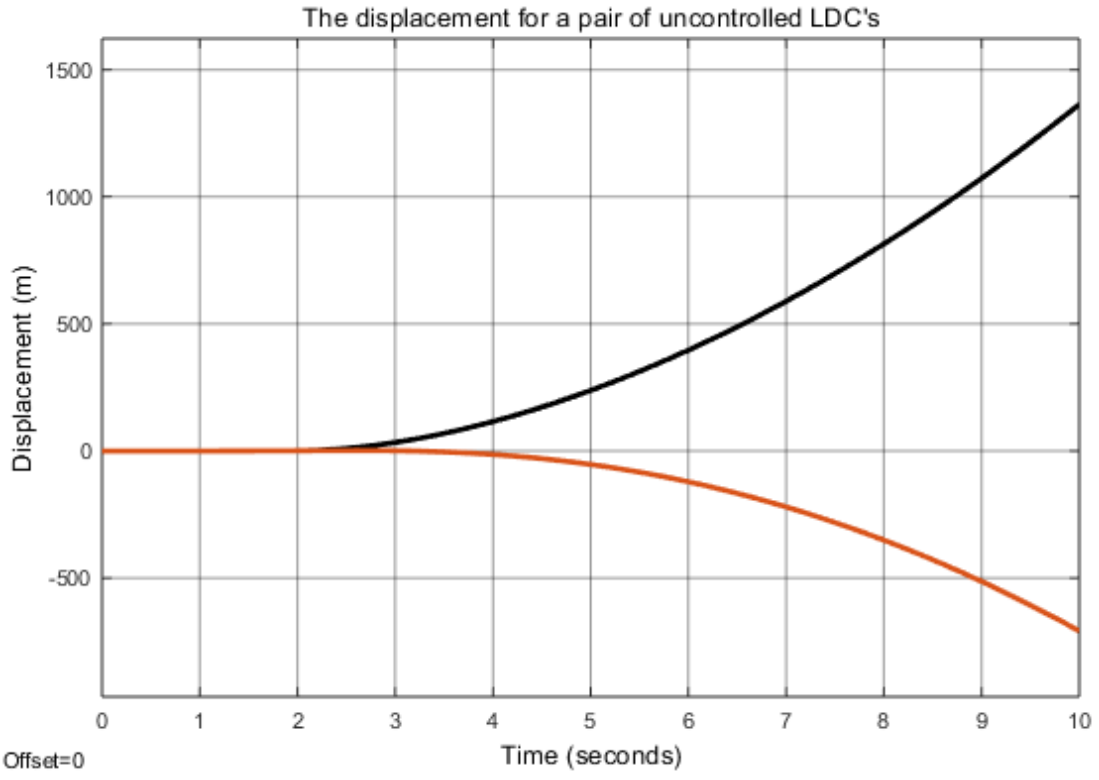

FIGURE 7.9: Displacement dynamics for mine locomotives

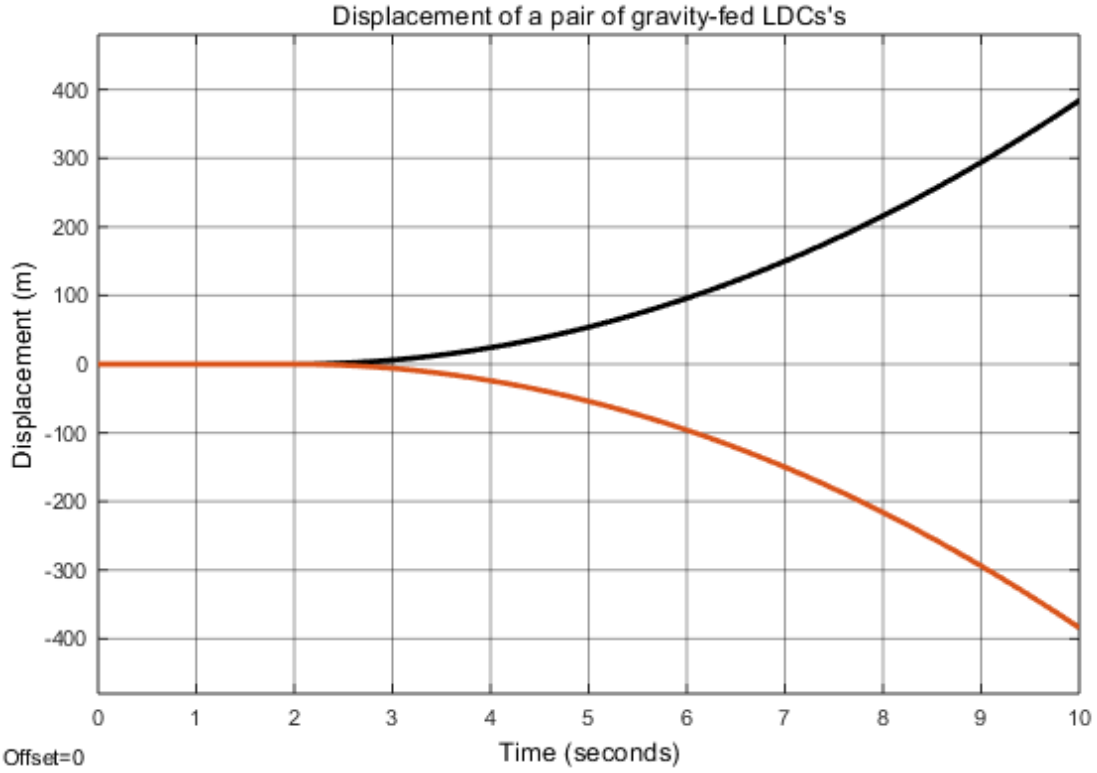

FIGURE 7.10: Optimal displacement for a pair of mine locomotives

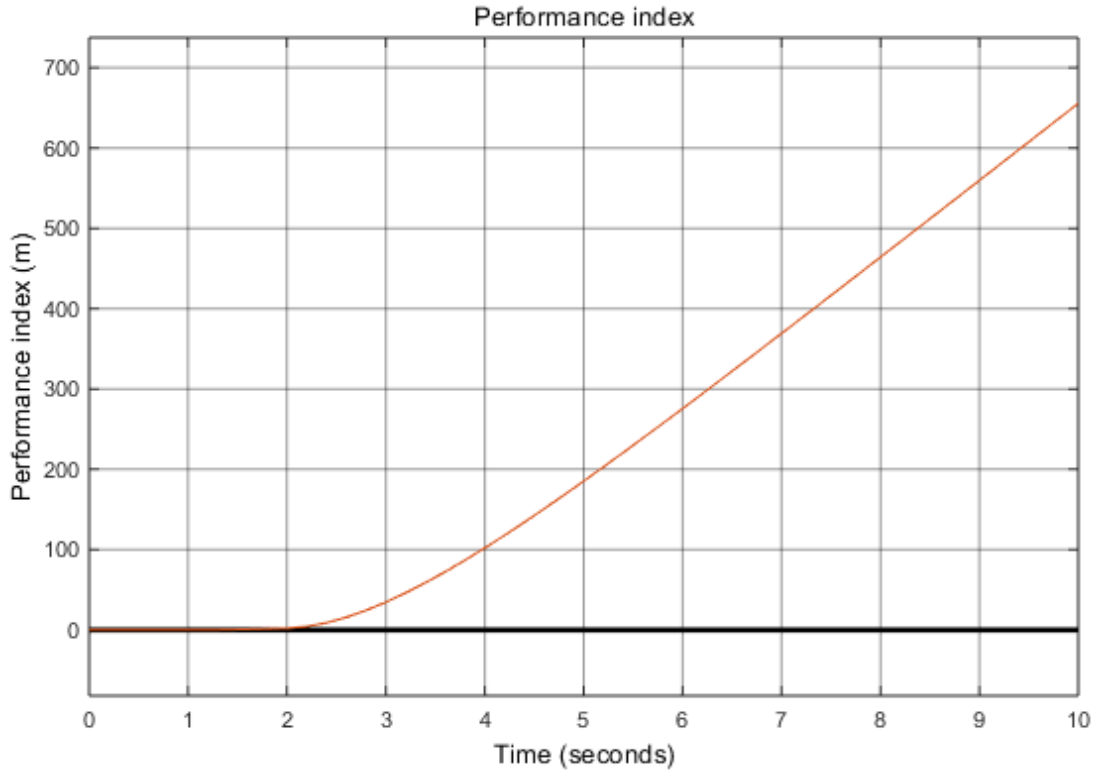

FIGURE 7.11: Performance index for a pair of linear DC machines

7.6 Summary

A condition for singular optimal control for a tandem pair of gravity fed linear DC machines is presented. A Chiasson mathematical model of the linear DC machine is used. These linear DC machines are connected in series hence, share the same current. Thereafter, an optimal control is formulated targeting; the singularity analysis and also, aiming for the one of the linear DC machines operating as a generator to drive the DC machine operating as motor. The results for a pair of gravity fed linear DC machines are also shown and it can be deduced from the results that a solution for the optimal control is found.

Conclusion and Future Work

7.7 Conclusion

Four key contributions have been demonstrated, highlighted and thoroughly discussed in the dissertation. These contributions are:

- Formulation of an magnetic field based, Lagrange analysis of a linear DC machine.
- Optimal singularity analysis for a pair of linear DC machines.
- Extension of Pacejka's, LuGre based friction model for rotating motion to sliding translational motion.
- Demonstration of a Lagrange based model order reduction.

A Lagrange based linear DC machine has been formulated and presented. The novelty of the Lagrange based linear DC machine formulation lies in the fact the Lagrange has been applied on an electromagnetic circuit based on a magnetic field. The challenge in the study has been identifying the type of energy (kinetic/potential energy) associated with the magnetic field. The electromagnetic circuit Lagrange formulations are compared with the formulations found by Chiasson for the same model. The formulations from the Lagrange analysis and Chiasson are found to be same, and the formulations also show that equations found using Newtons laws, Faraday's laws and Kirchhoff's laws can be found using the Lagrange. The linear DC machine in this study is further used for mining applications where the linear DC machine is used to power a mine locomotive. A speed controller based on the MIMO pole placement technique is developed to improve the performance of the locomotive. The controller ensures that the speed of the locomotive is maintained at 3 m/s and also that a settling time of 0.6s is achieved. A friction model (for the locomotive) which is an extension of the work done by Pacejka is formulated and presented. The friction model takes into consideration the static

and kinetic regime. Also, the friction model is a function of a sliding friction opposing the motion of the bar of the linear DC machine, and the rolling friction opposing the motion of the wheels of the locomotive on the rail. Practically, the friction model makes sense. The velocity dynamics of the locomotive are represented and the locomotive is found to have a higher velocity when there is no friction, and the locomotive has a low velocity in the presence of friction force. The effects of loading the locomotive and friction force are also investigated. From the investigation, it is found that the more loaded the locomotive, the higher the friction and the lower the velocity of the locomotive compared to an unloaded locomotive. Effects of variable voltages and friction force are also investigated. The results show that the locomotives with a higher supply tend to have lower losses compared to a locomotive with a lower voltage. The aforementioned necessitates the need for a comprehensive friction model.

Model order reduction based on Lagrange is also presented. A reduced model is achieved using Lagrange by taking advantage of transformation formulae, using degrees of order analysis and conditions that make sense physically. The model order reduction is performed on a pair of locomotives on an inclined plane. Practical systems have constrained motion, the same applies to the locomotives which are constrained to move down a slope. Identifying these constraints helps in identifying the generalized coordinates. Moreover, imposing constraints on the locomotives reduces the number of degrees of freedom which means, having reduced generalized coordinates. The aforementioned results in a lower order. The lowest order achieved for the locomotives is three whilst the highest order is 14.

A Hamiltonian based optimal controller focusing on singularity analysis for the pair of locomotives on an inclined plane is presented and developed. The optimal controller should be able to minimize the relative displacement between the machines. Mine locomotive dynamics results are also presented to show that the differential velocity and displacement are minimized. The performance index and Lagrangian are also minimized. The optimal control formulation is demonstrated via switching function differential calculus. The solution is shown to improve mine locomotive energy performance.

7.8 Future Work

Future work in this study could include thermal modelling to extend the model presented in the document. Also, the stick-slip effects will be incorporated in the friction model. According to [105], the LuGre friction model does not address this limitation. Including the stick-slip effects could result in a better approximation of a real life linear DC machine model. Slip consideration are other factors that could looked at when extending the work done on the friction model. Noise could also be injected in the system of locomotives. Practical systems have non-linearities and stochastic behaviour. It would be interesting to simulate and analyze the effects of the non-linearities. After extending and improving the linear DC machine model presented in this study, a complex model such as a diesel generator model could be formulated based on the Lagrange analysis. In fact, the macroscopic view of a synchronous machine based on the work done by [13] could be formulated using the Lagrange analysis. A comprehensive diesel generator model could also formulated in the future.

References

[1] L.J. Adamson, S. Fichera, B. Mokrani, and J.E. Mottershead. Pole placement in uncertain dynamic systems by variance minimisation. volume 127, pages 290–305. Elsevier, mechanical systems and signal processing, 2019.

[2] K.J. Astrom. Control of systems with friction. pages 1–8. Swedish Research Council for Eng. Science, 1995.

[3] K.J. Astrom and C. Canudas de Wit. Revisiting the lugre model stick-slip motion and rate dependence. BME MOGI, 2008.

[4] E.J. Berger. Friction modeling for dynamic system simulation. pages 535–577. American Society of Mechanical Engineers, 2002.

[5] L.D. Berkovitz and N.G. Medhin. Nonlinear optimal control. CRC Press, 2012.

[6] U. Boscain and B. Piccoli. An introduction to optimal control. page 99–66. Semantic Scholar, 2016.

[7] R.S Burns. Advanced control engineering. pages 35–266. Butterworth Heinemann, 2001.

[8] J.M. Carnicer, Y. Khiar, and J.M. Peña. Optimal stability of the lagrange formula and conditioning of the newton formula. volume 238, pages 52–66, 2019.

[9] E. Celledoni and Eirik H. Høiseth. Control of port hamiltonian systems by dissipative devices and application to improve semi-active suspension behaviour. IEEE transaction of automatic control, 2017.

[10] J. Cervera, A.J. van der Schaftb, and A. Baños. Interconnection of port-hamiltonian systems and composition of dirac structures. Elsevier, 2006.

[11] S.J. Chapman. Electric machinery fundamentals. pages 1–66. Mcgrawhill, 2005.

[12] S.J. Chapman. Electric machinery fundamentals. pages 191–264. Mcgrawhill, 2012.

[13] J. Chiasson. Modeling and high performance control of electric machines. pages 1–400. IEEE Power engineering, 2005.

[14] T. Chingozha, O.T. Nyandoro, M.A. van Wyk, and J.E.D Ekoru. Stabilizability preserving quotients and partial feedback linearization. volume 50, pages 203– 208. Elsevier, Computers and Structures, 2017.

[15] D. Chou. Dahl friction modeling. pages 1–60. Massachusetts Institute of Technology, 2004.

[16] C. Civeleka and T.F. Bechteler. Lagrangian formulation of electromagnetic fields in nondispersive medium by means of the extended euler–lagrange differential equation. volume 46, pages 1218–1227, 2008.

[17] M.N Sadiku C.K. Alexandra. Fundamentals of electric circuits. McGraw-Hill Companies, 2007.

[18] J. Van Coller. Advanced power system. *Power Sytems, Witwatersrand*, pages 29–38.

[19] P. Combes, A.K Jebai, F. Malrait, P. Martin, and P. Rouchon. Energy-based modeling of electric motors. pages 1–8. IEEE, 2014.

[20] P. Combes, A.K Jebai, F. Malrait, P. Martin, and P. Rouchon. Energy-based modeling of ac motors. pages 1–14. Researchgate, 2016.

[21] P.R. Dahl. A solid friction model. pages 1–24. Aerospace Corporation, 1968.

[22] C.C. de Wit, H. Olsson, K.J. Åström, and P. Lischinsky. A new model for control of systems with friction. volume 40, pages 419–425. IEEE, Transactions on automatic control, 1995.

[23] H. Duan, W. Liu, J. Ma, R.C.E. Tan, and S. Zhang. A family of optimal lagrange elements for maxwell's equations. pages 1–32, 2019.

[24] G.M. Eaton. The development of the electric mine locomotive. volume 33, pages 517–528. IEEE, Proceedings of the American Institute of Electrical Engineers, 1914.

[25] P.R. Evans. Rotations and rotation matrices. International Union of Crystallography.

[26] S. Fiaz, D. Zonetti, R. Ortega, J.M.A. Scherpen, and A.J. van der Schaft. On port-hamiltonian modeling of the synchronous generator and ultimate boundedness of its solutions. IFAC, 2012.

[27] J. Fábio, S. Santos, P.C. Pellanda, and A.M. Simões. Robust pole placement under structural constraints. volume 116, pages 8–14. Elsevier, systems and control letters, 2018.

[28] Y. Gao, D. Liang, and Y. Li. Directed and undirected network evolution from euler–lagrange dynamics. volume 000, 2018.

[29] Y. Gao, D. Liang, and Y. Li. Optimal weighted upwind finite volume method for convection-diffusion equations in 2d. pages 1–28, 2019.

[30] S. Garatti and S. Bittanti. Parameter estimation in the pacejka's tyre model through the ts method. volume 42, pages 1304 – 1309. IFAC proceedings Symposium on System Identification, 2009.

[31] T.E. Green. Mine locomotives. volume 103, pages 517–528. IET, Proceedings of the IEE - Part A: Power Engineering, 1956.

[32] M.T. Hale, Y. Wardi, H. Jaleel, and M. Egerstedt. Hamiltonian-based algorithm for optimal control. page 1–8. Elsevier, 2016.

[33] D. Halliday, R. Resnick, and J. Walker. Fundamentals of physics extended. pages 764–818. John Wiley and sons, 2011.

[34] K. Hashiguchi and S. Ozaki. Constitutive equation for friction with transition from static to kinetic friction and recovery of static frictions. page 2102–2124. International Journal of Plasticity 24, Elsevier, 2008.

[35] T. Herold. The art of modelling electrical machines. pages 1–6. Researchgate, 2014.

[36] G.W. Holl and E.G. Fairon. A review of some aspects of shaft design. The Southern African Institute of Mining and Metallurgy, 1973.

[37] M.C. Jain. Textbook of engineering physics. pages 1–99. PHI Learning, 2009.

[38] A.K Jebai, F. Malrait, P. Martin, and P. Rouchon. Estimation of saturation of permanent-magnet synchronous motors through an energy-based model. pages 1316–1321. IEEE International Electric Machines Drives Conference, 2011.

[39] Y. Jiang, Z. Li, G. Yang, Y. Zhang, and X. Zhang. Recent progress on smart mining in china: Unmanned electric locomotive. volume 9, pages 1–10. SAGE, Advances in Mechanical Engineering, 2017.

[40] Y. Jiang and W. Wang. H2 optimal model order reduction of the discrete system on the product manifold. volume 69, pages 593–603. Elsevier, Applied Mathematical Modelling, 2019.

[41] N. Kim, S. Cha, and H. Peng. Optimal control of hybrid electric vehicles based on pontryagin's minimum principle. volume 19, pages 1279–1287. IEEE transactions on control systems technology, 2011.

[42] P.N.V Kluge, D.K. Germaine, and K.T. Crépin. Dry friction with various frictions laws: From wave modulated orbit to stick-slip modulated. pages 28–40. Scientific Research Publishing, 2015.

[43] Redefining Knowledge. Simple pendulum. Redefining Knowledge, 2018. [Online; accessed 13-January-2019].

[44] V.A Kononov. Telecontrol for mining machinery. IFAC Automation in mining, mineral and metal processing, 1995.

[45] P. Korondi, J. Halas, K. Samu, A. Bojtos, and P. Tamás. Robot applications. BME MOGI, 2014.

[46] W. Kwak, J. Lee, and Y. Lee. Effects of friction models on the compaction behavior of copper powder. volume 122, pages 125–132. Elsevier, tribology international, 2018.

[47] W. Kwak, J. Lee, and Y. Lee. Numerical analysis of the friction-induced oscillator of duffing's type with modified lugre friction model. volume 440, pages 23–33. Elsevier, journal of sound and vibration, 2019.

[48] W. Kwak, J. Lee, and Y. Lee. Theoretical and experimental approach to ball bearing frictional characteristics compared with cryogenic friction model and dry friction model. volume 124, pages 424–438. Elsevier, mechanical systems and signal processing, 2019.

[49] G.H. Kwatny, F.M. Massimo, and L.Y. Bahar. volume 4, page 220–233. The Generalized Lagrange formulation for nonlinear RLC networks, 1982.

[50] J. Lamor. Ether and matter. *Electronics Letters*, 1900.

[51] B.P. Lathi. Linear systems and signal. pages 35–266. Oxford university press, 2005.

[52] H. Lee, D. Woo, B. Lee, G. Moon, G. Lee, M. Tahk, and H. Shin. Parameter-robust linear quadratic gaussian technique for multi-agent slung load transportation. volume 71, page 119–127. Elsevier, aerospace science and technology, 2017.

[53] V.J.S. Leite and P.L.D. Peres. Pole location control design of an active suspension system with uncertain parameters. volume 43, page 561–579. International Journal of Vehicle Mechanics and Mobility, 2005.

[54] F.L. Lewis, D.L. Vrabie, and V.L. Syrmos. Optimal control 3rd edition. pages 1–500. Wiley, 2012.

[55] C.J. Lin, H.T. Yau, and Y.C. Tian. Identification and compensation of nonlinear friction characteristics and precision control for a linear motor stage. volume 18, pages 1385–1396. American Society of Mechanical Engineers, 2013.

[56] F. Liu and S.D. Bopardikar. Sparse linear-quadratic-gaussian control in networked systems. volume 50, page 10748–10753. Elseveier, IFAC, 2017.

[57] Y. Liu, X. Wang, and Y. Gao. Three-dimensional multifilamentfinite element models of bi-2212 high-temperature superconducting round wire under axial load. volume 211, pages 273–286. Elsevier, composite structures, 2019.

[58] Y.F. Liu, J. Li, Z.M. Zhang, X.H. Hu, and W. J. Zhang. Experimental comparison of five friction models on the same test-bed of the micro stick-slip motion system. pages 15–28. Mechanical Science, 2015.

[59] Y.F. Liu, Z.M. Zhang, X.H. Hu, and W.J. Zhang. Experimental comparison of five friction models on the same test-bed of the micro stick-slip motion system. volume 6, pages 15–28. Copernicus, Mechanical sciences, 2015.

[60] W. Ludwig, D. Zajac, G. Ligus, and P. Korman. Analysis of pneumatic nozzle operation with the stochastic euler-lagrange model. volume 197, pages 386–403, 2019.

[61] SE Lyshevski. Analysis of Electromechanical Systems and Devices. In *Electromechanical Systems and Devices*, pages 15–70. CRC Press, 2008.

[62] A. Machelli. Port hamiltonian systems: A unified approach for modeling and control finite and infinite dimensional physical systems. pages 1 – 180. University of Bologna Dept. of Electronics, Computer Science and Systems, 2003.

[63] B. Mashadi, H. Mousavi, and M. Montazeri. Obtaining relations between the magic formula coefficients and tire physical properties. volume 5, pages 911 – 922. International Journal of Automotive Engineering, 2015.

[64] A. Masmoud. Control oriented modelling of ac electric machines. pages 1–20. Springer, 2018.

[65] M. McGrath, D. Howard, and R. Baker. A lagrange-based generalised formulation for the equations of motion of simple walking models. volume 55, 2017.

[66] Lagrangian Mechanics. Lagrangian mechanics. pages 1–28. `http://astrowww.phys.uvic.ca/~tatum/classmechs/class13.pdf`. [Online; accessed 15-Octoberber-2018].

[67] G. Miller. Nonlinear model-based friction compensation in control systems: Theory and experiment. pages 1–92. Queens University, Department of Mathematics and Statistics, 1997.

[68] R. Mittal and M. Bhandari. Design of robust pi controller for active suspension system with uncertain parameters. pages 333–337. IEEE, International conference on signal processing, 2015.

[69] K. Miyamoto, J. She, D. Sato, and N. Yasuo. Automatic determination of lqr weighting matrices for active structural control. volume 174, pages 308–321. Elsevier, 2018.

[70] R. Morselli and R. Zanas. Lagrange and hamiltonian methods for non-linear control. volume 2. IFAC conference by Elsevier, 2003.

[71] R. Morselli and R. Zanas. Control of port hamiltonian systems by dissipative devices and application to improve semi-active suspension behaviour. IFAC, 2006.

[72] D. Nataliia, G. Erik, Z. Igor, and Z. Klaus. Mathematical modeling of friction stir welding considering dry and viscous friction. volume 67, pages 1–8. Elsevier, applied mathematical modelling, 2019.

[73] O.T. Nyandoro, J.O. Pedro, O.A. Dahunsi, and B. Dwolatzky. Linear slip control formulation for vehicular anti-lock braking system with suspension effects. pages 4779–4784. The International Federation of Automatic Control Milano (Italy), 2011.

[74] R.T. O'Brien. Bang-bang control of lightly damped systems robust pole placement under structural constraints. pages 150–153. IEEE, 39th south-eastern symposium on system theory, 2007.

[75] H. Olsson, K.J. Åström, C.C. de Wit, M. Gäfvert, and P. Lischinsky. Friction models and friction compensation. pages 1–37. Department of Automatic Control, Lund Institute of Technology, 1997.

[76] R. Ortegs, A. Loria, P.J. Nicklasson, and H.B. SIra-Ramirez. Passitivity-based control of euler-lagrange systems. pages 1–37. Springer, 1998.

[77] H.B. Pacejka. Tire and vehicle dynamics. Butterworth-Heinemann, 2012.

[78] H.B. Pacejka and R. S. Sharp. "shear force developments by psneumatic tires in steady-state conditions: A review of modeling aspects. volume 20, pages 121–176. Vehicle Systems Dynamics,, 1991.

[79] T. Piatkowski. Dahl and lugre dynamic friction models—the analysis of selected properties. volume 73, pages 91–100. Elsevier, Mechanism and Machine Theory, 2014.

[80] B. Polnik, Z. Budzynski, and B. Miedzinski. Effective control of a battery supplied mine locomotive unit. volume 20, pages 39–43. Elektronika Ir Elektrotechnika, 2014.

[81] G. Prassad and M. Mohan. A contemporary adaptive air suspension using lqr control for passenger vehicles. pages 1–11. Elsevier, ISA transactions, 2019.

[82] P. Quevedo. Controllabilty and observabilty for time-invariant systems. pages 1–28. University of paderborn, faculty of electrical enegineering, 2018.

[83] H.D. Raut, A. Singh, and M.D. Patil. Design of digital controller using pole placement method. pages 1–5. IEEE, International conference on control and automation, communication and energy conservation, 2009.

[84] I.M. Ross. An optimal control theory for nonlinear optimization. volume 354, pages 39–51. Elsevier, journal of computational and appied mathematics, 2018.

[85] R. Rupprecht. Mine development – access to deposit. The Southern African Institute of Mining and Metallurgy Platinum, 2012.

[86] J.A. Russer and P. Russer. Lagrangian and hamiltonian formulations for classical and quantum circuits. Elsevier, IFAC proceedings.

[87] M. Rydel, R. Stanislawski, K.J. Latawiec, and M. Galek. Model order reduction of commensurate linear discrete-time fractional-order systems. volume 51, pages 536–541. Elsevier, 2018.

[88] S. Sarata, T. Kiyama, Y. Takahashi, and M. Seish. Development of a locomotive mechanism for underground coal mines. IFAC Automation in mining, mineral and metal processing, 1986.

[89] D. Sbarbaro. On the port-hamiltonian models of some electrochemical processes. volume 51, pages 38–43. IFAC, 2018.

[90] R.D Schultz and L. Zhao. Coenergy based transient model of interior permanent synchronous machines. *Communications, IEEE Transactions on Power Engineering*, pages 1–7, 2015.

[91] H. Shi and X. Yu. An effective euler–lagrange model for suspended sediment transport by open channel flows. volume 30, 2015.

[92] L. Slotine. Applied nonlinear control. Prentice hall, 1991.

[93] D. Spdek. Electric and magnetic forces in lagrangian and hamiltonian formalism. volume 143, pages 99–102. IEEE, 1996.

[94] M.R. Spiegel. Schaum's theory and problems of theoretical mechanics. pages 1–310. Mcgraw-Hill book company, 1967.

[95] D.S. Stutts. Analytical dynamics: Lagrange's equation and its application – a brief introduction. pages 1–23. Missouri University of Science and Technology, 2017.

[96] J. Swevers, F. Al-Bender, C.G. Ganseman, and T. Prajogo. An integrated friction model structure with improved presliding behavior for accurate friction compensation. volume 45, pages 675–686. IEEE, Transactions on automatic control, 2000.

[97] W.E. Ting and J.S. Lin. Nonlinear backstepping design of anti-lock braking system with assistance of active suspensions. volume 38, pages 97 – 102. IFAC proceedings Symposium on System Identification, 2005.

[98] W.E. Ting and J.S. Lin. Nonlinear backstepping design of anti-lock braking systems with assistance of active suspensions. volume 5, pages 97 – 102. Elsevier, IFAC, 6th Triennial World Congress, Prague, Czech Republic, 2005.

[99] P. Tsiotras. On the optimal braking of wheeled vehicles. pages 569–573. Proceedings of the American Control Conference, 2000.

[100] V. van Geffen. A study of friction models and friction compensation. Technische Universiteit Eindhoven, Department, Mechanical Engineering Dynamics and Control Technology Group, 2009.

[101] N. Vu, L. Lefevre, and B. Maschke. Geometric spatial reduction for port-hamiltonian systems. volume 125, pages 1–8. Elsevier, systems and control letters, 2019.

[102] P. Wach. *Dynamics and Control of Electric Drives*. Springer, 2011.

[103] J. Wang and D.A. WILSON. Mixed gl2/h2/gh2 control with pole placement and its application to vehicle suspension systems. volume 74, pages 1353–1369. International Journal of Control, 2001.

[104] C.C. De Wit and P. Tsiotras. Dynamic tire friction models for vehicle traction control. volume 5, pages 3746 – 3751. IEEE, Proceedings of the 38th Conference on decision and phoenix, Arizona USA, 1999.

[105] J. Wojewoda, A. Stefanski, , M. Wiercigroch, and T. Kapitaniak. Hysteretic effects of dry friction: modelling and experimental studies. volume 366, pages 747–765. Philosophical transactions of royals society, 2009.

[106] H. Zhou Y. Hu and C. Zhieng. Elsevier, Computer and structures.

[107] Z. Li Z. Yang, X. Deng. Numerical modeling of dynamic frictional rolling contact with an explicit finite element method. volume 129, pages 214–231. Elsevier, Tribology International, 2019.

[108] Z. Zhihui and L. Yuren. Numerical and analytical modeling of switched reluctance machines. volume 7, pages 3036–3043. Journal of Computer, 2012.